

AD _____

Award Number: W81XWH-04-1-0630

TITLE: Surface Enhanced Raman Spectroscopy for Monitoring Lactate and Glucose

PRINCIPAL INVESTIGATOR: Matthew R. Glucksberg, Ph.D.
Joseph Walsh, Ph.D.
Richard Van Duyne, Ph.D.

CONTRACTING ORGANIZATION: Northwestern University
Evanston, IL 60208-1110

REPORT DATE: July 2005

TYPE OF REPORT: Annual

20060215 116

PREPARED FOR: U.S. Army Medical Research and Materiel Command
Fort Detrick, Maryland 21702-5012

DISTRIBUTION STATEMENT: Approved for Public Release;
Distribution Unlimited

The views, opinions and/or findings contained in this report are those of the author(s) and should not be construed as an official Department of the Army position, policy or decision unless so designated by other documentation.

REPORT DOCUMENTATION PAGE				Form Approved OMB No. 0704-0188	
Public reporting burden for this collection of information is estimated to average 1 hour per response, including the time for reviewing instructions, searching existing data sources, gathering and maintaining the data needed, and completing and reviewing this collection of information. Send comments regarding this burden estimate or any other aspect of this collection of information, including suggestions for reducing this burden to Department of Defense, Washington Headquarters Services, Directorate for Information Operations and Reports (0704-0188), 1215 Jefferson Davis Highway, Suite 1204, Arlington, VA 22202-4302. Respondents should be aware that notwithstanding any other provision of law, no person shall be subject to any penalty for failing to comply with a collection of information if it does not display a currently valid OMB control number. PLEASE DO NOT RETURN YOUR FORM TO THE ABOVE ADDRESS.					
1. REPORT DATE (DD-MM-YYYY) 01-07-2005		2. REPORT TYPE Annual		3. DATES COVERED (From - To) 1 Jul 2004 – 30 Jun 2005	
4. TITLE AND SUBTITLE Surface Enhanced Raman Spectroscopy for Monitoring Lactate and Glucose				5a. CONTRACT NUMBER	
				5b. GRANT NUMBER W81XWH-04-1-0630	
				5c. PROGRAM ELEMENT NUMBER	
6. AUTHOR(S) Matthew R. Glucksberg, Ph.D. Joseph Walsh, Ph.D. Richard Van Duyne, Ph.D. E-mail: m-glucksberg@northwestern.edu				5d. PROJECT NUMBER	
				5e. TASK NUMBER	
				5f. WORK UNIT NUMBER	
7. PERFORMING ORGANIZATION NAME(S) AND ADDRESS(ES) Northwestern University Evanston, IL 60208-1110				8. PERFORMING ORGANIZATION REPORT NUMBER	
9. SPONSORING / MONITORING AGENCY NAME(S) AND ADDRESS(ES) U.S. Army Medical Research and Materiel Command Fort Detrick, Maryland 21702-5012				10. SPONSOR/MONITOR'S ACRONYM(S)	
				11. SPONSOR/MONITOR'S REPORT NUMBER(S)	
12. DISTRIBUTION / AVAILABILITY STATEMENT Approved for Public Release; Distribution Unlimited					
13. SUPPLEMENTARY NOTES					
14. ABSTRACT The development of robust, portable, and simple biomedical device for the monitoring of glucose, lactate and other metabolites of interest is of great practical importance to routine treatment of diabetes and to the evaluation of individuals under high-stress situations, e.g. warfighters and astronauts. Raman spectroscopy is a powerful analytical tool that permits the unambiguous identification of molecules based on their unique vibrational modes. This spectral fingerprinting of molecules is well suited to multi-analyte detection without cumbersome sample preparation or separation. The Surface Enhanced Raman Scattering (SERS) phenomenon increases by up to a trillion fold the Raman signal from molecules near gold and silver nanoscale materials. We have shown that the incorporation of chemically tailored coatings on SERS active surfaces may serve as a partitioning layer, selectively concentrating the molecules of interest near the surface, thus simultaneously increasing target signal and decreasing the noise signal from interferants even with low power (~1mW) lasers. We have successfully developed and tested these SERS active substances in vitro and in vivo in the subcutaneous space of a rat. Work continues in rat models of hyperglycemia and hyperlactatemia.					
15. SUBJECT TERMS No subject terms provided.					
16. SECURITY CLASSIFICATION OF:			17. LIMITATION OF ABSTRACT	18. NUMBER OF PAGES	19a. NAME OF RESPONSIBLE PERSON
a. REPORT	b. ABSTRACT	c. THIS PAGE			USAMRMC
U	U	U	UU	70	19b. TELEPHONE NUMBER (include area code)

Table of Contents

Cover.....	1
SF 298.....	2
Table of Contents.....	3
Introduction.....	4
Body.....	4
Key Research Accomplishments.....	12
Reportable Outcomes.....	13
Conclusions.....	14
References.....	14
Appendices.....	15

INTRODUCTION

The overall project goal is to demonstrate a sensor based on surface-enhanced Raman spectroscopy (SERS) that measures glucose and lactate. We have successfully demonstrated feasibility of using this system for detection *in vitro* and *in vivo* as specified in the original proposal.

The specific aims, as proposed in the original "statement of work" included:

Task 1. To develop and optimize SERS (Surface Enhanced Raman Active) surfaces and partition layers for the detection of glucose and lactate, *in vitro*.

- a. Determine optimal nanoscale geometry for SERS-active substrate.
- b. Optimize, *in vitro*, partition layers for best selectivity to target molecules glucose and lactate.
- c. Test effectiveness of probe configurations.

Task 2. Use a rat model to monitor analyte concentrations and assess performance.

- a. Control experiments.
- b. Use indwelling probes to quantitatively measure glucose levels *in vivo*.
- c. Use indwelling probes to quantitatively measure lactate levels *in vivo*.
- d. Use indwelling probes to quantitatively measure lactate and glucose levels *in vivo*.

BODY

TASK 1 – Development and Optimization of the SERS-active substrate

Self-Assembled Monolayer (SAM) Development As with most research projects, there were obstacles to overcome. While we anticipated some of these, we did not expect an inability to find a consistent supplier of a basic and critical chemical need. In our proposal, we submitted preliminary SERS data using tri(ethylene glycol) alkanethiol (EG3) as the SAM to partition glucose. The EG3 SAM consists of a hydrophobic chain with a hydrophilic head group. The SAM captures the glucose and concentrates it within the first few nanometers of the SERS-active Ag or Au surface. This is a critical requirement since SERS has a short-range (0-2 nm) distance dependence and can only detect analytes within this narrow zone. We found that neither the commercial or academic suppliers of EG3 could provide us material capable of reproducing our previous SERS work even in the simplest of environments (i.e. glucose in water). Consequently, the first months of the project were consumed with the task of isolating the problem to the EG3 SAM and then developing an alternative. The non-trivial breakthrough that has allowed us to rapidly move forward in the past 6 months was the development of a new mixed SAM based on two commercially available components, decanethiol (DT) and mercaptohexanol (MH). The DT/MH SAM was designed to have dual hydrophobic/hydrophilic functionality analogous to EG3, glucose-sized pockets formed by the shorter OH-terminated chains (Figure 1), and partitioning

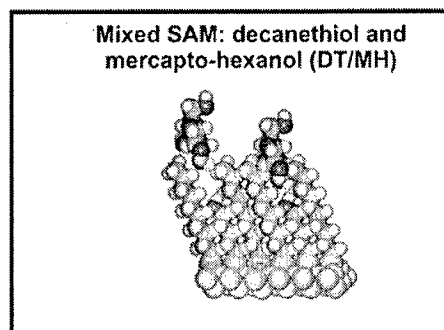


Figure 1: Schematic representation of DT/MH mixed SAM for partitioning and departitioning of glucose.

of glucose even closer to the SERS-active surface than EG3. We have experimentally confirmed that the DT/MH mixed SAM has better performance as a partitioning layer than the DT¹ and EG3^{2,3} SAMs used previously.

Nanowells. Nanowells were fabricated using reactive ion etching (RIE) and the resulting structure was verified by AFM. A flow diagram illustrating this procedure is shown in Figure 2A. Hexagonally close-packed polystyrene nanospheres, diameter 510 nm, were used as the etching mask. Tetrafluoromethane (CF₄) gas was used to etch glass surfaces with the polystyrene nanosphere mask using the following parameters: power 25 W, pressure 10 mTorr, and etching time 3 min. The AFM micrographs and the corresponding linescans confirm that the nanowells are approximately 10 nm deep (Figure 2B). Further, a 55-nm-thick layer of Ag was thermally deposited to form particles with a height of 45 nm above the glass surface. Figure 2C demonstrates that the Ag nanoparticles are actually in the nanowells. Embedding the particles in nanowells rather than fabricating them directly on a SiO₂ surface (e.g. periodic particle array (PPA)) improves their mechanical stability. This was verified spectroscopically as well as mechanically with AFM force measurements. Extinction spectra of PPAs and particles-in-nanowells substrates were measured over a period of four days in a constant flow aqueous environment. Particles-in-nanowells substrates retain their optical properties for three days while the PPA surfaces remain stable for only one day. Lateral forces required to move the metal particles were also measured for PPA and particles-in-nanowells substrates using AFM force calibration plots. The force needed to move most of the particles embedded in the nanowells was 29.8 nN, while the particles in a PPA move when only 11.1 nN was applied.

The structure of the nanoparticles embedded in nanowells was optimized to produce a localized surface plasmon resonance (LSPR) spectrum with an extinction band maximum at 836 nm, optimal for 785-nm excitation. Van Duyne and coworkers have demonstrated that the maximum SERS enhancement

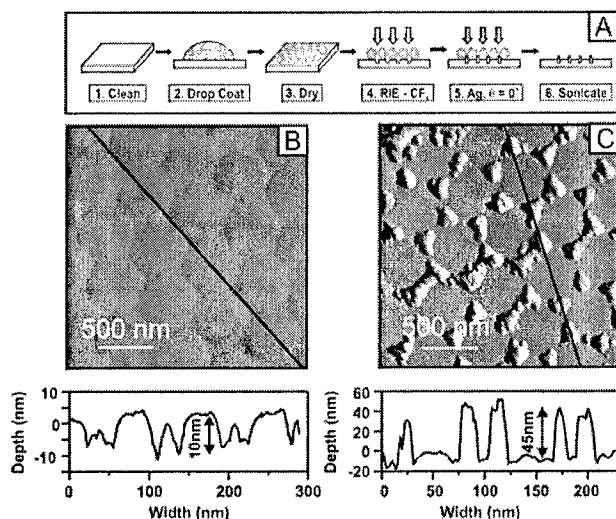


Figure 2. (A) Fabrication of a particles-in-nanowells substrate. Substrates were prepared using 510-nm-diameter spheres. Nanowells were manufactured using Reactive Ion Etching (RIE), $P = 25$ W, $P_r = 10$ mTorr, $t = 3$ min. (B) AFM micrograph of fabricated nanowells on glass substrate, depth ~ 10 nm. 55 nm of silver was deposited to form particles in nanowells. (C) AFM micrograph of particles in nanowells, height ~ 45 nm above the glass surface.

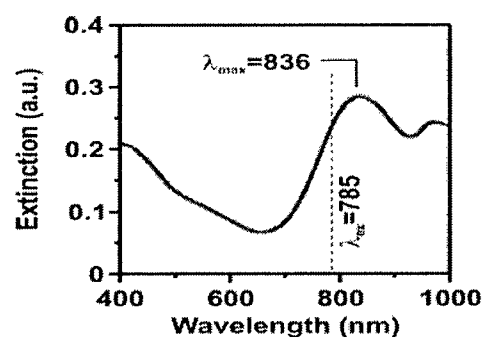


Figure 3. Extinction spectrum of the particles-in-nanowells substrate used for the SERS sensor substrate; the particles are functionalized with a DT/MH SAM and the spectrum is measured in aqueous solution. The LSPR maximum, $\lambda_{\text{max}} = 836$ nm, is optimized for 785-nm excitation.

can be achieved when the LSPR determined by the extinction maximum is slightly to the red of the excitation wavelength.⁴⁻⁶

To construct an optimized surface for 785-nm laser excitation, the nanowells were fabricated as described above and 65-nm-thick Ag was thermally deposited. These surfaces were then functionalized with the DT/MH mixed SAM and extinction spectra were measured in a flow cell in an aqueous environment. The extinction spectrum of the substrate is shown in Figure 3. The particles embedded in nanowells yield a LSPR spectrum with a rather narrow extinction band with $\lambda_{\text{max}} = 836$ nm, which is optimized for 785-nm excitation.

A benzenethiol monolayer was used to test the SERS-activity of the particles-in-nanowells surfaces. As shown by Van Duyne and coworkers, for nanoparticle array surfaces, the largest SERS signals are observed when the excitation wavelength is positioned slightly to the blue of the LSPR extinction λ_{max} .^{4,5} Similarly, particles-in-nanowells substrates exhibit a rather narrow extinction band and its location has a significant effect on the observed SERS signal intensity. It is a nontrivial task to optimize the optical characteristics of the particles-in-nanowells surfaces in order to use it to perform SERS measurements. A high signal-to-noise ratio SER spectrum of benzenethiol on particles in nanowells is shown in Figure 4. This demonstrates the feasibility of SERS measurements using the particles-in-nanowells format.

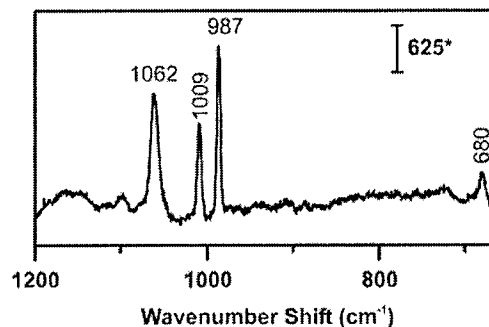


Figure 4. SERS spectrum of benzenethiol on Ag particles in nanowells. $\lambda_{\text{ex}} = 750$ nm, power = 1.6 mW, time = 2 min. *a.d.u.·mW⁻¹·min⁻¹

The data presented herein demonstrate the fabrication of nanowells and particles-in-nanowells on SiO₂ substrates. Moreover, we have explored alternative designs for fiber optic probes that use nanoparticles in nanowells as well as other SERS-active substrates. These designs focus on attaching the substrate to the tip of the fiber and might further improve light collection efficiency and ease of fabrication. They will be discussed in more detail in Task 2.

Particles-in-nanowells were fabricated on SiO₂ substrates with a SAM; however, the transition to the fiber tip has not yet been implemented. Several alternative designs for the optical fiber probe with SERS-active substrates attached to the tip of a fiber were developed (Figure 5). Figure 5A shows the design of a fiber probe with the particles-in-nanowells substrates attached to the tip of the fiber using optical epoxy such that the metal particles can be in contact with the sampling medium. This would allow utilization of large, well-packed, uniform areas of particles that are more difficult to achieve when nanoparticles are fabricated directly on

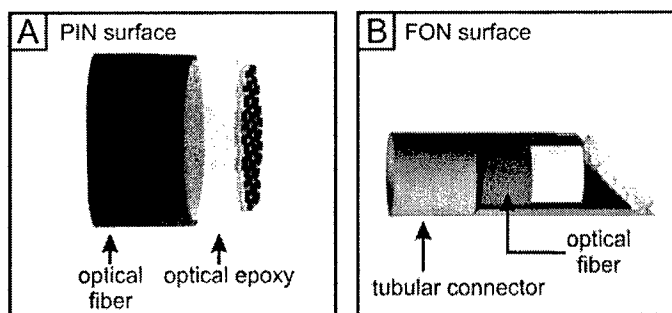


Figure 5. Proposed configurations. (A) Particles-in-nanowells (PIN) substrates attached directly to a fiber using optical epoxy. (B) A metal FON surface is used as a SERS-active surface; it is attached to the end of the fiber and interstitial fluid can flow in the space between the fiber and the AgFON surface.

the tip of the fiber. The optical epoxy will allow for transmission of the excitation beam and collection of the Raman scattered photons.

The second design utilizes a SERS-active, film over nanosphere (FON) surface (Figure 5B). The FONs will be fabricated by depositing 200 nm of Ag over the polystyrene nanosphere mask resulting in a nontransparent surface. This surface can be attached to the tip of a single optical fiber, a fiber pair (one for excitation and one for collection), or a fiber bundle (center fiber for excitation and ring of six for collection) using tubular connectors with slots to allow the flow of fluid to the surface. Although this type of substrate is not transparent, it provides 10 times the surface area in contact with the sample. As a result, AgFON surfaces produce larger net signal intensity than particles-in-nanowells substrates. Therefore, we employed AgFON surface to achieve the results shown in the rest of this report.

The structure of the AgFON surface is shown in the AFM micrograph in Figure 6A. The LSPR of AgFON substrates can also be tuned to create an optimized surface for 785-nm excitation.⁷ The tuning can be achieved by varying the diameter of the polystyrene nanospheres. Since AgFONs are not transparent, the LSPR spectra are measured in reflectance mode. Figure 6B shows the reflectance spectrum of the AgFON fabricated with 390-nm-diameter nanospheres, functionalized with DT/MH SAM in a flow cell in aqueous environment. The reflectance λ_{\min} occurs at 808 nm, which is optimal for 785-nm excitation.

To verify that a glucose spectrum can be collected in presence of the SAM, 0 and 100 mM aqueous glucose solutions were cycled through the flow cell with a DT/MH functionalized AgFON surface (Figure 7 inset). SER spectra were collected for each step (Figure 7A, B, C, D). The difference spectra are plotted in

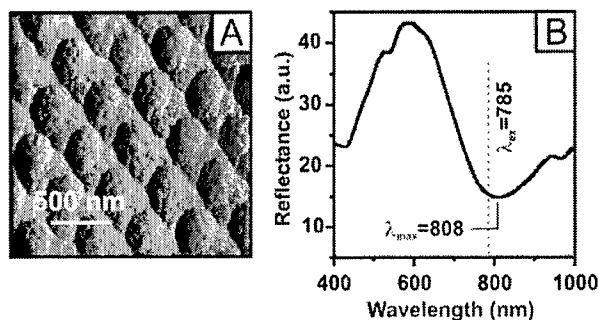


Figure 6. (A) AFM micrograph of AgFON manufactured using 390-nm-diameter nanospheres by depositing 200 nm of silver over the nanosphere mask. (B) Reflectance spectrum of AgFON substrate used for glucose sensing. The surface was optimized for 785-nm excitation. The reflectance minimum at 808 nm corresponds to the LSPR extinction maximum and is slightly red of the excitation wavelength.

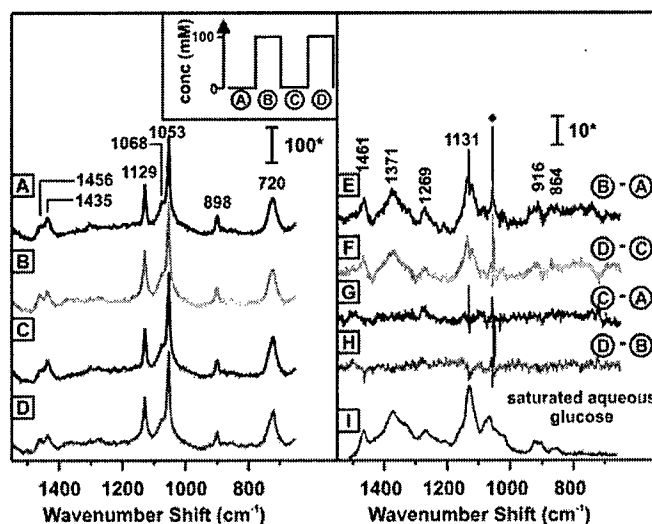


Figure 7. Glucose pulsing sequence on the SAM modified AgFON surface. (A, B, C, D) SER spectra of the sample cycled between 0 and 100 mM aqueous glucose solutions, $\lambda_{\text{ex}} = 532$ nm, $P_{\text{laser}} = 10$ mW, $t = 20$ min, $\text{pH} \sim 7$. (E, F, G, H) Difference spectra showing partitioning/departitioning of glucose. (I) Aqueous saturated glucose solution normal Raman spectrum. Inset represents the pulsing sequence of the experiment. ♦ Imperfect subtraction of the narrow band at 1053 cm^{-1} due to nitrate results in a very sharp peak in the difference spectra. *a.d.u.·mW⁻¹·min⁻¹

Figure 7E, F, G, H. Figure 7I shows the normal Raman spectrum of a saturated aqueous glucose solution for comparison. The glucose peaks in the difference spectra (Figure 7E, F) correspond to the peaks in the normal Raman spectrum of glucose (Figure 7I).

We were able to demonstrate that a DT/MH functionalized, AgFON, SERS-based, glucose sensor has *in vitro* accuracy and precision. For calibration, over 90% of measurements fell in the A+B ranges of the Clarke error grid in three model systems: water, water with lactic acid and urea, and bovine plasma. In addition, over 85% of the independent validation measurements fell in the A+B ranges in all three systems. No quantitative analysis was done in blood because *in vivo* measurements will be in interstitial fluid, not in blood. If this sensor is ever to be used in blood, a protective membrane will be utilized to filter blood cells and larger proteins such that the fluid in contact with the SERS substrate resembles blood plasma. Therefore, quantitative analysis of glucose in a whole-blood system is not required. A DT/MH functionalized, AgFON substrate was placed in a flow cell and the sensor was exposed to known concentrations of glucose ranging from 10 - 450 mg/dL in water at pH ~7. SER spectra were collected ($\lambda_{\text{ex}} = 632.8$ nm, $P = 13$ mW, $t = 2$ min) from two locations on the substrate for each concentration. Several different substrates were used to build the training set, and each of those substrates was exposed to glucose concentrations spanning the experimental concentration range in random order. A partial least squares (PLS) calibration model was built using 46 independent spectral measurements.

In addition, 23 independent measurements with glucose concentrations ranging from 10 - 450 mg/dL were used to validate the model. In Figure 8, the calibration and validation data points for

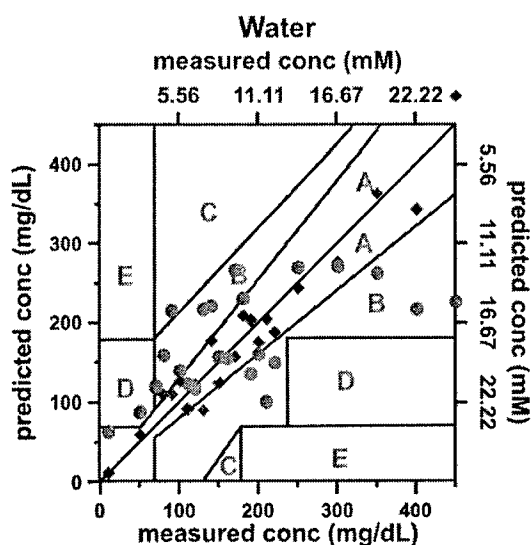


Figure 8. Calibration (♦) and validation (●) plot using two substrates and multiple spots. PLS calibration plot was constructed using 46 data points and validation plot was constructed using 23 data points taken over a range of glucose concentrations (10 - 450 mg/dL) in water at pH~7. RMSEC = 26.59 mg/dL (1.47 mM) and RMSEP = 85.95 mg/dL (4.78 mM). $\lambda_{\text{ex}} = 632.8$ nm, $P = 13$ mW, $t = 2$ min.

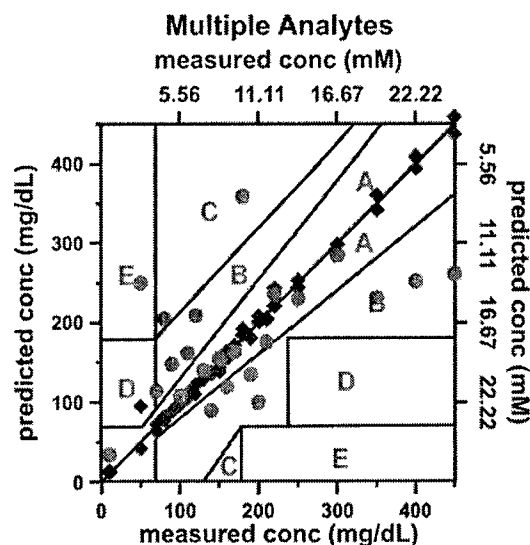


Figure 9. Calibration (♦) and validation (●) plot using two substrates and multiple spots. PLS calibration plot was constructed using 46 data points. The validation plot was constructed using 23 data points taken over a range of glucose concentrations (10 - 450 mg/dL) in 1 mM lactic acid and 2.5 mM urea at pH~7. RMSEC = 9.89 mg/dL (0.55 mM) and RMSEP = 92.17 mg/dL (5.12 mM). $\lambda_{\text{ex}} = 785$ nm, $P = 8.4$ mW, $t = 2$ min.

glucose in water are plotted on the Clarke error grid in order to evaluate the predictive capacity of the model. Diamonds (♦) represent the calibration with RMSEC of 26.59 mg/dL whereas circles (●) represent validation data with RMSEP of 85.95 mg/dL. In Figure 8, 98% of the calibration points and 91% of the validation points fall in the A+B ranges of the Clarke error grid. Furthermore, we demonstrated the quantitative detection of glucose in water (pH~7) with lactic acid (1 mM) and urea (2.5 mM) in physiological concentrations (Figure 9). We not only made our system more complex by adding small interfering analytes, but, we also advanced toward using a near-infrared laser source ($\lambda_{\text{ex}} = 785 \text{ nm}$, $P = 8.4 \text{ mW}$, $t = 2 \text{ min}$). Near-infrared sources are better suited for use in biological systems because of diminished protein autofluorescence. With PLS analysis, RMSEC was calculated to be 9.89 mg/dL and RMSEP was calculated to be 92.17 mg/dL. In Figure 9, 98% of the calibration points and 87% of the validation points fall in the A+B ranges of the Clarke error grid.

Once we were able to achieve acceptable calibration and validation plots for the systems mentioned above, we decided to skip the proposed steps of adding more analytes and move immediately to a more complex medium – bovine plasma. Bovine plasma was filtered using 0.45- μm -diameter pore filters. The filtered plasma was then spiked with glucose concentrations ranging from 10-450 mg/dL. SER spectra were collected at each concentration using multiple samples and multiple spots in random order ($\lambda_{\text{ex}} = 785 \text{ nm}$, $P = 10\text{-}30 \text{ mW}$, $t = 2 \text{ min}$). Figure 10 depicts 92 data points for the calibration plot with RMSEC of 34.3 mg/dL and 46 data points for the validation plot with RMSEP of 83.16 mg/dL. In the Clarke error grid, 98% for calibration and 85% for validation fall in A+B range.

We were able to demonstrate that the $1/e$ time constant in the water based media was 8 s for both partitioning and departitioning. For the plasma-based media the $1/e$ time constant was found to be 28 s for partitioning and 25 s for departitioning. The $1/e$ time constant data for the whole-blood based system was not measured for the reasons stated previously.

To demonstrate the real-time $1/e$ response to a step change in glucose concentration, we performed partitioning and departitioning of 50 mM glucose in an aqueous environment. DT/MH functionalized AgFON was placed in water (pH ~7) for ~5 hours. The AgFON surface was then placed in a flow cell. SER spectra were collected every 15 s ($\lambda_{\text{ex}} = 532 \text{ nm}$). Once the baseline was established, 50 mM glucose solution was injected at $t = 15 \text{ s}$. At $t = 225 \text{ s}$, 0 mM glucose solution was injected into the flow cell.

The data show that the intensity of the 1462 cm^{-1} glucose peak increased during partitioning and diminished during departitioning. This 1462 cm^{-1} peak was analyzed in PeakFit v4.12 program by fitting the data to the sum of two Lorentzian lineshapes. The amplitude for the 1462 cm^{-1} peak for each spectrum was thus obtained. The $1/e$

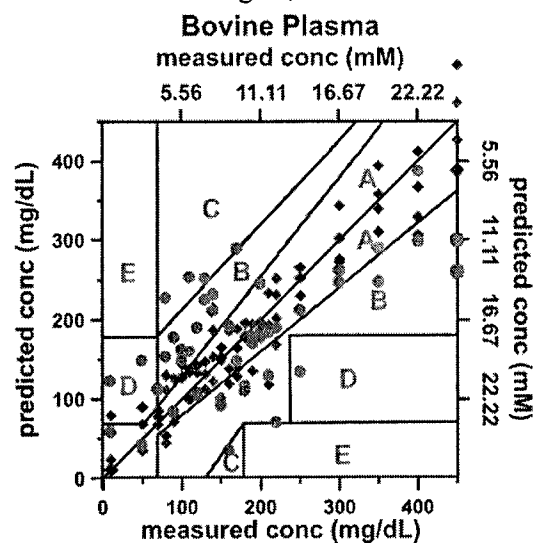


Figure 10. Calibration (♦) and validation (●) plot using three substrates and multiple spots acquired in two days. PLS calibration plot was constructed using 92 data points and validation plot was constructed using 46 data points taken over a range of glucose concentrations (10 - 450 mg/dL) in bovine plasma. RMSEC = 34.3 mg/dL (1.9 mM) and RMSEP = 83.16 mg/dL (4.62 mM). $\lambda_{\text{ex}}=785\text{nm}$, $P = 10\text{-}30 \text{ mW}$, $t = 2 \text{ min}$.

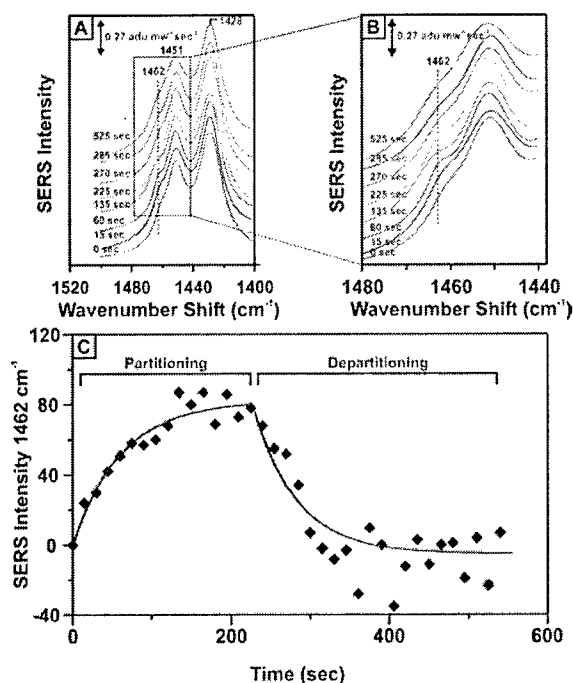


Figure 11. Real-time SERS response to a step change in glucose concentration in bovine plasma. A) SER spectra of the SAM and glucose at various times. Peaks at 1451 and 1428 cm^{-1} are features of SAM and 1462 cm^{-1} indicates glucose. Glucose was injected at $t = 15$ s and the cell was flushed with bovine plasma at $t = 225$ s. B) Expanded scale version of Figure 11A from 1480 to 1440 cm^{-1} . PeakFit v4.12 was used to determine the intensity of the 1462 cm^{-1} peak. C) Partitioning and departitioning of glucose. $\lambda_{\text{ex}} = 785$ nm, laser power = 100 mW, data acquisition $t = 15$ s. The $1/e$ time constants were calculated to be 28 s for partitioning and 25 s for departitioning.

time constant for the aqueous medium was 8 s for partitioning and 8 s for departitioning calculated from the exponential fit.

Since the $1/e$ experiment for the aqueous medium was successful, we moved towards conditions that are optimal for *in vivo* sensing by switching to 785-nm excitation for the bovine plasma experiments. The time constant for glucose in bovine plasma was determined under similar conditions as the glucose in water experiment. The spectra shown in Figure 11A and 11B demonstrate real-time amplitude changes in the 1462 cm^{-1} peak as the glucose concentration varies. The $1/e$ time constant was 28 s for partitioning and 25 s for departitioning, calculated from the exponential fit (Figure 11C).

TASK 2 – Development of rat model and *in vivo* testing

A Sprague-Dawley rat was weighed, anesthetized (Pentobarbital, Ovation Pharmaceuticals, Inc., 50 mg/kg ip induction, maintenance 25 m/kg ip hourly), and placed on a warming pad. The femoral vein was cannulated with PE 50 tubing (Clay Adams) for glucose infusion and the carotid artery was cannulated using PE 90 tubing for arterial blood sampling, including monitoring of blood glucose (One Touch II blood glucose meter)^a. The incisions were shut with surgical clips.

^a We should note here that a commercial paper strip-based test designed for human blood does give different results when used with rat blood. The differences are systematic, so it is a simple matter to account for this. Another concern is that the One Touch II and other consumer-grade systems likely introduce more scatter than our clinical-grade system (Corning 860). In subsequent chronic experiments we will make all measurements in a clinical-grade blood gas analyzer available for our use in a nearby lab.

To collect SER spectra, a 1-cm- diameter piece of skin was removed and replaced with a glass window held in a metal frame mounted on the rat's back. A DT/MH functionalized AgFON surface supported on a Cu mesh was positioned between the exposed subcutaneous tissue and the window such that the substrate was immersed in the subcutaneous interstitial milieu. Glucose (1 g/mL in saline) was infused at a constant rate (0.05-0.1 mL/min) through the venous catheter to increase and maintain blood glucose concentrations. A droplet of blood was drawn from the rat to measure the blood glucose level with the One Touch II blood glucose meter. After the blood glucose concentrations reached a stable plateau the SER spectra were acquired through the window using the Ti:sapphire laser ($\lambda_{\text{ex}} = 785 \text{ nm}$, $P = 50 \text{ mW}$, time = 2 min). The SER spectra showed clearly visible Raman bands characteristic of the SAM (data available, not shown). Additional bands were observed compared to the spectra collected in the plasma model; however, the Raman bands were not obscured by autofluorescence because of the near infra-red wavelength (785 nm) used for excitation.

All SER spectra were analyzed using PLS and represented on the Clarke error grid. In Figure 12, 21 data points were used to build the calibration model and five data points were used to validate the model. All the data points in both calibration and validation fall in A+B range of the Clarke error grid with the RMSEC = 7.46 mg/dL and RMSEP = 53.42 mg/dL.

Glucose was varied in the rat through intermittent intravenous infusion for three hours. A droplet of blood was drawn from the rat, the glucose level was measured with the One Touch II blood glucose meter, and corresponding SERS measurements were taken. Figure 13 shows the glucose concentration variation in the rat measured using SERS and the One Touch II blood glucose meter with respect to time.

After being implanted in the rat for 5 hr, the DT/MH functionalized AgFON surface was removed and placed in a flow cell containing bovine plasma. Then 1/e time constant response to a step change in glucose concentration was determined (Figure 14). The AgFON surface was exposed to 50 mM glucose in plasma at $t = 15 \text{ s}$ and then flushed with plasma at $t = 240 \text{ s}$. SER spectra were collected every 15 s ($\lambda_{\text{ex}} = 785 \text{ nm}$). Based upon amplitude calculation for 1462 cm^{-1} peak, the 1/e time constant was 9 s for partitioning and 27 s for departitioning.

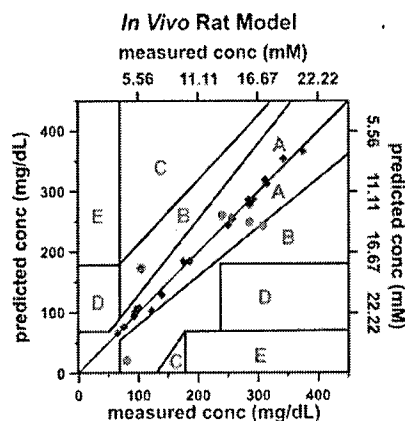


Figure 12. Calibration (\diamond) and validation (\bullet) plot using a single substrate and a single spot on a DTMH functionalized AgFON on a mesh. PLS calibration plot was constructed using 21 data points and validation plot was constructed using 5 data points taken over a range of glucose concentrations (10 - 450 mg/dL) in vivo (rat). RMSEC = 7.46 mg/dL (0.41 mM) and RMSEP = 53.42 mg/dL (2.97 mM). $\lambda_{\text{ex}} = 785 \text{ nm}$, $P = 50 \text{ mW}$, $t = 2 \text{ min}$.

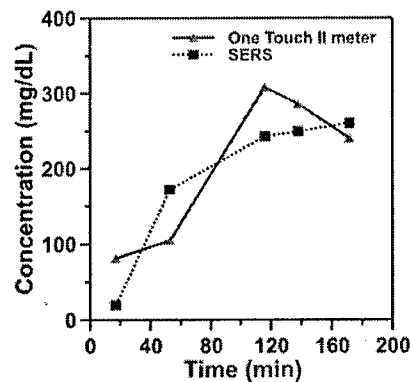


Figure 13. Real-time response of the in vivo blood glucose concentration. Triangles (\blacktriangle) are measurements made using One Touch II blood glucose meter and squares (\blacksquare) are measurements made using a SERS sensor ($\lambda_{\text{max}} = 785 \text{ nm}$, $P = 50 \text{ mW}$, $t = 2 \text{ min}$).

Lactate Sensing by SERS

We have verified (Figure 15) that the SERS spectrum of lactate can be collected from a SAM functionalized Ag surface and the SAM provides a reversible sensing platform. The SAM used for lactate partitioning/departitioning is a mixed monolayer of decanethiol and mercaptohexanol (DT/MH). The same SAM was also used for glucose sensing. It has dual hydrophobic/hydrophilic functionality to allow preconcentration of the analyte of interest in an aqueous environment. To show reversibility of the SAM, 0 and 100 mM aqueous lactate solutions were cycled through the flow cell with a DT/MH functionalized AgFON surface (figure inset). The difference spectra of lactate were then obtained by subtracting step 1 from step 2, and step 3 from step 4 (Figure 15 F, G). The Raman bands in the difference spectra correspond to the peaks in the normal Raman spectrum of aqueous lactate (figure E). This indicates that lactate partitions into the SAM and SER spectra of lactate can be obtained. The subtraction of steps 3 and 1, and 4 and 2, results in flat baseline spectra (figure H, I), which indicates that departitioning of lactate also occurs successfully.

Key Research Accomplishments

- Developed a system for fabrication of nanowells on the tip of an optical fiber. The resulting structure was to be verified using Atomic Force Microscopy (AFM).
- Achieved Surface functionalization of the particles embedded in nanowells on the tip of a fiber with a self-assembled monolayer (SAM).
- Optimized the structure of Ag nanoparticles embedded in nanowells to yield a narrow LSPR spectrum in the near-infrared for maximum enhancement with 785 nm or 830 nm laser excitation.
- Demonstrated that glucose may be measured in the presence of potentially interfering analytes using a SERS-based system. And that the $1/e$ time constant for response to a step change in glucose concentration is less than 1 minute.
- Demonstrated that glucose may be measured in bovine plasma using a SERS-based system. And that the $1/e$ time constant for response to a step change in glucose concentration is less than 1 minute.
- Demonstrated that glucose may be measured in rats using a SERS-based system.
- Demonstrated that lactate concentrations may be measured in vitro using a SERS-based system.

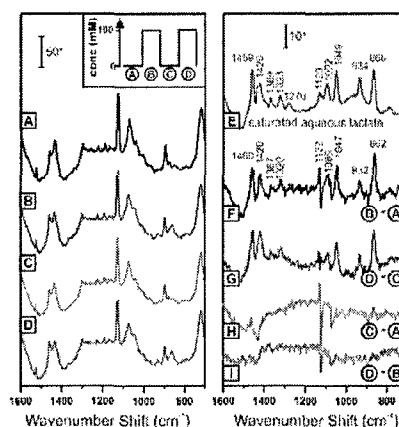


Figure 15. Lactate pulsing sequence on the SAM modified AgFON surface (inset). A, B, C, D: SER spectra of the sample cycled between 0 and 100 mM aqueous lactate solution, $\lambda_{\text{ex}} = 532$ nm, $P_{\text{laser}} = 20$ mW, $t = 20$ min, pH = 7.1. E is the normal Raman spectrum

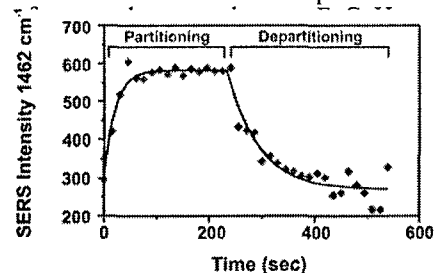


Figure 14. Real-time SERS response to a step change in glucose concentration after being implanted in a rat for 5 hours. Glucose was injected at $t = 15$ s and the cell was flushed with bovine plasma at $t = 240$ s. Partitioning and departitioning of glucose. $\lambda_{\text{ex}} = 785$ nm, laser power = 100 mW, data acquisition $t = 15$ s. The $1/e$ time constants were calculated to be 9 s for partitioning and 27 s for departitioning.

The accomplishments have or will be reported in various forms:

Conferences:

- Biomedical Engineering Society, October, 2004, Philadelphia, PA
- Third International Conference on Advanced Vibrational Spectroscopy, August, 2005, Delavan, WI
- Biomedical Engineering Society, October, 2005, Baltimore, MD
- Fifth Annual Diabetes Technology Meeting, November 2005, San Francisco, CA
- Pittsburgh Conference on Analytical Chemistry and Applied Spectroscopy, March 2006, Orlando, FL

Patent Disclosures:

- New partition layer for surface enhanced Raman nanobiosensor. M.R. Glucksberg, J.T. Walsh, C. Ranjit-Yonzon, N.C. Shah, O. Lyandres, July 26, 2005.

Manuscripts:

- Lyandres, O., N.C. Shah, C.R. Yonzon, J.T. Walsh Jr., M.R. Glucksberg, and R.P. Van Duyne. A Mixed Decanethiol/Mercaptohexanol Partition Layer Enables Real-Time Glucose Sensing by Surface-Enhanced Raman Spectroscopy in Bovine Plasma. *Anal. Chem.* (manuscript in review).

Reportable Outcomes

A new and promising method of detecting glucose, lactate, and other biological analytes has been shown to be feasible in *in vitro* and *in vivo* systems. The method takes advantage of the remarkable amplification in Raman signal afforded by the surface enhancement effect to measure concentrations of these analytes. In the first year of this project it was shown that reliable and repeatable measurements of interstitial glucose concentration in rats may be achieved. This work has contributed to five published papers included in the Appendix:

- Yonzon, C. R., Haynes, C. L., Zhang, X. Y., Walsh, J. T., Van Duyne, R. P. A Glucose Biosensor Based on Surface-Enhanced Raman Scattering: Improved Partition Layer, Temporal Stability, Reversibility, and Resistance to Serum Protein Interference. *Anal. Chem.* 76, 78-85, 2004.
- Stuart, D. A., Yonzon, C. R., Zhang, X., Lyandres, O., Shah, N., Glucksberg, M. R., Walsh, J. T., Van Duyne, R. P. Glucose Sensing Using Near-Infrared Surface-Enhanced Raman Spectroscopy: Gold Surfaces, 10-Day Stability, and Improved Accuracy. *Anal. Chem.* 77, 4013-4019, 2005.
- Zhang, X., Young, M. A., Lyandres, O., Van Duyne, R. P. Rapid Detection of an Anthrax Biomarker by Surface-Enhanced Raman Spectroscopy. *J. Am. Chem. Soc.*, 127, 4484, 2005.
- McFarland, A. D., Young, M. A., Dieringer, J. A., Van Duyne, R. P. Wavelength-tuned Surface-Enhanced Raman Excitation Spectroscopy. *J. Phys. Chem. B* 109, 11279-11285, 2005.
- Haes, A. J., Haynes, C. L., McFarland, A. D., Zou, S., Schatz, G. C., Van Duyne, R., P. Plasmonic Materials for Surface-Enhanced Sensing and Spectroscopy. *MRS Bulletin* 2005, 30, 368., 2005

Conclusions

This report summarizes achievements in year 1 of this project. We fabricated particles-in-nanowells on a glass substrate with a LSPR spectrum having an extinction band at 836 nm, which is optimized for 785-nm laser excitation. In addition, we developed several alternative designs to transition these particles-in-nanowells or AgFONs to the tip of a fiber. The AgFON was functionalized with a DT/MH mixed SAM, which allows for rapid partitioning and departitioning of glucose. The DT/MH functionalized AgFON SERS-active surface has *in vitro* accuracy and precision of detecting glucose in aqueous medium, aqueous medium with interfering analytes, and plasma such that over 90% of the measured data fall in A+B range of the Clarke error grid. The 1/e time constant for a response to step change in glucose concentration is less than a minute in both aqueous medium and plasma. Finally, we surgically implanted the SERS-active surface in a rat and quantitatively measured glucose concentrations *in vivo*. All the measured data fall in A+B range of the Clarke error grid. For a response to step change in glucose concentration, the 1/e time constant after being implanted in a rat for 5 hr is also less than a minute.

In summary, we have achieved or are well on the way to achieving the goals set forth in our original statement of work. The aims for the current year will be to complete the studies in rat, and to optimize the fiber optic probe.

References

- (1) Shafer-Peltier, K. E.; Haynes, C. L.; Glucksberg, M. R.; Van Duyne, R. P. *J. Am. Chem. Soc.* **2003**, *125*, 588.
- (2) Yonzon, C. R.; Haynes, C. L.; Zhang, X. Y.; Walsh, J. T.; Van Duyne, R. P. *Anal. Chem.* **2004**, *76*, 78.
- (3) Stuart, D. A.; Yonzon, C. R.; Zhang, X.; Lyandres, O.; Shah, N.; Glucksberg, M. R.; Walsh, J. T.; Van Duyne, R. P. *Anal. Chem.* **2005**, *accepted April 21*.
- (4) Haynes, C. L.; Van Duyne, R. P. *J. Phys. Chem. B* **2003**, *107*, 7426.
- (5) McFarland, A. D.; Young, M. A.; Dieringer, J. A.; Van Duyne, R. P. *J. Phys. Chem. B* **2005**, *accepted April 11*.
- (6) Haes, A. J.; Haynes, C. L.; McFarland, A. D.; Zou, S.; Schatz, G. C.; Van Duyne, R. P. *MRS Bulletin* **2005**, *30*, 368.
- (7) Zhang, X.; Young, M. A.; Lyandres, O.; Van Duyne, R. P. *J. Am. Chem. Soc.* **2005**, *127*, 4484.

APPENDIX

Patent disclosure

New Partition Layer for Surface Enhanced Raman Nanobiosensor. M.R. Glucksberg, J.T. Walsh, C. Ranjit-Yonzon, N.C. Shah, O. Lyandres, July 26, 2005

Reprints of the following publications follow

Yonzon, C. R., Haynes, C. L., Zhang, X. Y., Walsh, J. T., Van Duyne, R. P. A Glucose Biosensor Based on Surface-Enhanced Raman Scattering: Improved Partition Layer, Temporal Stability, Reversibility, and Resistance to Serum Protein Interference. *Anal. Chem.* 76, 78-85, 2004.

Stuart, D. A., Yonzon, C. R., Zhang, X., Lyandres, O., Shah, N., Glucksberg, M. R., Walsh, J. T., Van Duyne, R. P. Glucose Sensing Using Near-Infrared Surface-Enhanced Raman Spectroscopy: Gold Surfaces, 10-Day Stability, and Improved Accuracy. *Anal. Chem.* 77, 4013-4019, 2005.

Zhang, X., Young, M. A., Lyandres, O., Van Duyne, R. P. Rapid Detection of an Anthrax Biomarker by Surface-Enhanced Raman Spectroscopy. *J. Am. Chem. Soc.*, 127, 4484, 2005.

McFarland, A. D., Young, M. A., Dieringer, J. A., Van Duyne, R. P. Wavelength-tuned Surface-Enhanced Raman Excitation Spectroscopy. *J. Phys. Chem. B* 109, 11279-11285, 2005.

Haes, A. J., Haynes, C. L., McFarland, A. D., Zou, S., Schatz, G. C., Van Duyne, R., P. Plasmonic Materials for Surface-Enhanced Sensing and Spectroscopy. *MRS Bulletin* 2005, 30, 368., 2005

Lyandres, O., N.C. Shah, C.R. Yonzon, J.T. Walsh Jr., M.R. Glucksberg, and R.P. Van Duyne. A Mixed Decanethiol/Mercaptohexanol Partition Layer Enables Real-Time Glucose Sensing by Surface-Enhanced Raman Spectroscopy in Bovine Plasma. *Anal. Chem.* (manuscript in review).

Conference abstracts are also available upon request, but are not included in this appendix.

NU# _____
Date Received _____

NORTHWESTERN UNIVERSITY INVENTION DISCLOSURE

1. **Invention Title** New partition layer for surface enhanced Raman nanobiosensor

2. **Inventors**

<u>Name</u>	<u>Department</u>	<u>Position</u>
Richard P. Van Duyne H.	Chemistry	Charles E. and Emma Morrison Professor
Matthew R. Glucksberg	Biomedical Engineering	Professor
Joseph T. Walsh Jr.	Biomedical Engineering	Professor
Chanda Ranjit-Yonzon	Chemistry	Graduate student
Nilam C. Shah	Chemistry	Graduate student
Olga Lyandres	Biomedical Engineering	Graduate student

3. **Description of Invention:** please see the attached manuscript

- (a) Brief summary stating its novelty and utility
- (b) Background information, how it works, and improvements over existing technologies
- (c) Detailed description with photographs, drawings, graphs and relevant manuscripts
- (d) Expected commercial applications

4. **Date and place where discovery was made**

- (a) When was the idea conceived February, 2005
Where and how was it documented Lab notebook (CRY, NCS)
- (b) When was the idea reduced to practice March, 2005

5. **Sources of Support, Research Sponsor and Grant Numbers**

- (a) Northwestern University Funds,
Facilities _____
- (b) Federal Agency National Institutes of Health Grant No. DK066990-01A1
U. S. Army Medical Research and Materiel Command
Grant No. W81XWH-04-1-0630

SERS Measurement of GLucose and Lactate - MR Glucksberg, PI

National Science Foundation **Grant No. CHE0414554**

Air Force Office of Scientific Research MURI program

Grant No. F49620-02-1-0381

(c) **Foundation**

(d) **Corporate**

6. **Public Disclosure - Please state if any disclosure has been made or if any is planned in the next six (6) months. Give dates and places.**

- (a) **Journal article** Submission to *Analytical Chemistry*
- (b) **Oral Presentation**
- (c) **Poster Presentation** 2005 BMES Annual Fall Meeting, October, 2005, Baltimore, MD (BMES), Third International Conference on Advanced Vibrational Spectroscopy, August, 2005, Delavan, WI (ICAVS-3)
- (d) **Conference Abstract** BMES, ICAVS-3, Pittsburgh Conference on Analytical Chemistry and Applied Spectroscopy, March 2006, Orlando, FL (PITTCO)
- (e) **Disclosure to Industry**
- (f) **Grant Proposal**
- (g) **Other**

7. **Prior Art**

Have you done a literature search? YES X NO If yes, include references
What related work in this area by others do you know?

8. **Commercialization:**

- (a) **Are you aware of potential licensees for this invention?** YES X NO
If yes, give names of companies and contact persons known to you on a separate sheet

If no, what industry might have interest in this invention

- (b) **Would you like to develop this invention further with corporate research support** YES X NO
- (c) **Are you willing to participate in the marketing of this invention** YES X NO

9. **Materials Associated with Invention**

Did this invention use any Materials which were obtained with a Materials Transfer Agreement from a company or another institution YES (Please give details);
NO X

Did this invention use any materials (vectors, cell lines, animals, etc.) containing cDNA and/or lox DNA? YES (Please give details) NO X

Did this invention use information obtained from any Celera database?

YES _____ (Please give details) NO X

Did you transfer to any researcher outside Northwestern any new Materials (DNA, peptides, cell lines, vectors, catalysts, polymers, alloys, etc.) of this invention YES _____ NO

X

This disclosure is submitted pursuant to the Northwestern University Patent and Invention Policy and is subject to all the terms of that Policy. If this invention is accepted by Northwestern University's Technology Transfer Program, I/We hereby agree to execute all necessary documents, assigning to Northwestern our rights in any patent application filed on this invention.

Signature of Inventor(s)
Richard P. VanDuyne
Joseph T. Walsh Jr.
Matthew R. Glucksberg
William C. Miller
Chandana Venkatarayana

Date
July 26, 2005
July 26, 2005
July 26, 2005
July 26, 2005
July 26, 2005
July 26, 2005

Please place an asterisk next to the name of the Principal Investigator(s)

- A. Inventor: Name Richard P. VanDuyne*
Department Chemistry Department
Phone/Fax/e-mail 847-491-3516/ 847-491-7713/
vanduyne@chem.northwestern.edu
Home Address 1520 Washington Ave.,
Wilmette, IL 60091
Citizenship USA
- B. Inventor: Name Joseph T. Walsh Jr.
Department Department of Biomedical Engineering
Phone/Fax/e-mail 847-491-7118/847-491-
4928/jwalsh@northwestern.edu
Home Address 1310 Washington St., Evanston, IL 60202
Citizenship USA
- C. Inventor: Name Matthew R. Glucksberg
Department Department of Biomedical Engineering
Phone/Fax/e-mail 847-491-7121/847-491-4928/
m-glucksberg@northwestern.edu
Home Address 3450 N Lake Shore Dr, Chicago, IL 60657
Citizenship USA

- D. Inventor:** Name Chanda Ranjit-Yonzon
Department Chemistry Department
Phone/Fax/e-mail 847-491-2952/847-491-7713/c-
ranjit@northwestern.edu
Home Address 1915 Maple Ave. Engelhart Hall 0711,
Evanston, IL 60201
Citizenship Nepal
- E. Inventor:** Name Nilam C. Shah
Department Chemistry Department
Phone/Fax/e-mail 847-491-2952/847-491-7713/n-
shah5@northwestern.edu
Home Address 7649 N. Eastlake Terr. # 2A, Chicago, IL 60626
Citizenship USA
- F. Inventor:** Name Olga Lyandres
Department Department of Biomedical Engineering
Phone/Fax/e-mail 847-491-2952/847-491-4928/o-
lyandres@northwestern.edu
Home Address 532 W. Roscoe St. Apt. 365 Chicago, IL 60657
Citizenship USA

Please let us know your forwarding address before leaving Northwestern University:

Richard P. Van Duyne
Northwestern University Chemistry Department
2145 Sheridan Rd.
Evanston IL 60208-3113
Phone: 847-491-3516
Fax: 847-491-7713

Please submit completed disclosure to:

Attn: Allan E. Nader
Licensing Associate
Technology Transfer Program
Northwestern University
1880 Oak Avenue – Suite 100
Evanston, IL 60201
Phone: (847)491-4456
Fax: (847)491-3625

Question 8 (a) in the invention disclosure form

Company name: Abbott Laboratories

Contact person: Omar S. Khalil, Ph.D.
Senior Research Fellow
Abbott Laboratories
100 Abbott Park Road
Abbott Park, IL 60064
Phone: (847) 937- 4093
Fax: (847) 938-7072
Omar.khalil@abbott.com

A Glucose Biosensor Based on Surface-Enhanced Raman Scattering: Improved Partition Layer, Temporal Stability, Reversibility, and Resistance to Serum Protein Interference

Chanda Ranjit Yonzon,^{†,‡} Christy L. Haynes,^{†,‡} Xiaoyu Zhang,[†] Joseph T. Walsh, Jr.,[§] and Richard P. Van Duyne^{*,†}

Department of Chemistry and Department of Biomedical Engineering, Northwestern University, 2145 Sheridan Road, Evanston, Illinois 60208-3113

This work updates the recent progress made toward fabricating a real-time, quantitative, and biocompatible glucose sensor based on surface-enhanced Raman scattering (SERS). The sensor design relies on an alkane-thiolate tri(ethylene glycol) monolayer that acts as a partition layer, preconcentrating glucose near a SERS-active surface. Chemometric analysis of the captured SERS spectra demonstrates that glucose is quantitatively detected in the physiological concentration range (0–450 mg/dL, 0–25 mM). In fact, 94% of the predicted glucose concentrations fall within regions A and B of the Clarke error grid, making acceptable predictions in a clinically relevant range. The data presented herein also demonstrate that the glucose sensor provides stable SERS spectra for at least 3 days, making the SERS substrate a candidate for implantable sensing. Glucose sensor reversibility and reusability is evaluated as the sensor is alternately exposed to glucose and saline solutions; after each cycle, difference spectra reveal that the partitioning process is largely reversible. Finally, the SERS glucose sensor successfully partitions glucose even when challenged with bovine serum albumin, a serum protein mimic.

Improved glucose-sensing technology will yield a significant increase in the quality of life for the 17 million diabetics and 16 million prediabetics in the United States. Scientific advances will also considerably reduce the estimated \$132 billion in annual economic cost of diabetes.¹ Diabetes mellitus is a disease characterized by elevated blood glucose levels caused by the body's abnormal response to or production of insulin, a hormone responsible for glucose metabolism regulation. The long-term health outlook of diabetic patients improves with frequent glucose measurements and careful control of glucose levels.

Numerous studies have been performed in recent years toward developing in vivo, minimally invasive, biologically compatible, and quantitative real-time glucose sensors.^{2,3} Of these studies, electrochemical methods have been the most successful techniques, relying on the detection of hydrogen peroxide produced by the enzymatic oxidation of glucose.^{4,5} One of the disadvantages of this indirect detection method is that glucose oxidase, the enzyme that catalyzes the oxidation, needs to be replenished and, therefore, limits the lifetime of the sensor. Another serious problem inherent to enzymatic glucose sensors is the lack of stability due to the intrinsic nature of enzymes.⁶ To avoid the disadvantages of enzyme-based sensors, nonenzymatic detection of glucose has been recently developed using amperometric measurements on platinum electrodes.^{6–9} However, this method has insufficient selectivity over interfering species in a biocompatible potential range.^{6,9} Indirect detection of glucose is also done using fluorescence spectroscopy. The signal transduction mechanism in fluorescence sensors exploits the reversible glucose-binding characteristics of fluorophore-labeled concanavalin A (Con A); separation of the fluorophore from Con A yields a measurable signal.^{10,11} Though this is a very promising technique that features a physiologically relevant detection range, biomolecules similar to glucose can interfere in this multistep process, giving false positives. Diffraction spectroscopy, another indirect detection method, has been implemented by Asher and co-workers to detect glucose in aqueous humor.^{12,13} In this technique, the binding of glucose to boronic acid embedded in a polymerized crystalline

* To whom correspondence should be addressed: (e-mail) vanduyne@chem.northwestern.edu.

[†] Department of Chemistry.

[‡] These authors contributed equally to this work.

[§] Department of Biomedical Engineering.

(1) American Diabetes Association, [http://www.diabetes.org/main/application/commercewf?origin=*jsp&event=link\(B1\)](http://www.diabetes.org/main/application/commercewf?origin=*jsp&event=link(B1)), access date 07–22–2003.

(2) McNichols, R. J.; Cote, G. L. *J. Biomed. Opt.* **2000**, *5*, 5–16.

(3) Steffes, P. G. *Diabetes Technol. Ther.* **1999**, *1*, 129–133.

(4) Tamada, J. A.; Garg, S.; Jovanovic, L.; Pitzer, K. R.; Fermi, S.; Potts, R. O. *J. Am. Med. Assoc.* **1999**, *282*, 1839–1844.

(5) Kaufman, F. R.; Gibson, L. C.; Halvorson, M.; Carpenter, S.; Fisher, L. K.; Pitukcheewanont, P. *Diabetes Care* **2001**, *24*, 2030–2034.

(6) Park, S. C.; T. C.; Kim, H. C. *Anal. Chem.* **2003**, *75*, 3046–3049.

(7) Vassilyev, Y. B.; Khazova, O. A.; Nikolaeva, N. N. *J. Electroanal. Chem.* **1985**, *196*, 105–125.

(8) Beden, B.; Largeaud, F.; Kokoh, K. B.; Lamy, C. *Electrochim. Acta* **1996**, *41*, 701–709.

(9) Sun, Y. P.; Buck, H.; Mallouk, T. E. *Anal. Chem.* **2001**, *73*, 1599–1604.

(10) Russell, R. J.; Pishko, M. V.; Gefrides, C. C.; McShane, M. J.; Cote, G. L. *Anal. Chem.* **1999**, *71*, 3126–3132.

(11) Ballerstadt, R.; Schultz, J. S. *Anal. Chem.* **2000**, *72*, 4185–4192.

(12) Asher, S. A. A.; V. L.; Goponenko, A. V.; Sharma, A. C.; Lednev, I. K.; Wilcox, C. S.; Finegold, D. N. *J. Am. Chem. Soc.* **2003**, *125*, 3332–3329.

colloidal array (PCCA) induces a change in osmotic pressure, swelling the PCCA and red-shifting the diffraction peak. However, glucose binds with boronic acid most efficiently when the pH is higher than 8.5, a nonphysiological condition.

The direct glucose detection methods developed so far include laser polarimetry¹⁴ and vibrational spectroscopies.^{15–19} The laser polarimetry detection method is based on the rotation of polarized light caused by glucose in aqueous humor. Unfortunately, other chiral constituents in this biological environment, such as ascorbate and albumin, interfere during measurements.¹⁴ Further, the rotation caused by corneal birefringence, and eye movement-induced variation in this rotation, can greatly complicate the quantification of the glucose concentration in vivo.² Vibrational spectroscopic methods applied to date for glucose sensing include near-infrared absorption, normal Raman scattering (NRS), and surface-enhanced Raman scattering (SERS) spectroscopies. Both NRS and SERS yield unique vibrational signatures for small-molecule analytes, as well as quantitative information. The implementation of near- and mid-infrared spectroscopic methods has a fundamental limitation due to the competing absorption by water and spectral congestion. However, the application of multivariate calibration models presents a possible remedy.¹⁷ Raman spectroscopy, in all its forms, is a vibrational spectroscopic method that has the inherent ability to distinguish between molecules with great structural similarity, molecules such as glucose and fructose.²⁰ Moreover, normal Raman spectroscopy has been shown to be able to detect physiological concentrations of glucose in vitro from a simulated aqueous humor solution.¹⁸ However, high laser powers and long acquisition times are required due to the inherently small NRS cross section of glucose, $5.6 \times 10^{-30} \text{ cm}^2 \text{ molecule}^{-1} \text{ sr}^{-1}$.²¹ Higher intensity Raman signals and lower detection limits can be achieved using SERS. SERS produces very large enhancements in the effective Raman cross section of species spatially confined within range of the electromagnetic fields (viz. 0–4 nm)²² generated upon excitation of the localized surface plasmon resonance of nanostructured noble metal surfaces. The Raman signals of ensemble-averaged molecules show enhancement of up to 8 orders of magnitude,²³ while the signals from single molecules can show an increase by 14 or 15 orders of magnitude in special cases.^{24,25} In comparison with infrared and NRS spectroscopies, SERS enjoys both the advantage

of SERS measurement of glucose and lactate by MR. Glucksberg, R. Raman scattering cross section of water²¹ and the sensitivity for trace level detection.²⁶

In our previous work,¹⁹ the first systematic study of the direct detection of glucose was performed using SERS. Glucose was partitioned into a decanethiol monolayer adsorbed on a silver film over nanosphere (AgFON) surface and thereby preconcentrated within the zone of electromagnetic field enhancement. A chemometric method, specifically, leave-one-out partial least-squares (LOO-PLS) analysis, was used to demonstrate quantitative glucose detection in both large (0–4,500 mg/dL, 0–250 mM) and clinically relevant (0–450 mg/dL, 0–25 mM) concentration ranges. Chemometric methods, such as LOO-PLS, are exploited for analyte quantification when the spectrum of interest is embedded within a complex background spectrum.

The current work demonstrates effective glucose quantification with improved alkanethiolate selectivity for glucose over a blood serum protein mimic in aqueous humor by using (1-mercaptopundeca-11-yl)tri(ethylene glycol) (EG3) as the partition layer. In fact, the data presented herein demonstrate that the EG3-modified AgFON substrate provides stable SERS spectra for at least 3 days, making the SERS substrate a candidate for implantable sensing. The reusability of the SERS sensor is evident during experiments where the EG3-modified AgFON is alternately exposed to glucose and saline solutions. EG3 is known to form a 2-nm-thick monolayer on noble metal surfaces²⁷ and provides a resistance to adsorption of proteins and enzymes.^{28–30} The ability of ethylene glycol-terminated polymers to reject nonspecific binding by background proteins^{29–34} and its biocompatibility^{35–37} have been at the center of interest in several studies. While the fundamental mechanism of such repulsion is still being debated, these highly valued properties are exploited here to fabricate an improved SERS glucose sensor. The experiments presented herein demonstrate that an EG3 partition layer has the capability of capturing glucose near the surface, while showing resistance to serum albumin, the most abundant protein in plasma.³⁸

In our earlier publication introducing the possibility of a SERS-based glucose sensor,¹⁹ we identified seven milestones to be achieved on the path to a fully functional, continuous, minimally invasive, quantitative, real-time, in vivo glucose sensor for application in biological media including aqueous humor, interstitial fluid, and blood. The first milestone, demonstration that quantitative

- (13) Alexeev, V. L.; Sharma, A. C.; Goponenko, A. V.; Das, S.; Lednev, I. K.; Wilcox, C. S.; Finegold, D. N.; Asher, S. A. *Anal. Chem.* **2003**, *75*, 2316–2323.
- (14) Cameron, B. D.; Gorde, H. W.; Satheesan, B.; Cote, G. L. *Diabetes Technol. Ther.* **1999**, *1*, 125–143.
- (15) Klonoff, D. C.; Braig, J.; Sterling, B.; Kramer, C.; Goldberger, D.; Trebino, R. *IEEE LEOS News.* **1998**, *12*, 13–14.
- (16) Berger, A. J.; Koo, T. W.; Itzkan, I.; Horowitz, G.; Feld, M. S. *Appl. Opt.* **1999**, *38*, 2916–2926.
- (17) Zhang, L.; Small, G. W.; Arnold, M. A. *Anal. Chem.* **2002**, *74*, 4097–4108.
- (18) Lambert, J.; Storrie-Lombardi, M.; Borchert, M. *IEEE LEOS News.* **1998**, *12*, 19–22.
- (19) Shafer-Peltier, K. E.; Haynes, C. L.; Glucksberg, M. R.; Van Duyne, R. P. *J. Am. Chem. Soc.* **2003**, *125*, 588–593.
- (20) Soderholm, S.; Roos, Y. H.; Meinander, N.; Hotokka, M. *J. Raman Spectrosc.* **1999**, *30*, 1009–1018.
- (21) McCreery, R. L. *Raman Spectroscopy for Chemical Analysis*; John Wiley & Sons: New York, 2000.
- (22) Schatz, G. C.; Van Duyne, R. P. In *Handbook of Vibrational Spectroscopy*; Chalmers, J. M., Griffiths, P. R., Eds.; Wiley: New York, 2002; Vol. 1, pp 759–774.
- (23) Haynes, C. L.; Van Duyne, R. P. *J. Phys. Chem. B* **2003**, *107*, 7426–7433.
- (24) Nie, S.; Emory, S. R. *Science* **1997**, *275*, 1102–1106.

- (25) Kneipp, K.; Wang, Y.; Kneipp, H.; Perelman, L. T.; Itzkan, I.; Dasari, R. R.; Feld, M. S. *Phys. Rev. Lett.* **1997**, *78*, 1667–1670.
- (26) Sylvia, J. M.; Janni, J. A.; Klein, J. D.; Spencer, K. M. *Anal. Chem.* **2000**, *72*, 5834–5840.
- (27) Palegrosdemange, C.; Simon, E. S.; Prime, K. L.; Whitesides, G. M. *J. Am. Chem. Soc.* **1991**, *113*, 12–20.
- (28) Prime, K. L.; Whitesides, G. M. *Science* **1991**, *252*, 1164–1167.
- (29) Ostuni, E.; Chapman, R. G.; Liang, M. N.; Meluleni, C.; Pier, G.; Ingber, D. E.; Whitesides, G. M. *Langmuir* **2001**, *17*, 6336–6343.
- (30) Lahiri, J.; Isaacs, L.; Tien, J.; Whitesides, G. M. *Anal. Chem.* **1999**, *71*, 777–790.
- (31) Clark, S. L.; Hammond, P. T. *Adv. Mater.* **1998**, *10*, 1515–1519.
- (32) Prime, K. L.; Whitesides, G. M. *J. Am. Chem. Soc.* **1993**, *115*, 10714–10721.
- (33) Zolk, M.; Eisert, F.; Pipper, J.; Herrwerth, S.; Eck, W.; Buck, M.; Grunze, M. *Langmuir* **2000**, *16*, 5849–5852.
- (34) Dicke, C.; Hahner, G. *J. Am. Chem. Soc.* **2002**, *124*, 12619–12625.
- (35) Mauzac, M. A.; N.; Jozefonvicz, J. *Biomaterials* **1982**, *3*, 221–224.
- (36) Lee, J. H.; Kopecek, J.; Andrade, J. D. *J. Biomed. Mater. Res.* **1989**, *23*, 351–368.
- (37) Cohn, D. Y.; H. J. *Biomed. Mater. Res.* **1988**, *22*, 993–1009.
- (38) Baker, M. E. *FEBS Lett* **1998**, *439*, 9–12.

sensing of glucose using SERS could be done under these circumstances was accomplished therein. The work presented here demonstrates a set of four significant advances toward achieving these milestones: (1) replacement of the 1-decanthiol partition layer with an EG3 monolayer, (2) detection of glucose in the presence of serum albumin, (3) 3-day temporal stability of the EG3-modified AgFON surface, and (4) demonstration of the reversible nature of glucose partitioning. The remaining milestones yet to be achieved include the following: (1) glucose sensing in the presence of other small-molecule analytes, (2) fabrication of a AgFON substrate on the tip of a fiber-optic probe and in vivo testing of the SERS-active probe, (3) miniaturization of the implanted SERS-active surface, and (4) miniaturization of the SERS instrument. After achieving these milestones, one can envision the application of the SERS sensor as a biomedical glucose-sensing technology. Specifically, this miniaturized SERS substrate (microscale or nanoscale) will be implanted subcutaneously or incorporated as a component of a prosthetic lens in the eye, achieving glucose detection with external excitation and collection apparatus.

EXPERIMENTAL SECTION

Materials. All the chemicals were of reagent grade or better and used as purchased. Ag wire (99.99%, 0.04-in. diameter) was purchased from D. F. Goldsmith (Evanston, IL). Oxygen-free high-conductivity copper was obtained from McMaster-Carr (Chicago, IL) and cut into 18-mm-diameter disks. $\text{CH}_3\text{CH}_2\text{OH}$, H_2O_2 , and NH_4OH were purchased from Fisher Scientific (Fairlawn, VA). Surfactant-free, white carboxyl-substituted latex polystyrene nanosphere suspensions (390 ± 19.5 nm diameter, 4% solid) were acquired from Duke Scientific Corp. (Palo Alto, CA). Tungsten vapor deposition boats were purchased from R. D. Mathis (Long Beach, CA). For substrate and solution preparations, ultrapure water ($18.2 \text{ M}\Omega \text{ cm}^{-1}$) from a Millipore academic system (Marlborough, MA) was used. Bovine serum albumin (BSA), saline, and tris buffer (pH = 7.4) were obtained from Sigma (St. Louis, MO). The disposable filters with $0.45\text{-}\mu\text{m}$ pore size were acquired from Gelman Sciences (Ann Arbor, MI). (1-Mercaptoundeca-11-yl)tri(ethylene glycol) ($\text{HS}(\text{CH}_2)_{11}(\text{OCH}_2\text{CH}_2)_3\text{OH}$, EG3) was synthesized²⁷ and donated by the Mrksich group at the University of Chicago.³⁹

AgFON Fabrication and Incubation Procedure. AgFON substrates were used because of their stable SERS activity in electrochemical,^{40,41} ultrahigh vacuum,⁴² and ambient experiments.¹⁹ In this work, AgFONs were fabricated on copper substrates. The copper substrates were cleaned by sonicating in 10:1:1 $\text{H}_2\text{O}/30\% \text{H}_2\text{O}_2/\text{NH}_4\text{OH}$. Approximately $12 \mu\text{L}$ of nanosphere solution was drop-coated onto a clean copper substrate and allowed to dry at room temperature. Then, 200-nm-thick Ag films were deposited onto and through the nanosphere mask using a modified Consolidated Vacuum Corp. vapor deposition system (base pressure 10^{-7} Torr).⁴³ The mass thickness and deposition

Measurement of Glucose and Lactate by MR Glucksberg, IP Rybold Inficon XTM/2 quartz-crystal microbalance (East Syracuse, NY). AgFON substrates were first incubated in 1 mM EG3 in ethanol for more than 12 h. Then, the EG3-modified substrates were mounted into a small-volume flow cell and exposed to glucose solutions for 10 min to ensure complete partitioning of the glucose into the EG3 monolayer.

Surface-Enhanced Raman Scattering Spectroscopy. A Spectra-Physics model 120 HeNe laser was used to produce the 632.8-nm excitation wavelength (λ_{ex}); the laser spot size was less than 2 mm in diameter. The SERS measurement system includes an interference filter (Edmund Scientific, Barrington, NJ), a holographic notch filter (Kaiser Optical Systems, Ann Arbor, MI), a model VM-505 single-grating monochromator with the entrance slit set at $100 \mu\text{m}$ (Acton Research Corp., Acton, MA), and a LN₂-cooled CCD detector (Roper Scientific, Trenton, NJ). A collection lens with magnification 5 was used to collect the scattered light. The small-volume flow cell⁴⁴ was used to control the external environment of AgFON surfaces throughout the SERS experiment.

Chemometrics Method. All data processing was performed using MATLAB (MathWorks, Inc., Natick, MA) and PLS_Toolbox (Eigenvector Research, Inc., Manson, WA). Prior to analysis, cosmic rays were removed from the spectra using a derivative filter. The slowly varying background, commonly seen in SERS experiments, was removed mathematically by subtracting a fourth-order polynomial. This method minimally affected the SERS peaks while greatly reducing the background level. The SERS spectral intensities were normalized using the 1107-cm^{-1} peak from the EG3 partition layer spectrum. From each spectrum, the absolute peak intensity of the 1107-cm^{-1} peak was obtained by subtracting the peak from the background (at 1174 cm^{-1}). An average peak intensity was determined for each experiment. To obtain the normalization factor for each sample spectrum, the average peak intensity was divided by the absolute peak intensity measured in each spectrum. Each spectrum was normalized by multiplying the spectrum by the normalizing factor before chemometric analysis. Then, data analysis was performed using partial least-squares leave-one-out analysis.

UV-Visible Spectroscopy. Measurements were carried out in a model 5000 Cary UV-Vis-NIR spectrometer (Varian Inc., Palo Alto, CA) using deuterium lamps.

RESULTS AND DISCUSSION

Significant progress has been made toward achieving a real-time, minimally invasive, biocompatible SERS glucose sensor. In previous work by Van Duyne and co-workers,¹⁹ decanethiol was used as a partition layer for glucose, but the required sensor characteristics of temporal stability, reversibility, and biocompatibility were not studied in detail. Herein, EG3 was chosen as a partition layer because of its biocompatibility and hydrophilic properties, progressing toward the long-term goal of fabricating an implantable glucose sensor. The EG3-modified AgFON substrate was exposed to various concentrations of glucose under physiological conditions, promoting preconcentration of glucose near the AgFON surface (Figure 1). After data analysis using LOO-

(39) Hodneland, C. D.; Lee, Y. S.; Min, D. H.; Mrksich, M. *Proc. Natl. Acad. Sci. U.S.A.* **2002**, *99*, 5048–5052.

(40) Dick, L. A.; McFarland, A. D.; Haynes, C. L.; Van Duyne, R. P. *J. Phys. Chem. B* **2002**, *106*, 853–860.

(41) Dick, L. A.; Haes, A. J.; Van Duyne, R. P. *J. Phys. Chem. B* **2000**, *104*, 11752–11762.

(42) Litorja, M.; Haynes, C. L.; Haes, A. J.; Jensen, T. R.; Van Duyne, R. P. *J. Phys. Chem. B* **2001**, *105*, 6907–6915.

(43) Hulteen, J. C.; Van Duyne, R. P. *J. Vac. Sci. Technol. A* **1995**, *13*, 1553–1558.

(44) Malinsky, M. D.; Kelly, K. L.; Schatz, G. C.; Van Duyne, R. P. *J. Am. Chem. Soc.* **2001**, *123*, 1471–1482.

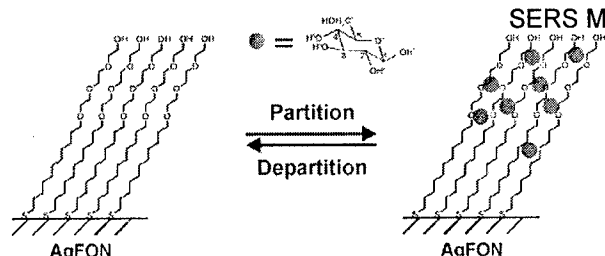


Figure 1. Schematic showing hypothetical glucose concentration gradient created by a (1-mercaptoundeca-11-yl)tri(ethylene glycol) (EG3) partition layer.

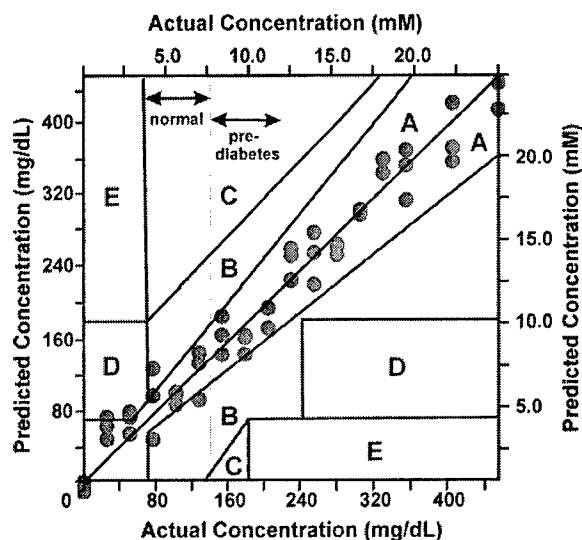


Figure 2. Clarke error grid of LOO-PLS predicted glucose concentration versus actual glucose concentration (5 loading vectors). AgFON samples were made ($D = 390$ nm, $d_m = 200$ nm), incubated for ~ 16 h in 1 mM EG3 solution, and dosed in glucose solution (range: 0–450 mg/dL, 0–25 mM) for 10 min. Each SERS measurement was made in the flow cell under saline with pH = 7.4, using $\lambda_{ex} = 632.8$ nm, $P_{laser} = 2.5$ mW, and $t = 30$ s.

PLS, the results are presented in a Clarke error grid (Figure 2). Clarke and co-workers established the Clarke error grid as the metric for evaluating glucose sensor efficacy in the clinical concentration range.⁴⁵ The Clarke error grid is divided into five major zones: zone A predictions lead to clinically correct treatment decisions; zone B predictions lead to benign errors or no treatment; zone C predictions lead to overcorrecting acceptable blood glucose concentrations; zone D predictions lead to dangerous failure to detect and treat; and zone E predictions lead to further aggravating abnormal glucose levels.

Quantitative Study of Glucose Using EG3 Partition Layer.

A viable glucose biosensor must be capable of detecting 0–450 mg/dL (0–25 mM) glucose under physiological conditions. Toward this goal, each EG3-modified AgFON sample was incubated for 10 min in a pH = 7.4 saline solution containing glucose concentrations from 0 to 450 mg/dL (0–25 mM). The samples were placed in an environmental control flow cell under saline, and SERS spectra were then measured ($\lambda_{ex} = 632.8$ nm, $P_{laser} = 2.5$ mW, $t = 30$ s). After spectral normalization using EG3 peak intensities, the SERS spectra were analyzed with the LOO-PLS

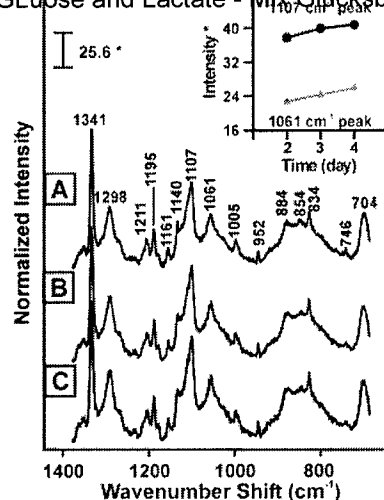


Figure 3. SERS spectra demonstrating the stability of an EG3-modified AgFON surface for at least 3 days. (A) After ~ 24 h of incubation in saline with pH = 7.4, $\lambda_{ex} = 632.8$ nm, $P_{laser} = 1.3$ mW, and $t = 60$ s. (B) After ~ 48 h of incubation in saline with pH = 7.4, $\lambda_{ex} = 632.8$ nm, $P_{laser} = 1.3$ mW, and $t = 60$ s. (C) After ~ 72 h of incubation in saline with pH = 7.4, $\lambda_{ex} = 632.8$ nm, $P_{laser} = 1.2$ mW, and $t = 60$ s. Inset shows the intensity variation for 1107- and 1061- cm^{-1} peaks with time. * denotes $\text{adu mW}^{-1} \text{s}^{-1}$.

method. In the data presented in Figure 2, five loading vectors were found to minimize the root-mean-squared error of cross-validation (RMSECV). The resulting cross-validated glucose concentration predictions are presented in the Clarke error grid (Figure 2).

The EG3-modified AgFON sensor quantitatively detects glucose in the physiological range with a corresponding RMSECV of 82 mg/dL (4.5 mM). In Figure 2, 94% of the predictions fall in zones A and B, while a few data points overlap in zone D within the hypoglycemic area (< 70 mg/dL, < 3.9 mM). The cross-validation error of 82 mg/dL (4.5 mM) can be partially attributed to variation of the SERS enhancement factor on different AgFON samples. The nanostructure on a AgFON substrate varies from point to point, affecting the localized surface plasmon resonance and, accordingly, the SERS enhancement factor.²³ In an effort to reduce the cross-validation error, the data later presented in Figure 7 used a single AgFON sample with a single point of detection. In addition to demonstrating quantitative glucose detection in a clinically relevant concentration range, other characteristics of the EG3-modified AgFON glucose sensor, such as durability, reusability, and selectivity, also need to be evaluated.

Temporal Stability of the EG3-Modified Substrate. Implantable glucose sensors must be stable for at least a 3-day period.⁵ Previous work has demonstrated that bare AgFON surfaces display extremely stable SERS activity when challenged with high potentials⁴⁰ and high temperatures in ultrahigh vacuum.⁴² Here, the stability of the EG3-modified AgFON SERS substrate is studied over a period of 3 days in saline with pH = 7.4 at room temperature. SERS spectra were captured every 24 h from the same sample location ($\lambda_{ex} = 632.8$ nm, $t = 60$ s) (Figure 3). The EG3 spectral band positions do not vary significantly over the course of 72 h. However, peaks at 1107 and 1061 cm^{-1} increase in intensity by 7.5 and 13% over 48 h, respectively (inset in Figure 3). The molecular order of self-assembled monolayers (SAMs)

(45) Clarke, W. L.; Cox, D.; Gonder-Frederick, L. A.; Carter, W.; Pohl, S. L. *Diabetes Care* **1987**, *10*, 622–628.

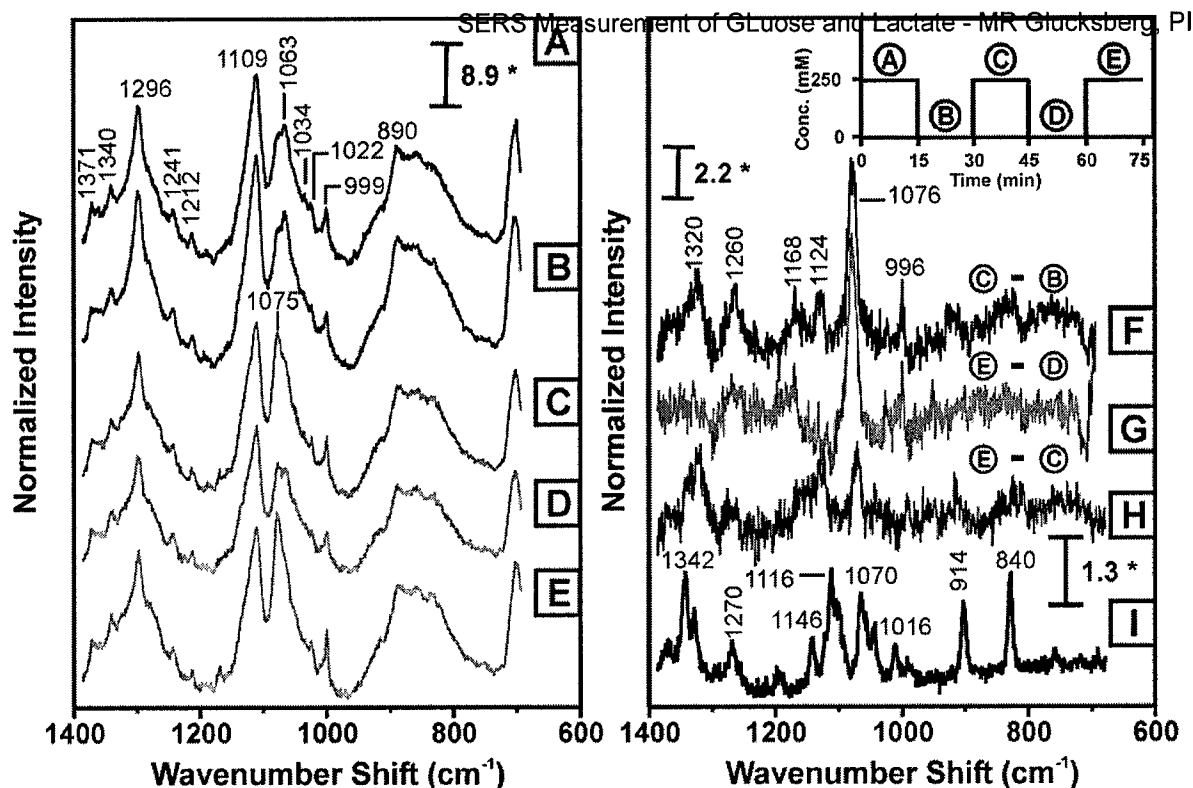


Figure 4. SERS spectra demonstrating the partition/departition capability of the EG3-modified AgFON substrate. The left panel displays SERS spectra of the sample cycled between 250 and 0 mM glucose solutions using $\lambda_{\text{ex}} = 632.8$ nm, $P_{\text{laser}} = 1.5$ mW, and $t = 30 \times 20$ s. (F) and (G) Difference spectra illustrating the glucose partitioning obtained by subtracting (B) from (A) and (D) from (E), respectively. (H) Difference spectra illustrating the glucose departitioning obtained by subtracting (C) from (E). Inset shows the schematic of the partition/departition concentration pulse experiment. (I) NRS of crystalline glucose for comparison, $\lambda_{\text{ex}} = 632.8$ nm, $P_{\text{laser}} = 5$ mW, and $t = 30$ s. * denotes $\text{adu mW}^{-1} \text{s}^{-1}$.

increases with incubation time;⁴⁶ the rearrangement of the SAM gives rise to peaks with increasing intensity. The SERS peaks at 1341 and 834 cm^{-1} have been identified as a signature of highly ordered SAMs^{47,48} and are the subject of further investigation.

Reversible Glucose Sensing. While the quantitative detection of glucose using the EG3-modified AgFON sensor and the stability of the sensor has been demonstrated, an implantable sensor must also be reusable. To examine the partition/departition capability of the EG3-modified AgFON sensor, it was exposed to cycles of 250 and 0 mM glucose solutions without flushing the sensor with saline between measurements (Figure 4 inset). SERS spectra were captured after each concentration variation ($\lambda_{\text{ex}} = 632.8$ nm, $P_{\text{laser}} = 1.5$ mW, $t = 30 \times 20$ s) (Figure 4, left panel). Traces F and G of Figure 4 are the difference spectra representing glucose partitioned into the EG3 SAM. Figure 4I is the Raman spectrum of crystalline glucose for comparison. Vibrational modes at 1342 (C–C–H bend), 1270, 1164, 1116 (C–C + C–O stretch), 1070 (C1–OH stretch), 914 (O–C1–H1 bend), and 840 cm^{-1} (C–C stretch) are known to be signatures of crystalline glucose.²⁰ The literature has shown that SERS spectral bands shift up to 25 cm^{-1} when compared to the NRS bands of the same analyte.⁴⁹ Peaks

in the SERS difference spectrum (Figure 4F) at 1320, 1260, 1168, 1124, and 1076 cm^{-1} correspond with the Raman spectrum of crystalline glucose. To evaluate the glucose departitioning, spectral subtraction of two glucose-containing cycles was performed (Figure 4H). Figure 4H shows spectral features that match with the glucose peaks at 1320 and 1076 cm^{-1} , but with lower intensities. Based on the 1076- cm^{-1} peak area, up to 33% of the glucose may remain in the EG3 layer after the 0 mM glucose cycle. The high glucose concentration used in this experiment caused incomplete departitioning after each cycle, and accordingly, the glucose accumulated in each step. However, physiological concentrations (0–450 mg/dL, 0–25 mM) of glucose will not likely cause such accumulation in the partition layer, and the natural flow of aqueous humor⁵⁰ or interstitial fluid will assist glucose departitioning.

Selectivity of the Sensor for Glucose in the Presence of Blood Serum Protein Mimic. Quantitative detection, temporal stability, and reusability are important characteristics of a viable biosensor; however, the glucose sensor must be effective in the presence of interfering proteins. Serum albumin is a blood serum protein mimic for challenging the glucose sensor. Prior to use, BSA solutions were filtered using track-etch membranes with 0.45- μm -diameter pores to remove any undissolved particulate, and UV absorption spectra were taken to determine the BSA concentration. BSA solutions of 0.00, 0.63, 1.25, and 2.50 mg/mL were made

(46) Biebuyck, H. A.; Bain, C. D.; Whitesides, G. M. *Langmuir* **1994**, *10*, 1825–1831.

(47) Clark, B. K.; Gregory, B. W.; Avila, A. J. *Phys. Chem. B* **1999**, *103*, 8201–8204.

(48) Gregory, B. W.; Clark, B. K.; Standard, J. M.; Avila, A. J. *Phys. Chem. B* **2001**, *105*, 4684–4689.

(49) Stacy, A. M.; Van Duyne, R. P. *Chem. Phys. Lett.* **1983**, *102*, 365–370.

(50) Vanlandingham, B. D.; Brubaker, R. F. *Am. J. Ophthalmol.* **1998**, *126*, 191–196.

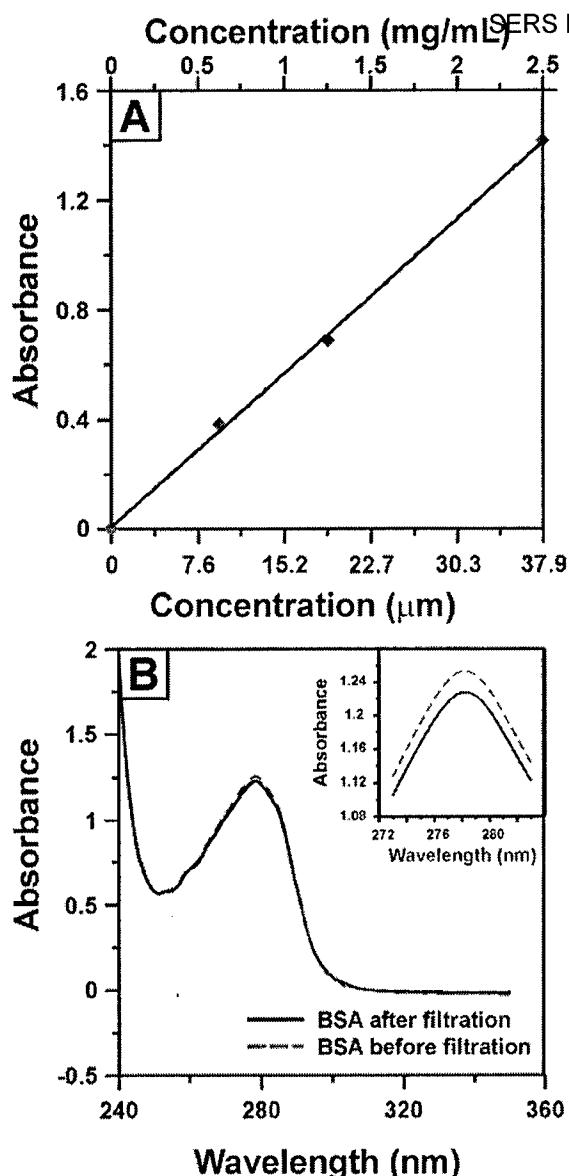


Figure 5. BSA concentration determination using UV absorption. (A) Calibration using 0.00, 0.63, 1.25, and 2.50 mg/mL BSA in saline, pH = 7.4. (B) UV absorption of 33.2 μ M (2.19 mg/mL) BSA before and after filtration using track-etch membranes with 0.45- μ m-diameter pores. The inset magnifies the absorption difference between the filtered BSA and nonfiltered BSA.

to create a Beer–Lambert calibration curve with R^2 of 0.9990 (Figure 5A). The molar extinction coefficient at 277 nm, ϵ_{277} of BSA was calculated to be $3.7 \times 10^4 \text{ M}^{-1} \text{ cm}^{-1}$. This correlates with literature values ranging from 4.36×10^4 to 2.77×10^4 at wavelengths 279–288 nm.⁵¹ Figure 5B shows the UV absorption spectra of 33.2 μ M (2.19 mg/mL) BSA before and after filtration. The calculated BSA concentration after filtration was 32.6 μ M (2.15 mg/mL), indicating a loss of 1.8% during filtration through 0.45- μ m-diameter pores. The inset in Figure 5B magnifies the absorption difference between the BSA before and after filtration.

Figure 6A shows the SERS spectrum of the EG3-modified AgFON substrate in saline ($\lambda_{\text{ex}} = 632.8 \text{ nm}$, $P_{\text{laser}} = 0.8 \text{ mW}$, $t =$

the flow cell, the SERS spectrum was collected throughout the 240-s incubation (Figure 6B). Finally, the sample was exposed to 100 mM glucose, and the SERS spectrum was collected (Figure 6C). Figure 6D is the difference spectrum demonstrating that serum albumin does not have a measurable SERS spectrum. The lack of SERS serum albumin bands could be due either to the small Raman scattering cross section of serum albumin or to the inefficient adsorption of serum albumin to the EG3 partition layer. Figure 6E demonstrates that the SERS glucose sensor is still effective after substrate exposure to an interfering protein. The peaks at 1449, 1433, 1339, 1291, 1108, 1077, 1059, and 855 cm^{-1} (Figure 6E) correspond with the crystalline glucose peaks shown in Figure 6F. Note that the glucose difference spectrum in Figure 6E has an altered appearance when compared to the glucose difference spectra shown in Figure 4F and G. This is the case because difference spectra highlight the glucose features versus the background spectral features. Varied background solution components yield varied glucose difference spectra. As long as the spectral locations of the peaks are comparable to the bulk glucose spectrum, it is fair to conclude that glucose is present. This experiment shows that glucose partitioning into EG3 is not affected by the presence of large molecules such as serum albumin. The peak at 695 cm^{-1} (Figure 6A) shifts to 710 cm^{-1} (Figure 6C) in the presence of glucose. This shift may be due to the rearrangement of the SAM when the glucose molecules partition into EG3. The observed shift further supports the hypothesis of glucose penetrating deeply into the EG3 monolayer, affecting even the character of the C–S bond.

Further studies of the effects of interfering protein were performed using glucose solutions (25–450 mg/dL, 1.4–25 mM) made in pH = 7.4 tris buffer containing 2 mg/mL serum albumin (filtered before addition). The EG3-modified AgFON was placed in a flow cell with the glucose solution, and SERS spectra were then measured ($\lambda_{\text{ex}} = 632.8 \text{ nm}$, $P_{\text{laser}} = 3 \text{ mW}$, $t = 60 \text{ s}$). After spectral capture, the glucose solution was flushed from the flow cell, and the next glucose solution was injected. The next spectrum was captured from the same spatial location on the AgFON after 10-min incubation. The AgFON sensor was not flushed with saline between incremental glucose measurements in order to mimic the characteristics of in vivo measurements. After spectral normalization using EG3 peak intensities, the SERS spectra were analyzed with the LOO-PLS method. In the data presented in Figure 7, four loading vectors were found to minimize the RMSECV. The resulting cross-validated glucose concentrations are presented in the Clarke error grid format (Figure 7).

This work demonstrates that the EG3-modified AgFON sensor can be used to quantitatively detect glucose in the presence of serum albumin in the physiological range with a RMSECV of 54 mg/dL (3 mM). In Figure 7, nearly all the predictions lie in zones A and B, with the exception of one data point, which lies in zone D within the hypoglycemic region of the Clarke error grid (<70 mg/dL, <3.9 mM). When comparing the RMSECV calculated in Figure 7 to that calculated in Figure 1, great improvement is apparent when a single sample and a single detection point are used. The RMSECV in Figure 7 may be further improved by eliminating excitation laser power fluctuation and solution turbulence present in the cell. In addition, the longevity of the EG3-

(51) Fasman, G. D. *Handbook of Biochemistry and Molecular Biology*, 3rd ed.; CRC Press Inc.: Cleveland, OH, 1976.

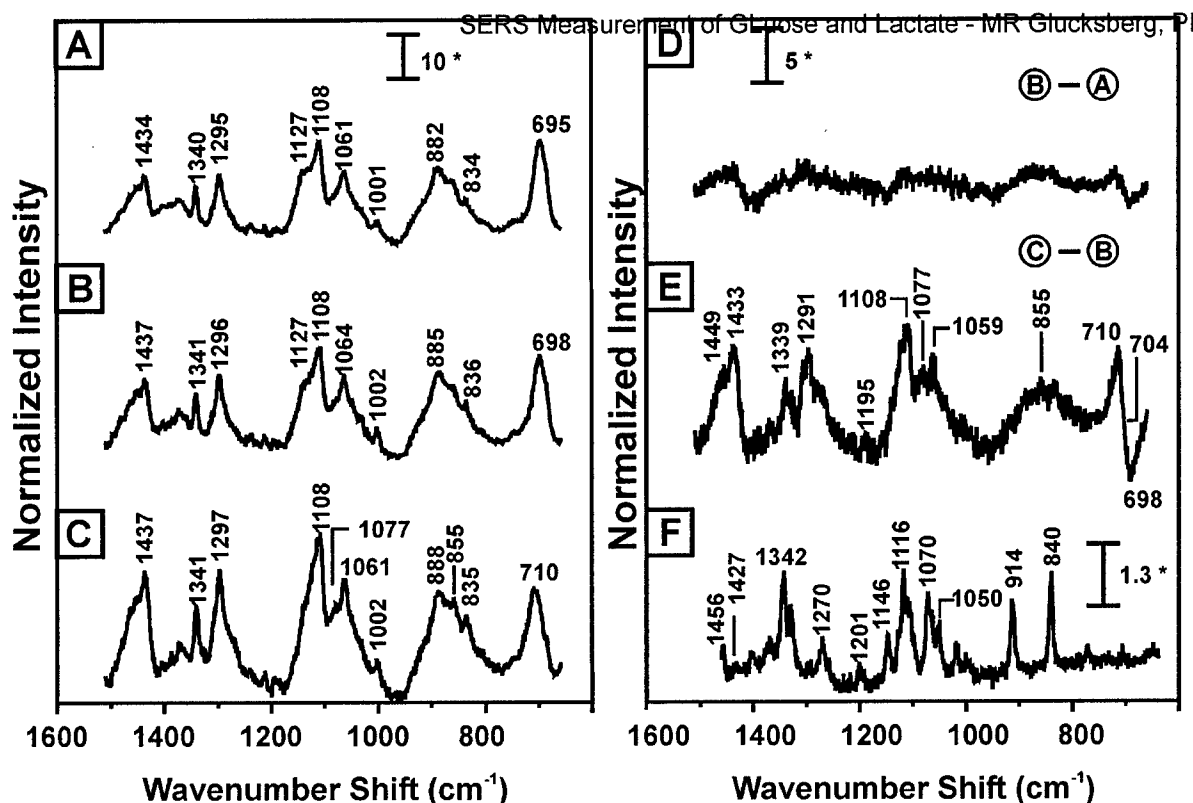


Figure 6. SERS spectra showing detection of glucose in the presence of serum albumin. (A) EG3 monolayer on AgFON substrate, $\lambda_{\text{ex}} = 632.8$ nm, $P_{\text{laser}} = 0.8$ mW, and $t = 240$ s. (B) A 1 mg/mL solution of serum albumin injected into the flow cell to challenge the EG3-modified AgFON, $\lambda_{\text{ex}} = 632.8$ nm, $P_{\text{laser}} = 0.8$ mW, and $t = 240$ s. (C) A 100 mM solution of glucose injected into the flow cell, $\lambda_{\text{ex}} = 632.8$ nm, $P_{\text{laser}} = 0.8$ mW, and $t = 240$ s. (D) Difference spectrum obtained by subtracting (A) from (B) revealing the lack of SERS spectrum for adsorbed serum albumin. (E) Difference spectrum obtained by subtracting (B) from (C) indicating serum albumin exposure does not interfere with glucose detection. (F) Normal Raman spectrum of crystalline glucose for comparison, $\lambda_{\text{ex}} = 632.8$ nm, $P_{\text{laser}} = 5$ mW, and $t = 30$ s. * denotes $\text{adu mW}^{-1} \text{s}^{-1}$.

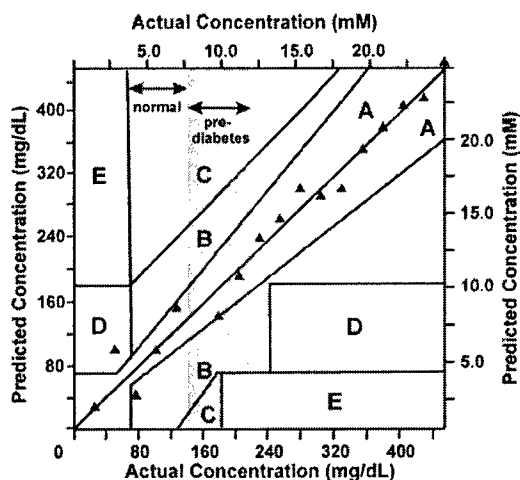


Figure 7. Clarke error grid of LOO-PLS predicted glucose concentration versus actual glucose concentration in the presence of 2 mg/mL BSA (4 loading vectors). An AgFON sample was made ($D = 390$ nm, $d_m = 200$ nm), incubated in 1 mM EG3 solution for ~ 16 h, and dosed in glucose solution (range: 25–450 mg/dL, 1.4–25 mM) with 2 mg/mL BSA for 10 min. Each SERS measurement was made in the flow cell under tris buffer with pH = 7.4, using $\lambda_{\text{ex}} = 632.8$ nm, $P_{\text{laser}} = 3$ mW, and $t = 60$ s.

modified AgFON surface was investigated by incubating the substrate in 2 mg/mL BSA for 6 h during data collection.

Measured SERS spectra indicate that the surface is durable as well as SERS-active even when exposed to the blood serum protein mimic for several hours. Future studies will investigate 3-day exposure to the blood serum protein mimic before detection of glucose.

CONCLUSIONS

Significant progress has been made toward achieving a real-time, quantitative, and biocompatible SERS glucose sensor. In our previous work, decanethiol was used as an effective partition layer for glucose, but the required sensor characteristics of stability, reversibility, and selectivity were not studied in detail. This technology is further advanced by demonstration of quantitative detection of glucose in the physiological range (0–450 mg/dL, 0–25 mM) under physiological conditions, 3-day sensor stability, partition/departition efficacy of the sensor using an optimized partition layer, and glucose detection in the presence of an interfering protein.

The accuracy of the SERS glucose sensor is evaluated using the Clarke error grid, the accepted metric for judging the prediction capability of glucose sensors in the clinical concentration range.⁴⁵ In fact, 94% of the predictions fall in zones A and B, signifying that correct treatment choices can be made using this sensor. Additionally, the EG3-modified AgFON sensor quantitatively detects glucose in the physiological range with a corresponding cross-validation error of 82 mg/dL (4.5 mM). A large

portion of the calculated error can be attributed to SERS enhancement factors due to sample-to-sample variation.

The stability of the EG3-modified AgFON SERS substrate is evident as the SERS bands and intensities do not change significantly during a 3-day incubation period in saline with pH = 7.4 at room temperature. The molecular order of the EG3 SAM increases with incubation time,⁴⁶ and this rearrangement gives rise to slightly larger SERS intensities.

Moreover, the glucose partition/departition capability of the EG3-modified AgFON sensor is demonstrated by exposing the sensor to cycles of 250 and 0 mM glucose solutions. The relatively high glucose concentration used in this experiment caused incomplete departitioning after each cycle, and accordingly, the glucose accumulated in each step. However, physiological concentrations of glucose will not likely cause such accumulation in the partition layer, and the natural flow of aqueous humor⁵⁰ or interstitial fluid will assist glucose departitioning. In future experiments, simulation of aqueous humor flow and more advanced difference spectroscopy methods will be applied.

Finally, this work also demonstrates that an EG3 partition layer can preconcentrate glucose near the surface quantitatively, while showing resistance to serum albumin, the most abundant protein

in the presence of other interfering proteins and analyte mixtures found in aqueous humor, interstitial fluid, and blood.

ACKNOWLEDGMENT

The authors acknowledge the technical assistance of Adam D. McFarland, Dr. Douglas Stuart, and Ms. Olga Lyandres. The authors are grateful to Professor Milan Mrksich and Dr. Eunhee Jeoung at the University of Chicago for the donation of the EG3 and to Professor Joeseeph T. Hupp at Northwestern University for access to the Cary UV-visible spectrometer. This project was supported by the Institute for Bioengineering and Nanoscience in Advanced Medicine at Northwestern University, the National Institutes of Health (EY13002 and EY13015), the National Science Foundation (EEC-0118025 and DMR-0076097), the Air Force Office of Scientific Research MURI program (F49620-02-1-0381), and a Northwestern University Presidential Fellowship (C.L.H.).

Received for review September 26, 2003. Accepted October 24, 2003.

AC035134K

Glucose Sensing Using Near-Infrared Surface-Enhanced Raman Spectroscopy: Gold Surfaces, 10-Day Stability, and Improved Accuracy

Douglas A. Stuart,[†] Chanda Ranjit Yonzon,[†] Xiaoyu Zhang,[†] Olga Lyandres,[‡] Nilam C. Shah,[†] Matthew R. Glucksberg,[‡] Joseph T. Walsh,[‡] and Richard P. Van Duyne^{*†}

Department of Chemistry and Department of Biomedical Engineering, Northwestern University, 2145 Sheridan Road, Evanston, Illinois, 60208-3113

This research presents the achievement of significant milestones toward the development of a minimally invasive, continuously monitoring, glucose-sensing platform based on the optical quantitation of glucose in interstitial fluid. We expand our initial successes in the measurement of glucose by surface-enhanced Raman scattering (SERS), demonstrating substantial improvements not only in the quality and optical properties of the substrate system itself but also in the robustness of the measurement methodology and the amenability of the technique to compact, diode laser-based instrumentation. Herein, we compare the long-term stability of gold to silver film over nanosphere (AuFON, AgFON) substrates functionalized with a partitioning self-assembled monolayer (SAM) using both electrochemical and SERS measurements. AuFONs were found to be stable for a period of at least 11 days. The switch to AuFONs not only provides a more stable surface for SAM formation but also yields better chemometric results, with improved calibration and validation over a range of 0.5–44 mM (10–800 mg/dL). Measured values for glucose concentrations in phosphate-buffered saline (pH ~7.4) based on 160 independent SERS measurements on AuFONs have a root-mean-square error of prediction of 2.7 mM (49.5 mg/dL), with 91% of the values falling within an extended A–B range on an expanded Clarke error grid. Furthermore, AuFONs exhibit surface plasmon resonances at longer wavelengths than similar AgFONs, which make them more efficient for SERS at near-infrared wavelengths, enabling the use of low-power diode lasers in future devices.

The routine electrochemical determination of blood glucose concentrations by diabetics is arguably the single most common analytical measurement made on a given day in the United States. Therefore, analytical methods that can improve on existing technologies by lowering cost, improving accuracy, or increasing ease of use stand to directly benefit the 18 million American diabetics.¹ The accurate measurement of glucose is challenging,

particularly in complex biological fluids, which by nature vary greatly in their constituents, not only between individuals but also throughout the day for a particular individual.

Currently, the most successful methods for glucose detection are indirect measurements that rely on the natural affinities of proteins such as glucose oxidase.^{2,3} The uncomfortable “finger stick” measurement familiar to diabetics relies on the electrochemical detection of the redox species produced by the enzymatic reduction of glucose by glucose oxidase.² Given the success of the enzymatic technique, due primarily to the protein’s inherent amenability to biological environments and high affinity for glucose, many research groups have attempted to utilize glucose-sensitive enzymes in novel, nonelectrochemical techniques. For example, Pishko and co-workers used fluorescence resonance energy transfer (FRET) to measure glucose by incorporating fluorescently labeled concanavalin A and dextran in a poly(ethylene glycol) hydrogel matrix.⁴ Glucose competitively binds to the concanavalin A, displacing the dextran, thus separating the protein/dextran FRET pair. The increase in the fluorescence of the dextran label was used to track changes in the glucose concentration. Pei and co-workers recently reported on a microcantilever system sensitive to glucose.⁵ Glucose oxidase was immobilized onto a microfabricated cantilever surface, which undergoes bending due to surface stress changes upon binding of glucose. The above methods all experience similar limitations because they rely on the same core chemistry—the protein-mediated binding of glucose. Proteins have inherently finite stability, particularly in terms of enzyme turnover lifetime, leading to a need to replenish the protein. Such sensors are also sensitive to interferences, e.g., similar monosaccharides, uric acid, acetaminophen, or dissolved oxygen.^{3,6} The binding of enzymes is also known to be temperature and pH dependent, variables frequently beyond experimental control in real-world systems.

* To whom correspondence should be addressed: (e-mail) vanduyne@chem.northwestern.edu.

[†] Department of Chemistry.

[‡] Department of Biomedical Engineering.

(1) *All About Diabetes*; American Diabetes Association, <http://www.diabetes.org/about-diabetes.jsp> (access date 09–08–2004).

(2) Heller, A. *Annu. Rev. Biomed. Eng.* **1999**, *1*, 153.

(3) Wilson, G. S.; Hu, Y. *Chem. Rev.* **2002**, *100*, 2693.

(4) Russell, R. J.; Pishko, M. V.; Gefrides, C. C.; McShane, M. J.; Cote, G. L. *Anal. Chem.* **1999**, *71*, 3126.

(5) Pei, J. H.; Tian, F.; Thundat, T. *Anal. Chem.* **2004**, *76*, 292.

(6) Turner, A. P. F.; Chen, B. N.; Piletsky, S. A. *Clin. Chem.* **1999**, *45*, 1596.

Others have mimicked the specificity of proteins for SERS measurement of glucose and lactate. MR Glucksberg and co-workers have used boronic acid derivatives by using compounds such as boronic acids,^{7,8} molecularly imprinted polymers (MIPs),^{9,10} or other nonbiological molecules that bind glucose¹¹ and undergo a subsequent physically observable change. These chemistries have been featured in numerous indirect detection methods including diffraction spectroscopy,^{8,12} fluorescence,^{4,7,13–15} and colorimetric UV–visible spectroscopy.^{16,17} The aforementioned methods have all been used—to varying degrees of success—for glucose detection. However, both boronic acid and imprinted polymer sensors are generally less sensitive to glucose than to other sugars.^{11,13} Many of the boronic acids optimally bind glucose at higher than physiological pH, although progress is being made toward synthesizing boronic acid derivatives that bind glucose at lower pH.¹⁸ MIPs similarly exhibit difficulty with selectivity, due to the structural specificity of the “glucose-shaped” binding cavity.¹¹ Such indirect methods offer a potentially unlimited number of sensitive detection modalities, including signal multiplication. However, they have many possible sources of error, particularly from competing species. Therefore, it is desirable to be able to directly assess the concentration of glucose in solution.

The direct detection of glucose has been a more challenging analytical problem than the indirect measures detailed above. While glucose can be directly assayed by a variety of laboratory techniques (mass spectrometry, chromatography, etc.),^{19,20} the number of methods amenable to clinical or personal use is more limited. The majority of the direct glucose detection techniques are optical because of the reagentless, nondestructive, and rapid nature of spectroscopic analysis. Polarimetry has been used to measure glucose levels based on the rotation of light in aqueous humor.^{21,22} Unfortunately, other chemical species in aqueous humor, such as ascorbate and albumin, are also optically rotationally active and can mask the concentration of glucose. Furthermore, the birefringence of the cornea itself complicates such polarimetric measurements. Vibrational spectroscopies enable quantitative, molecularly specific data to be acquired that can readily distinguish analytes based on their unique spectroscopic

infrared and near-infrared (NIR) absorbance^{23–30} and Raman spectroscopies for glucose detection.^{31–38} Current NIR results are impressive, but the instrumental constraints, i.e., size, cost, and power, are presently prohibitive for portable applications. For example, several groups have recently published results demonstrating both sensitive and accurate glucose measurements using infrared absorbance. Unfortunately, the acquisition of high-quality spectral data can require high powers delivered at the sample and lengthy collection times. Raman spectroscopic methods applied to glucose detection also require high powers and long acquisition times due to the very small Raman scattering cross section of glucose, $5.6 \times 10^{-30} \text{ cm}^2 \text{ molecule}^{-1} \text{ sr}^{-1}$, as determined by McCreery and co-workers.³⁹ This is particularly important when samples consisting of complex mixtures are used because other molecules, such as hemoglobin, may be strong scatterers. If sufficiently high in concentration or scattering cross section, the nontarget molecules' Raman scattering can overwhelm the glucose signal. Detection in less complicated media such as interstitial fluid, tears, or the aqueous humor of the eye could potentially ameliorate the difficulties inherent in interpreting spectra with many confounding analytes,⁴⁰ but is complicated by the low level of glucose in these fluids relative to blood and the time differential in glucose concentration between blood and secondary fluid levels.^{22,41} The higher signal intensity gained from the surface-enhanced Raman scattering (SERS) phenomenon overcomes the limitations imposed by weak signal strength, enabling the use of lower power and shorter acquisition times.⁴² When molecules are brought into proximity to nanoscale roughened metal surfaces, the intensified local electromagnetic field generated by the nanoscale structures is able to enhance the observed Raman scattering by 10^6 – 10^8 , and in exceptional cases as much as 10^{14} times.^{43–49} Furthermore, SERS is highly surface selective, such

- (7) Karnati, V. V.; Gao, X.; Gao, S.; Yang, W.; Ni, W.; Sankar, S.; Wang, B. *Bioinorg. Med. Chem. Lett.* **2002**, *12*, 3373.
- (8) Alexeev, V. L.; Sharma, A. C.; Goponenko, A. V.; Das, S.; Lednev, I. K.; Wilcox, C. S.; Finegold, D. N.; Asher, S. A. *Anal. Chem.* **2003**, *75*, 2316.
- (9) Parmpi, P.; Kofinas, P. *Biomaterials* **2004**, *25*, 1969.
- (10) Byrne, M. E.; Park, K.; Peppas, N. A. *Adv. Drug Delivery Rev.* **2002**, *54*, 149.
- (11) James, T. D.; Shinkai, S. Artificial receptors as chemosensors for carbohydrates. In *Host–Guest Chemistry*; Springer–Verlag: Berlin, 2002; Vol. 218; p 159.
- (12) Asher, S. A. A.; V. L.; Goponenko, A. V.; Sharma, A. C.; Lednev, I. K.; Wilcox, C. S.; Finegold, D. N. *J. Am. Chem. Soc.* **2003**, *125*, 3332.
- (13) Badugu, R.; Lakowicz, J. R.; Geddes, C. D. *Anal. Chem.* **2004**, *76*, 610.
- (14) Cao, H. S.; Diaz, D. I.; DiCesare, N.; Lakowicz, J. R.; Heagy, M. D. *Org. Lett.* **2002**, *4*, 1503.
- (15) James, T. D.; Shinkai, H.; Shinkai, S. *Chem. Commun.* **1997**, 71.
- (16) DiCesare, N.; Lakowicz, J. R. *Org. Lett.* **2001**, *3*, 3891.
- (17) Aslan, K.; Zhang, J.; Lakowicz, J. R.; Geddes, C. D. *J. Fluoresc.* **2004**, *14*, 391.
- (18) Das, S.; Alexeev, V. L.; Sharma, A. C.; Geib, S. J.; Asher, S. A. *Tetrahedron Lett.* **2003**, *44*, 7719.
- (19) Blanco Gomis, D.; Muro Tamayo, J.; Alonso, M. *Anal. Chim. Acta* **2001**, *436*, 173.
- (20) Di Gioia, M. L.; Leggio, A.; Le Pera, A.; Liguori, A.; Napoli, A.; Siciliano, C.; Sindona, G. *J. Chromatogr., B* **2004**, *801*, 355.
- (21) Cameron, B. D.; Gorde, H. W.; Satheesan, B.; Cote, G. L. *Diabetes Technol. Ther.* **1999**, *1*, 125.
- (22) Klonoff, D. C. *Diabetes Care* **1997**, *20*, 433.
- (23) Kasemsumran, S.; Du, Y. P.; Murayama, K.; Huehne, M.; Ozaki, Y. *Anal. Chim. Acta* **2004**, *512*, 223.
- (24) Jensen, P. S.; Bak, J.; Ladefoged, S.; Andersson-Engels, S. *Spectrosc. Acta, Part A* **2004**, *60*, 899.
- (25) Zhang, L.; Small, G. W.; Arnold, M. A. *Anal. Chem.* **2003**, *75*, 5905.
- (26) Wabomba, M. J.; Small, G. W.; Arnold, M. A. *Anal. Chim. Acta* **2003**, *490*, 325.
- (27) Shen, Y. C.; Davies, A. G.; Linfield, E. H.; Taday, P. F.; Arnone, D. D.; Else, T. S. *J. Biol. Phys.* **2003**, *29*, 129.
- (28) Maruo, K.; Tsurugi, M.; Tamura, M.; Ozaki, Y. *Appl. Spectrosc.* **2003**, *57*, 1236.
- (29) Jensen, P. S.; Bak, J.; Andersson-Engels, S. *Appl. Spectrosc.* **2003**, *57*, 28.
- (30) Arnold, M. A. *Abst. Pap. Am. Chem. Soc.* **2002**, *224*, U114.
- (31) Bell, A. F.; Barron, L. D.; Hecht, L. *Carbohydr. Res.* **1994**, *257*, 11.
- (32) Berger, A. J.; Wang, Y.; Feld, M. S. *Appl. Opt.* **1996**, *35*, 209.
- (33) Lambert, J.; Storrie-Lombardi, M.; Borchert, M. *IEEE LEOS Newslett.* **1998**, *12*, 19.
- (34) Enejder, A. M. K.; Koo, T. W.; Oh, J.; Hunter, M.; Sasic, S.; Feld, M. S.; Horowitz, G. L. *Opt. Lett.* **2002**, *27*, 2004.
- (35) Mrozek, M. F.; Weaver, M. J. *Anal. Chem.* **2002**, *74*, 4069.
- (36) Yonzon, C. R.; Haynes, C. L.; Zhang, X. Y.; Walsh, J. T.; Van Duyne, R. P. *Anal. Chem.* **2004**, *76*, 78.
- (37) Berger, A. J.; Itzkan, I.; Feld, M. S. *Spectrosc. Acta, Part A* **1997**, *53*, 287.
- (38) Shafer-Peltier, K. E.; Haynes, C. L.; Glucksberg, M. R.; Van Duyne, R. P. *J. Am. Chem. Soc.* **2003**, *125*, 588.
- (39) McCreery, R. L. *Raman Spectroscopy for Chemical Analysis*; John Wiley & Sons: New York, 2000; Vol. 157.
- (40) Lambert, J. L.; Morookian, J. M.; Sirk, S. J.; Borchert, M. S. *J. Raman Spectrosc.* **2002**, *33*, 524.
- (41) Bantle, J. P.; Thomas, W. J. *Lab. Clin. Med.* **1997**, *130*, 436.
- (42) Chang, R. K.; Furtak, T. E. *Surface Enhanced Raman Scattering*; Plenum Press: New York, 1982.
- (43) Campion, A.; Kambhampati, P. *Chem. Soc. Rev.* **1998**, *27*, 241.

that the observed enhancements drop ~ 1 order of magnitude for a 10 nm distance between the molecule and the metal surface.⁵⁰ Selective substrates can be fabricated that effectively concentrate the target analyte at the SERS active surface, often rendering signal subtraction, particularly of water, unnecessary.^{51–58}

We have previously demonstrated that SERS can be used to directly detect glucose on silver surfaces functionalized with alkanethiol monolayers.^{36,38} A SAM of *n*-decane- ω -thiol or (1-mercaptopentadeca-11-yl)tri(ethylene glycol) partitioned glucose from aqueous buffer into the zone of electromagnetic field enhancement extending from a silver film over nanosphere (AgFON) surface. Due to the low affinity of glucose toward noble metal surfaces, no SERS spectra of glucose could be obtained in the absence of a partitioning layer. Using appropriate multivariate calibration techniques, we could detect glucose over a very wide range of concentrations, both large (0–4500 mg/dL, 0–250 mM) and clinically relevant (0–450 mg/dL, 0–25 mM).³⁸ The second-generation sensor was robust enough to survive 3 days in solution and could operate effectively in the presence of serum albumin as a blood serum mimic.³⁶

The present work demonstrates significant improvements in all aspects of the SERS glucose sensor. Most importantly, this sensor shows higher predictive accuracy than the second-generation sensor and greater stability of the crucial partitioning SAM. We have striven to increase the glucose SERS signal by concentrating the glucose in proximity to the metal by using a glycosylated thiol with a shorter alkane spacer. Spectroscopic and electrochemical measurements indicate that the novel SAM is stable on gold films over nanospheres (AuFONs) for at least 11 days. We attribute the greater temporal stability of the SAM to the switch from silver to gold FON surfaces. The improved surface chemistry is due to the greater strength of the S–Au bond (~ 420 kJ/mol) relative to the S–Ag bond (217 kJ/mol).⁵⁹ We hypothesize that the greater ordering in the SAMs on gold versus silver surfaces is also partially responsible for the observed improvement in glucose measurement. Furthermore, the localized surface plasmon for AuFONs occurs at longer wavelengths than similar AgFONs. AuFONs work well with red and NIR lasers because the optimal SERS enhancements occur when the excitation

lasers will present several advantages in subsequent device development. NIR diode lasers are relatively compact, inexpensive, and power efficient. Furthermore, switching to NIR wavelengths will reduce not only the interference from biological autofluorescence in future in vivo applications but also the potential for tissue damage due to the low water and tissue absorption of NIR light.^{61,62}

EXPERIMENTAL SECTION

Materials. All the chemicals were of reagent grade or better and were used as purchased. Ag and Au wire (99.99%) were purchased for thermal deposition (D. F. Goldsmith, Evanston, IL). Oxygen-free high-conductivity copper (McMaster-Carr, Chicago, IL) was cut into 18-mm-diameter disks for supporting substrates. NH_4OH , H_2O_2 , and $\text{CH}_3\text{CH}_2\text{OH}$ (Fisher Scientific, Fairlawn, VA) were used to clean the substrates and as solvents for the SAM. Surfactant-free white carboxyl-substituted latex polystyrene nanosphere suspensions (390 ± 19.5 nm diameter, 4% solid) were obtained from a commercial vendor (Duke Scientific Corp., Palo Alto, CA). Tungsten vapor deposition boats (R. D. Mathis, Long Beach, CA) were used to evaporate the metal. For substrate and solution preparations, ultrapure water ($18.2 \text{ M}\Omega \text{ cm}^{-1}$) from Millipore academic system (Millipore, Marlborough, MA) and phosphate-buffered saline (pH ~ 7.4) (Sigma, St. Louis, MO) were used. 1-Mercaptoocta-8-yltri(ethylene glycol), EG3, was custom synthesized (SensoPath Technologies, Bozeman, MT). Ruthenium hexamine was purchased from Strem (Strem Chemicals, Newburyport, MA).

Substrate Fabrication and Incubation Procedure. The design and fabrication of the SAM-functionalized SERS sensors are shown in Figure 1. Ag- and AuFONs were fabricated on copper substrates, which provide better mechanical stability of the FON than on glass. The copper substrates were cleaned by sonicating in 10:1:1 $\text{H}_2\text{O}/30\% \text{H}_2\text{O}_2/\text{NH}_4\text{OH}$. To form a nanosphere deposition mask, $\sim 12 \mu\text{L}$ of nanosphere solution was drop-coated onto a clean copper substrate and allowed to dry at room temperature. Then, 200-nm-thick Ag or Au films were deposited onto and through the nanosphere mask using a modified vapor deposition system (Consolidated Vacuum Corp., Rochester, NY) with a base pressure 10^{-7} Torr. The mass thickness and deposition rate (~ 1 nm/s) of the metal were measured by an Inficon XTM/2 quartz crystal microbalance (Leybold, East Syracuse, NY). The FON substrates were first incubated in 1 mM solutions of the EG3 in ethanol for at least 12 h. Then, the SAM-modified substrates were mounted into a small-volume flow cell. Finally, the substrates were exposed to glucose solutions for at least 5 min, and spectra data were acquired.

UV-Visible Diffuse Reflectance Spectroscopy. Measurements were carried out in a home-built flow cell using an SD2000 spectrometer (Ocean Optics, Dunedin, FL) coupled to a reflectance probe and a model F-O-Lite H halogen lamp (World Precision Instruments, Sarasota, FL). The reflectance probe consists of a tight bundle of 12 read fibers ($200 \mu\text{m}$) around 1 illumination fiber ($400 \mu\text{m}$), optimized for the UV–NIR (250–

- (44) John T. Krug, I., Geoffrey D. Wang, Steven R. Emory, and Shuming Nie. *J. Am. Chem. Soc.* **1999**, *121*, 9208.
- (45) Nie, S.; Emory, S. R. *Science* **1997**, *275*, 1102.
- (46) Kneipp, K.; Wang, Y.; Kneipp, H.; Perelman, L. T.; Itzkan, I.; Dasari, R. R.; Feld, M. S. *Phys. Rev. Lett.* **1997**, *78*, 1667.
- (47) Otto, A.; Mrozek, I.; Grabhorn, H.; Akemann, W. *J. Phys. Condens. Matter* **1992**, *4*, 1143.
- (48) Schatz, G. C.; Van Duyne, R. P. *Electromagnetic Mechanism of Surface-Enhanced Spectroscopy*. In *Handbook of Vibrational Spectroscopy*; Chalmers, J. M., Griffiths, P. R., Eds.; Wiley: New York, 2002; Vol. 1; pp 759.
- (49) Haynes, C. L.; Van Duyne, R. P. *J. Phys. Chem. B* **2003**, *107*, 7426.
- (50) Kennedy, B. J.; Spaeth, S.; Dickey, M.; Carron, K. T. *J. Phys. Chem. B* **1999**, *103*, 3640.
- (51) Deschaines, T. O.; Carron, K. T. *Appl. Spectrosc.* **1997**, *51*, 1355.
- (52) Carron, K.; Peitersen, L.; Lewis, M. *Environ. Sci. Technol.* **1992**, *26*, 1950.
- (53) Sulk, R.; Chan, C.; Guicheteau, J.; Gomez, C.; Heyns, J. B. B.; Corcoran, R.; Carron, K. *J. Raman Spectrosc.* **1999**, *30*, 853.
- (54) Sulk, R. A.; Corcoran, R. C.; Carron, K. T. *Appl. Spectrosc.* **1999**, *53*, 954.
- (55) Wachter, E. A.; Storey, J. M. E.; Sharp, S. L.; Carron, K. T.; Jiang, Y. *Appl. Spectrosc.* **1995**, *49*, 193.
- (56) Mosier-Boss, P. A.; Boss, R. D.; Lieberman, S. H. *Langmuir* **2000**, *16*, 5441.
- (57) Mosier-Boss, P. A.; Lieberman, S. H. *Appl. Spectrosc.* **2003**, *57*, 1129.
- (58) Carron, K. T.; Corcoran, R. *Abstr. P. Am. Chem. Soc.* **1997**, *214*, 18.
- (59) *CRC Handbook of Chemistry and Physics*, 81 ed.; Lide, D. R., Ed.; CRC Press: Boca Raton, FL, 2000; p 2556.

- (60) McFarland, A. D., Ph.D. Northwestern University, Evanston, IL, 2004.
- (61) Anderson, R. R.; Parrish, J. A. *Optical Properties of Human Skin*. In *The Science of Photomedicine*; Regan, J. D., Parrish, J. A., Eds.; Plenum Press: New York, 1982; p 147.
- (62) Weissleder, R. *Nat. Biotechnol.* **2001**, *19*, 316.

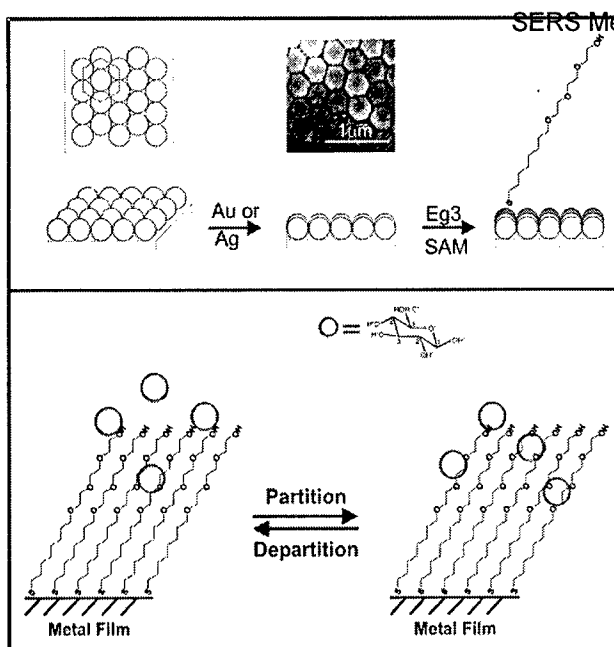


Figure 1. Schematic of sensing surface. Polymer nanospheres are self-assembled onto a supporting substrate, and allowed to form a hexagonal close-packed 2D crystal. Metal (Au or Ag) is then deposited via vacuum thermal deposition over the nanosphere lattice. A SEM micrograph is shown. The Au or Ag FON is then incubated in a solution of EG3, forming a SAM of the EG3. Glucose is able to partition and depart into the monolayer.

2100 nm) in a stainless steel ferrule. All reflectance spectra were collected using a mirrorlike Ag film over copper substrate as a reference.

Electrochemistry. The home-built smooth Ag working electrode was embedded into a glass body using Torr Seal (Varian Vacuum Products, Lexington, MA). Prior to use, surfaces were polished with 0.3- and 0.05- μm alumina, successively (Buehler Ltd., Lake Bluff, IL), and sonicated in MQ water. The Au working electrode, Pt auxiliary electrode, Ag/AgCl reference electrode, and BAS 100B/W electrochemical workstation were acquired commercially (Bioanalytical Systems Inc., West Lafayette, IN). The potential of the Ag/AgCl reference electrodes is -35 mV relative to the saturated calomel electrode.

Surface-Enhanced Raman Scattering Spectroscopy. A Spectra-Physics model Millennia Vs laser was used to excite a Spectra-Physics model 3900 Ti-sapphire laser to produce the 750-nm excitation wavelength (λ_{ex}); the laser spot size on the sample was less than 0.5 mm in diameter. The SERS measurement system includes an interference filter (Edmund Scientific, Barrington, NJ), a holographic notch filter (Kaiser Optical Systems, Ann Arbor, MI), a model VM-505 single-grating monochromator with the entrance slit set at 100 μm (Acton Research Corp., Acton, MA), and a LN₂-cooled CCD detector (Roper Scientific, Trenton, NJ). A collection lens with magnification 5 was used to collect the scattered light. The small-volume flow cell was used to control the external environment of the metal FON surfaces throughout the SERS experiments.

Quantitative Multivariate Analysis. All data processing was performed using MATLAB (MathWorks, Inc., Natick, MA) and PLS_Toolbox (Eigenvector Research, Inc., Manson, WA). Prior

to the SERS measurement of glucose and lactate, the PLS method with a second-order polynomial and window size of 9. Cosmic rays were removed from the spectra using a derivative filter. The slowly varying background, commonly seen in SERS experiments, was removed mathematically by subtracting a fourth-order polynomial. This method minimally affected the SERS peaks while greatly reducing the background level. The SERS spectral intensities were normalized using the 700 ± 10 cm^{-1} peak from the EG3 partition layer spectrum. The 700-cm^{-1} band arises from the S-C bond stretch and serves as a convenient reference for SERS of thiol SAMs on metal surfaces.⁶³ From each spectrum, the absolute peak intensity of the 700-cm^{-1} peak was obtained and the entire spectrum was divided by that value, such that the intensity of the 700-cm^{-1} peak is unity. Then, data analysis was performed using the partial least-squares (PLS) analysis and leave-one-out cross-validation algorithm.

RESULTS AND DISCUSSION

The results presented below detail the achievement of a substantial advance toward the development of a practical, portable, SERS-based glucose measuring device. Our previous work demonstrated the feasibility of using SERS to detect and quantify glucose. Subsequent work addressed the performance of the SERS sensor in terms of short-term stability, reversibility, and selectivity in the presence of interferences. Herein, we report on the development of a substrate that is optimized for SERS using NIR laser excitation with not only enhanced spectral and physical stability but also the capability of superior quantitative measurements.

Optical Properties of Au- and AgFONs. In normal Raman scattering, the signal intensity scales with the inverse fourth power of the excitation wavelength. Thus, the ratio of normal Raman scattering intensities for 750- versus 632.8-nm excitation is 0.51. In contrast, the SERS signal intensity is actually larger when using far-red excitation due to the smaller imaginary portion of the complex dielectric constants of Ag and Au. The optical properties of nanoscale noble metal materials, including FONs, are dominated by the surface plasmon.⁶⁴ The position and intensity of the surface plasmon is sensitive to the morphology (size and shape) and composition of the material.^{65,66} In FONs, the position of the plasmon can be tuned by controlling the size of the spheres used in the underlying nanosphere mask. The surface plasmon is responsible for the intense local electromagnetic fields that give rise to SERS. The maximum SERS enhancements occur when the excitation laser is of slightly shorter wavelength than the surface plasmon, enabling electromagnetic enhancements of both the incoming photons and the scattered, Raman-shifted photons.⁴⁹ Therefore, by tuning the physical properties of the FON surface, we are able to tune the surface plasmon to maximize the SERS enhancements. As illustrated in Figure 2, using an AuFON rather than an AgFON enables us to position the plasmon peak nearer the excitation wavelength (λ_{ex}) with greater facility. Although the maximum SERS enhancements on silver surfaces are greater than

(63) Bryant, M. A.; Pemberton, J. E. *J. Am. Chem. Soc.* **1991**, *113*, 8284.

(64) Kreibig, U.; Vollmer, M. *Optical Properties of Metal Clusters*; Springer: New York, 1995.

(65) Haynes, C. L.; Van Duyne, R. P. *Abstr. Pap. Am. Chem. Soc.* **2001**, *222*, U89.

(66) Haynes, C. L.; Van Duyne, R. P. *J. Phys. Chem. B* **2001**, *105*, 5599.

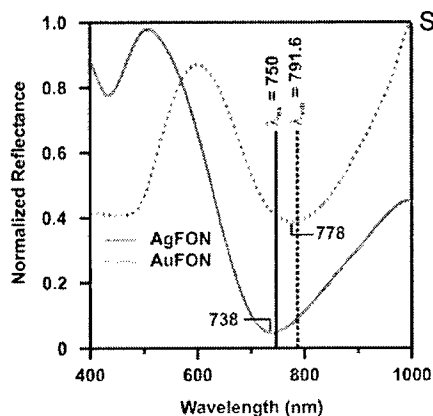


Figure 2. Reflectance spectra from EG3-functionalized Au and AgFONs. The position of the LSPR λ_{\min} for the AgFON (738 nm) occurs at shorter wavelengths than that of the AuFON (778 nm). The AuFON is therefore better tuned to the wavelength of the excitation laser used in these experiments (750 nm). The 700-cm^{-1} band of the EG3 SAM occurs at 791.6 nm under 750-nm excitation.

the maximum enhancements on gold surfaces, the efficiency of SERS on silver is highest in the visible region. Thus, gold surfaces become as effective SERS substrates as silver surfaces when λ_{ex} occurs at longer wavelengths. Experimentally, the magnitude of the observed SERS is slightly higher on the gold surfaces than silver, as described below.

SAM Stability. To continuously monitor glucose levels in vivo, a SERS-based sensor must have an implantable substrate that can be optically addressed either directly through the skin or via an optical fiber. Such an implantable glucose sensor must be stable for at least a three-day period. Three days has been chosen as a target milestone because more frequent changing of the implant would be burdensome on the subject, and the implantable insulin pump has a three-day lifetime. Previous work has demonstrated that bare AgFON surfaces display extremely stable SERS activity when challenged with high potentials,⁶⁷ and high temperatures in ultrahigh vacuum,⁶⁸ and when studied over a three-day period in the presence of saline and interfering analytes such as blood protein mimics.³⁶ Toward developing a more stable glucose sensor, we have performed an extensive surface study comparing AgFON versus AuFON using cyclic voltammetry (CV) and SERS.

Electrochemical Analysis. It is essential to have a stable, well-packed SAM on the sensor surface since the SAM is essential to partition glucose for SERS detection. Electrochemical measurements of heterogeneous electron transfer were exploited in order to probe the average behavior of the EG3 assemblies on Ag and Au surfaces and the extent of structural defects over the course of 11 days. Ideally, electron transfer through a well-packed monolayer of alkyl chains occurs via a highly nonadiabatic pathway in which the kinetics exhibit an exponential dependence on the separation distance between the electron donor and the electron acceptor.⁶⁹ As the extent of structural defects of the monolayer increases, e.g., due to appearance of pinholes and trapped solvent, the current of heterogeneous electron transfer will be strongly

SERS Measurement of Glucose and Lactate. MR. Glucksberg, et al. of ruthenium(III/II) hexamine on EG3-modified Ag and Au electrodes. The complexes were selected because both $\text{Ru}(\text{NH}_3)_6^{3+}$ and $\text{Ru}(\text{NH}_3)_6^{2+}$ are substitutionally inert in aqueous media and undergo rapid heterogeneous electron-transfer reactions in a convenient range of potentials.

The initial voltammograms for the $\text{Ru}(\text{NH}_3)_6^{3+/2+}$ couple at the EG3-covered surfaces are shown as the day 1 samples. After electrochemical examination in 5 mM $\text{Ru}(\text{NH}_3)_6\text{Cl}_3$ PBS solution, the EG3-modified electrodes were removed from the cell, thoroughly rinsed with PBS solution, and then reimmersed into the PBS solution before measuring the next cyclic voltammogram. CV of the $\text{Ru}(\text{NH}_3)_6^{3+/2+}$ couple on clean, unmodified surfaces is also shown in gray lines in Figure 3 for purposes of comparison. At bare Ag and Au electrodes, the shapes of the current–potential curves and $\sim 60\text{-mV}$ separation between the cathodic and anodic peak currents indicate a diffusion-limited or electrochemically reversible one-electron redox process. The voltammograms for the EG3-modified electrodes are remarkably different: the current is much lower, and most of the current comes from the double layer capacitance. For EG3-modified Ag electrodes, the reduction current increases with the immersion time in PBS, owing to an increase in monolayer defects. However, even after 11-day immersion into the PBS solution, the EG3-coated Au electrode shows much lower reduction current in comparison to the EG3-coated Ag electrode.

The percentages of current maximum obtained in voltammetry from PBS-immersed samples vary with time, as shown in Figure 3C. The percentage represents the average of the absolute value of cathodic and anodic peak current divided by the same value calculated from a clean, unmodified surface.⁷⁰ As Figure 3C shows, the percentages of the current maximum increase to 20.0% after 10 days for SAM functionalized silver electrodes, while only 2.4% after 11 days for those made with gold. These results agree with the literature⁶³ and indicate that SAMs are more stable and better ordered on gold than silver surfaces.

SERS Stability. While the electrochemical measurements confirmed that the SAM was adequately blocking the electroactive surface, they did not directly indicate that the FON retained its SERS properties over that time. Therefore, the stability of the EG3-modified metal FON SERS substrates was studied over a period of 10 days in pH 7.4 PBS buffer at room temperature. SERS spectra were captured every 24 h from the same sample ($\lambda_{\text{ex}} = 750\text{ nm}$, $t = 60\text{ s}$) on an AgFON and an AuFON. Figure 4A and B represents the initial EG3 spectra on AgFON and AuFON, respectively. Figure 4C is the peak intensity at 699 cm^{-1} for EG3 on the AgFON, and Figure 4D is the peak intensity at 698 cm^{-1} for EG3 on the AuFON. The EG3 spectral band positions and relative intensities did not vary significantly over the course of 10 days. Although the peak intensities of EG3 on AgFONs and AuFONs were comparable on the first day, peak intensities decreased as time progresses for the AgFON sample. By the fifth day, the peak intensities of the EG3 on the AgFON diminished to the point where no data could be acquired. The peak intensities of the EG3 on the AuFON, however, remained constant over the period of 10 days. These spectral data not only indicate that the

(67) Zhang, X.; Yonzon, C. R.; Van Duyne, R. P. *Proc. SPIE-Int. Soc. Opt. Eng.* 2003, 5221, 82.

(68) Litorja, M.; Haynes, C. L.; Haes, A. J.; Jensen, T. R.; Van Duyne, R. P. *J. Phys. Chem. B* 2001, 105, 6907.

(69) Li, T. T. T.; Liu, H. Y.; Weaver, M. J. *J. Am. Chem. Soc.* 1984, 106, 1233.

(70) Flynn, N. T.; Tran, T. N. T.; Cima, M. J.; Langer, R. *Langmuir* 2003, 19, 10909.

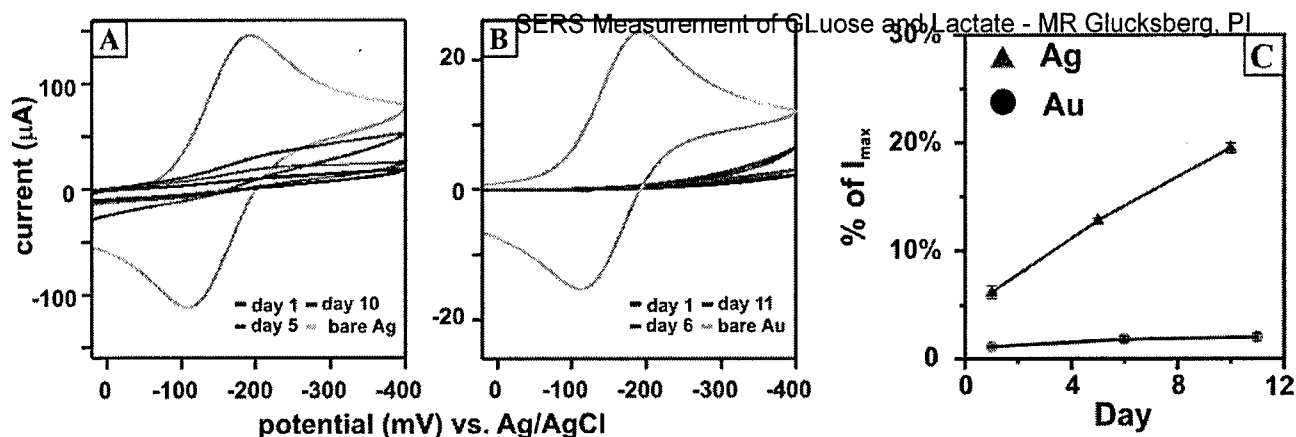


Figure 3. Electrochemical determination of monolayer stability. Both Ag (A) and Au (B) electrodes were functionalized with a SAM and immersed in a solution of 1 mM $\text{Ru}(\text{NH}_3)_6 \text{Cl}_3$ in PBS buffer. Cyclic voltammograms were taken of the electrodes daily for 10 days, with a scan rate of 200 mV/s. Shown are representative voltammograms for days 1 (black), 5 (red), and 10 (blue) on the silver electrode, and days 1 (black), 6 (red), and 11 (blue) on the gold electrode, as well as a reference voltammogram (gray) from a bare (control) electrode (both Au and Ag electrodes). Desorption of the protective monolayer permits direct access to the electrode surface by the electroactive species and was observed as an increase in the total current over time. (C) shows the percentages of current maximum vary with time.

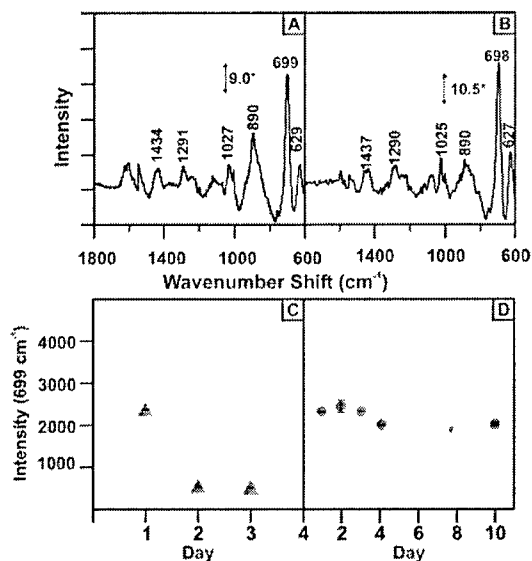


Figure 4. Comparative SERS spectra of EG3 on (A) AgFON and (B) AuFON surfaces. FONs were prepared by coating 390-nm nanospheres with 200 nm of metal. (C) and (D) show the time course of the intensity of the $\sim 699\text{-cm}^{-1}$ peak. Signal intensities from the AuFON remained stable for a period of 10 days. The AgFONs rapidly lost signal, and no spectra were observed by day 4. For all cases, $\lambda_{\text{ex}} = 750 \text{ nm}$, 7–8 mW power, and 60-s acquisition.

AuFON surface remains SERS active but also confirm that the SAM is intact and well ordered.

Quantitative Detection. A PLS calibration model was built using 160 independent spectral measurements on sensors exposed to known concentrations of glucose. Data were collected by immersing prepared substrates in glucose solutions and acquiring SERS spectra ($\lambda_{\text{ex}} = 750 \text{ nm}$, 10-s integration \times 12 averages). Spectra from two locations on the substrate were acquired for each concentration. Several different substrates were used to build the training set, and each of those substrates was exposed to glucose concentrations spanning the experimental concentration range. Based on the calibration, 95% of the data is represented by nine latent variables.

The number of latent variables can be interpreted as the inherent dimensionality of the system, in other words, the number of variables present including the concentration of the analyte of interest. These variables can include, and are not limited to, the temperature and humidity conditions in the laboratory on the day of the experiment, the focusing of the optical elements, the enhancement of the sensing surface at different locations, and the laser power and mode fluctuations, as well as noise in the data. Although using too many latent variables can cause over-modeling of the data, including all of the above-mentioned variation in the experimental design is necessary to build a robust calibration model.⁷¹ For example, the training set needs to be able to accurately predict glucose concentrations at more than one temperature to account for thermal fluctuations in vivo and to still function if subject movement alters the position of the optical focus.

The use of nine latent variables resulted in a model with a root-mean-square error of calibration (RMSEC) of 49.5 mg/dL (2.7 mM). The RMSEC describes the accuracy of the model itself. Our previous work modeled the response for a single sensor surface optically addressed at a single spot. This approach led to a lower RMSEC, i.e., a precise model, but predictions based on models generated in this manner performed poorly when applied to data collected from either a different focal point or another substrate. Because real-world applications of the sensor will include a number of independent and uncontrolled variables, a versatile mathematical model is needed, and it is reasonable that the dimensionality of the system can be as high as 9. Including a large number of samples in the calibration set helps generate a robust mathematical model by including data that may be affected by the uncontrolled variables. The 160 data points were collected on several unique substrates, and measurements were made on at least two spots on each surface to account for possible differences in the SERS signals arising from variation in the AuFON/SAM microenvironment. Furthermore, the data for the calibration were collected at different times of the day, over a

(71) Beebe, K. R.; Pell, R. J.; Seasholtz, M. B. *Chemometrics: A Practical Guide*; Wiley-Interscience: New York, 1998.

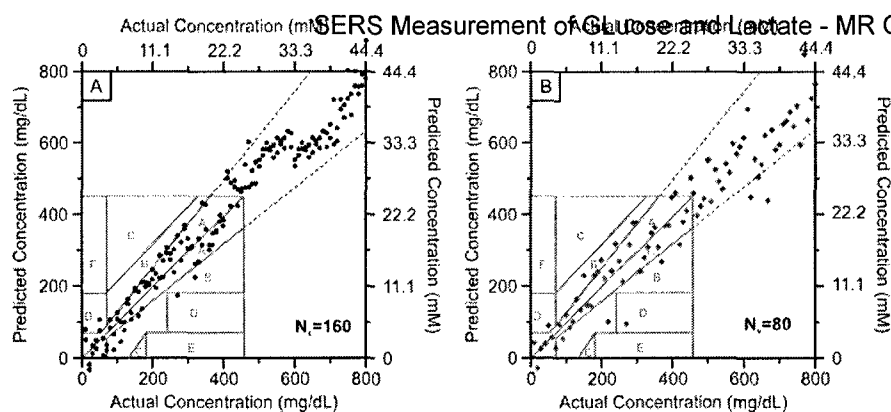


Figure 5. Calibration and prediction/validation plots using multiple substrates. PLS calibration plots were constructed using 160 data points taken over a range of concentrations (10–800 mg/dL) on a number of separately prepared AgFON substrates (5). Each substrate was interrogated at three different locations. Nine latent variables were used to generate the mathematical model, which had an RMSEC of 49.5 mg/dL. The central line represents the ideal prediction axis, not a best-fit curve. An independent validation set was used to test the predictive capability of the mathematical model. Predictions fall primarily within the extended A or B range of the Clarke error grid, with an RMSEP of 69.9 mg/dL.

period of several days. This helps account for random fluctuations in the data and minimizes the residuals and errors in the data analysis. By increasing the number of data samples, we can decrease the RMSEC as well as improve the quantitative prediction of glucose concentration.

A low RMSEC is necessary for, but does not in itself ensure, accurate prediction of concentrations based on measurements from samples outside the training set. Therefore, a separate set of spectra consisting of 80 independent data points was used to validate the model. Validation tests the ability of the model to predict the concentration of samples not used in the calibration, and more precisely reflects the accuracy of the sensor. The RMSEP was calculated to be 69.87 mg/dL (3.88 mM).

In Figure 5, the calibration and prediction data points are plotted against the Clarke error grid, a standard metric for the performance of glucose sensors, to evaluate the predictive capacity of the model.⁷² The calibration and prediction shown in Figure 5 are constructed for a range higher than the clinically relevant range (0–450 mg/dL, 0–25 mM) of the Clarke error grid because patients can have elevated blood glucose levels as high as 650–800 mg/dL during initial diagnosis of diabetes. Extending the A lines of the Clarke error grid over the entire range, 94% of the data points in the calibration plot and 91% of data points in the prediction plot fall within the acceptable region. These results indicate that the AuFON sensor is capable of making acceptably accurate concentration measurements even when challenged with a diverse sample population.

CONCLUSIONS

This work details our improvements in detecting and measuring glucose using SERS. Most notably, the sensor system is now able to perform more accurately over a wide range of glucose concentrations, over a long period of time, and on multiple substrates. Validation of the PLS model with 80 independent measurements yields an RMSEP of 2.7 mM (49.5 mg/dL), with

91% of the values falling within an extended A–B range on an expanded Clarke error grid. These analytical figures of merit compare favorably with existing detection methods, which have instrument-dependent coefficients of variation of 0.96–26.9% (0.096–2.69 mM, 1.75–49 mg/dL at 10 mM).^{73,74} The partition layer was improved by using 1-mercaptoocta-8-yltri(ethylene glycol), which has a shorter alkyl chain than the SAMs used previously. This shorter spacer is sufficiently alkane in nature to form ordered SAMs on the surface but is shorter thereby increasing the electromagnetic enhancement of the partitioned glucose. Additionally, the underlying SERS substrate transitioned from an AgFON to an AuFON. We have experimentally determined that the SAM is more stable on the gold surface by both cyclic voltammetry and SERS spectroscopy. We have also demonstrated that there are spectroscopic advantages to using AuFONs. The optimal laser wavelengths for SERS can be extended into the red and NIR because the fundamental plasmon wavelength for gold occurs at longer wavelength than silver. Red and NIR wavelengths will reduce background from biological autofluorescence and help prevent signal loss due to tissue and water absorption. Further experiments will test the capability of the sensor for interfacing with compact instrumentation, including fiber delivery and collection optics. In the near term, we will apply this sensor to the measurement of glucose levels in interstitial fluid in rodents.

ACKNOWLEDGMENT

The authors thank Erin M. Hicks for the SEM image used in Figure 1. This work was supported by the Institute for Bioengineering and Nanoscience in Advanced Medicine at Northwestern University, the National Institutes of Health (EY13002 and EY13015), the National Science Foundation (EEC-0118025 and DMR-0076097), and the Air Force Office of Scientific Research MURI program (F49620-02-1-0381).

Received for review January 21, 2005. Accepted April 20, 2005.

AC0501238

(72) Clarke, W. L.; Cox, D.; Gonder-Frederick, L. A.; Carter, W.; Pohl, S. L. *Diabetes Care* **1987**, *10*, 622.

(73) Solnica, B.; Naskalski, J. W.; Soeradzki, J. *Clin. Chim. Acta* **2003**, *331*, 29.

(74) Johnson, R. N.; Baker, J. R. *Clinica Chim. Acta* **2001**, *307*, 61.

Rapid Detection of an Anthrax Biomarker by Surface-Enhanced Raman Spectroscopy

Xiaoyu Zhang,[†] Matthew A. Young,[†] Olga Lyandres,[§] and Richard P. Van Duyne^{*,†}

Contribution from the Departments of Chemistry and Biomedical Engineering,
Northwestern University, 2145 Sheridan Road, Evanston, Illinois 60208-3113

Received October 20, 2004; E-mail: vanduyne@chem.northwestern.edu

Abstract: A rapid detection protocol suitable for use by first-responders to detect anthrax spores using a low-cost, battery-powered, portable Raman spectrometer has been developed. *Bacillus subtilis* spores, harmless simulants for *Bacillus anthracis*, were studied using surface-enhanced Raman spectroscopy (SERS) on silver film over nanosphere (AgFON) substrates. Calcium dipicolinate (CaDPA), a biomarker for bacillus spores, was efficiently extracted by sonication in nitric acid and rapidly detected by SERS. AgFON surfaces optimized for 750 nm laser excitation have been fabricated and characterized by UV–vis diffuse reflectance spectroscopy and SERS. The SERS signal from extracted CaDPA was measured over the spore concentration range of 10^{-14} – 10^{-12} M to determine the saturation binding capacity of the AgFON surface and to calculate the adsorption constant ($K_{\text{spore}} = 1.7 \times 10^{13} \text{ M}^{-1}$). At present, an 11 min procedure is capable of achieving a limit of detection (LOD) of $\sim 2.6 \times 10^3$ spores, below the anthrax infectious dose of 10^4 spores. The data presented herein also demonstrate that the shelf life of prefabricated AgFON substrates can be as long as 40 days prior to use. Finally, these sensing capabilities have been successfully transitioned from a laboratory spectrometer to a field-portable instrument. Using this technology, 10^4 bacillus spores were detected with a 5 s data acquisition period on a 1 month old AgFON substrate. The speed and sensitivity of this SERS sensor indicate that this technology can be used as a viable option for the field analysis of potentially harmful environmental samples.

Introduction

The rapid and accurate identification of bioagents is a vital task for first-responders in order to facilitate timely and appropriate actions in the event of a biological attack. *Bacillus anthracis*, a spore-forming bacterium and a dangerous pathogen for the disease anthrax, is an important example. *B. anthracis* bacteria exist in two different forms: rod-shaped organisms and spores. Rod-shaped organisms grow and divide in a nutrient-rich environment. When the food supply is depleted, the organisms turn into spores that can survive for decades. Structurally, a spore consists of a central core cell surrounded by various protective layers. Calcium dipicolinate (CaDPA) exists in these protective layers and accounts for $\sim 10\%$ of the spore's dry weight;¹ therefore, it is a useful biomarker for bacillus spores.²

Among the potential biological warfare agent candidates, *B. anthracis* spores are of particular concern. First, they are highly resistant to environmental stress and are relatively easily produced into weapon-grade material outside the laboratory. Second, anthrax is an infectious disease, requiring medical attention within 24–48 h of initial inhalation of more than

10^4 *B. anthracis* spores.³ However, the diagnosis of anthrax is not immediate because it takes 1–60 days for anthrax symptoms to appear in humans.⁴ Therefore, the rapid detection of *B. anthracis* spores in the environment prior to infection is an extremely important goal for human safety.

In the last two decades, various biological and chemical techniques have been developed to detect bacillus spores. Two important biological methods are the polymerase chain reaction (PCR)^{5–7} and immunoassays.^{8,9} PCR, a primer-mediated enzymatic DNA amplification method, requires expensive reagents, molecular fluorophores, and considerable sample processing prior to analysis. The limit of detection (LOD) based on PCR detection of bacterial *pagA* gene is $\sim 10^3$ spores in 3 h.⁷ Immunoassays, which rely on the interaction between antibodies and *B. anthracis* cell surface antigens, can detect 10^5 spores in 15 min.⁹ However, in immunoassays, it is necessary to employ specific antibodies for the desired agents and to individually

[†] Department of Chemistry.

[§] Department of Biomedical Engineering.

(1) Bailey, G. F.; Karp, S.; Sacks, L. E. *J. Bacteriol.* **1965**, *89*, 984–987.
(2) Goodacre, R.; Shann, B.; Gilbert, R. J.; Timmins, E. M.; McGovern, A. C.; Alsberg, B. K.; Kell, D. B.; Logan, N. A. *Anal. Chem.* **2000**, *72*, 119–127.

(3) Walt, D. R.; Franz, D. R. *Anal. Chem.* **2000**, *72*, 738A–746A.

(4) Chin, J. E. *Control of Communicable Diseases Manual*; American Public Health Association: Washington, D.C., 2000; pp 20–25.

(5) De Wit, M. Y.; Faber, W. R.; Krieg, S. R.; Douglas, J. T.; Lucas, S. B.; Montrewasuwat, N.; Pattyn, S. R.; Hussain, R.; Ponnighaus, J. M.; Hartskeerl, R. A. *J. Clin. Microbiol.* **1991**, *29*, 906–910.

(6) Hurtle, W.; Bode, E.; Kulesh, D. A.; Kaplan, R. S.; Garrison, J.; Bridge, D.; House, M.; Frye, M. S.; Loveless, B.; Norwood, D. *J. Clin. Microbiol.* **2004**, *42*, 179–185.

(7) Fasanella, A.; Losito, S.; Adone, R.; Ciuchini, F.; Trotta, T.; Altamura, S. A.; Chiocco, D.; Ippolito, G. *J. Clin. Microbiol.* **2003**, *41*, 896–899.

(8) Yolken, R. H.; Wee, S. B. *J. Clin. Microbiol.* **1984**, *19*, 356–360.

(9) King, D.; Luna, V.; Cannons, A.; Cattani, J.; Amuso, P. *J. Clin. Microbiol.* **2003**, *41*, 3454–3455.

adjust the mobile-phase conditions for their capture, elution, and separation.

Recently, relatively rapid chemical methods for the detection of bacillus spores have been developed. For instance, photoluminescence detection based on the formation of terbium (Tb(III)) dipicolinate was found to have a LOD of 10^3 *B. subtilis* colony-forming-units·mL⁻¹ in 5–7 min.¹⁰ This method compares the enhanced luminescence of the terbium dipicolinate complex to Tb(III) alone. However, an increase in the luminescence intensity can also occur by the complexation of Tb(III) with aromatic compounds other than dipicolinic acid.¹¹ Due to the frequency of false positives and its limited ability for target analyte identification, alternative approaches with improved selectivity would be a welcome addition to the arsenal of anthrax detection methods.

Compared to photoluminescence, vibrational spectroscopy possesses highly specific chemical information content and, therefore, is capable of uniquely identifying target analytes. Both Fourier transform infrared (FT-IR)¹² and Raman^{13,14} spectroscopies have demonstrated the ability to discriminate among different bacterial spores. However, the implementation of near-infrared (NIR) and mid-infrared spectroscopies has fundamental limitations due to the competitive absorption of water and inherent spectral congestion. In contrast, Raman spectroscopy is well-suited to applications in aqueous environments because of the small Raman scattering cross section of water.¹⁵ Recently, for example, single bacterial spores have been detected using micro-Raman spectroscopy.¹⁴ As a consequence of different individual sporulations, however, the micro-Raman spectra vary significantly from one spore to another. Additionally, the applications that require complex instrumentation used in this approach restrict its applicability in field-portable measurements. The detection of bacillus spores by normal Raman spectroscopy (NRS) has also been demonstrated;¹⁶ however, NRS suffers from low sensitivity, so that long data acquisition times (5–13 min) and high laser powers (400 mW) are required. In comparison, surface-enhanced Raman spectroscopy (SERS) yields more intense Raman signals at much lower laser excitation power. SERS produces very large enhancements in the effective Raman cross section of species spatially confined within the electromagnetic fields generated by excitation of the localized surface plasmon resonance (LSPR) of nanostructured noble metal surfaces.¹⁷ The SERS signals of ensemble-averaged molecules show enhancements up to 8 orders of magnitude over NR signals.¹⁸ Furthermore, the low power required by SERS allows the development of a compact, field-portable detection system.

In the present paper, we describe a procedure for the rapid

SERS Measurement of Glucose and Lactate - MR Glucksberg, PI

extraction of CaDPA from *B. subtilis* spores, simulants for *B. anthracis* spores, followed by SERS detection on reproducible,¹⁹ stable^{20,21} silver film over nanosphere (AgFON) substrates. Our previous studies have shown that when the localized surface plasmon resonance (LSPR) maximum of a AgFON substrate closely matches the laser excitation wavelength, the maximum SERS signal intensity results.^{18,22} In this study, AgFON surfaces were fabricated using 600 nm spheres in order to optimize SERS intensity for 750 nm laser excitation. We demonstrate a LOD of $\sim 2.6 \times 10^3$ spores with a data acquisition period of 1 min and a laser power of 50 mW. To place these results in context, it should be noted that previous published SERS studies of anthrax detection via the CaDPA biomarker were 200 times less sensitive and required 3 times more laser power.²³ Similarly, previous published NRS studies were 200 000 times less sensitive and required 8 times more laser power.¹⁶ The data presented herein also demonstrate that AgFON substrates provide stable SERS spectra for at least 40 days. Finally, a portable SERS device successfully produces a SERS spectrum from 10^4 spores in 5 s using a 1 month old prefabricated AgFON. This is, to our knowledge, the first reported result that utilizes a compact vibrational spectrometer for the detection of bacillus spores.

Experimental Section

Materials. All of the chemicals used were of reagent grade or better. Ag (99.99%) was purchased from D. F. Goldsmith (Evanston, IL). Glass substrates were 18 mm diameter, No. 2 cover slips from Fisher Scientific (Pittsburgh, PA). Pretreatment of substrates required H₂SO₄, H₂O₂, and NH₄OH, all of which were purchased from Fisher Scientific (Fairlawn, NJ). Surfactant-free white carboxyl-functionalized polystyrene latex nanospheres with diameters of 390, 510, 600, and 720 nm were obtained from Duke Scientific Corporation (Palo Alto, CA) and Interfacial Dynamics Corporation (Portland, OR). Tungsten vapor deposition boats were purchased from R. D. Mathis (Long Beach, CA). Nitric acid 70% (Fisher Scientific), dipicolinic acid (2,6-pyridinedicarboxylic acid, DPA), calcium hydroxide, and benzenethiol (Aldrich Chemical Co., Milwaukee, WI) were used as purchased. Water (18.2 MΩ/cm) was obtained from an ultrafilter system (Milli-Q, Millipore, Marlborough, MA). Calcium dipicolinate (CaDPA) was prepared from DPA and calcium hydroxide according to the method of Beiley and co-workers.¹

Spore Samples. *B. subtilis* was purchased from the American Type Culture Collection (Manassas, VA). Spore cultures were cultivated by spreading the vegetative cells on sterile nutrient agar plates (Fisher Scientific), followed by incubating at 30 °C for 6 days. The cultures were washed from the plates using sterile water and centrifuged at 12 000g for 10 min. The centrifuging procedure was repeated five times. The lyophilized spores were kept at 2–4 °C prior to use. Approximately 1 g of sample was determined to contain 5.6×10^{10} spores by optical microscopic measurements (data not shown). The spore suspension was made by dissolving spores in 0.02 M HNO₃ solution and by sonicating for 10 min.

AgFON Substrate Fabrication. Glass substrates were pretreated in two steps. (1) Piranha etch (*CAUTION: piranha solution should be handled with great care*), 3:1 H₂SO₄/30% H₂O₂ at 80 °C for 1 h, was

- (10) Pellegrino, P. M.; Fell, N. F.; Gillespie, J. B. *Anal. Chim. Acta* **2002**, *455*, 167.
- (11) Beltyukova, S. V.; Poluektov, N. S.; Tochilovskaya, T. L.; Kucher, A. A. *Dokl. Akad. Nauk.* **1986**, *291*, 1392–1395.
- (12) Thompson, S. E.; Forster, N. S.; Johnson, T. J.; Valentine, N. B.; Amonette, J. E. *Appl. Spectrosc.* **2003**, *57*, 893–899.
- (13) Jarvis, M. R.; Goodacre, R. *Anal. Chem.* **2004**, *76*, 40–47.
- (14) Chan, J. W.; Esposito, A. P.; Talley, C. E.; Hollars, C. W.; Lane, S. M.; Huser, T. *Anal. Chem.* **2004**, *76*, 599–603.
- (15) McCreery, R. L. *Raman Spectroscopy for Chemical Analysis*; John Wiley & Sons: New York, 2000; Vol. 157, p 420.
- (16) Farquharson, S.; Grigely, L.; Khitrov, V.; Smith, W.; Sperry, J. F.; Fenerty, G. J. *Raman Spectrosc.* **2004**, *35*, 82–86.
- (17) Schatz, G. C.; Van Duyne, R. P. Electromagnetic Mechanism of Surface-Enhanced Spectroscopy. In *Handbook of Vibrational Spectroscopy*; Chalmers, J. M., Griffiths, P. R., Eds.; Wiley: New York, 2002; Vol. 1, pp 759–774.
- (18) Haynes, C. L.; Van Duyne, R. P. *J. Phys. Chem. B* **2003**, *107*, 7426–7433.

- (19) Dick, L. A.; McFarland, A. D.; Haynes, C. L.; Van Duyne, R. P. *J. Phys. Chem. B* **2002**, *106*, 853–860.
- (20) Zhang, X.; Yonzon, C. R.; Van Duyne, R. P. *Proc. SPIE-Int. Soc. Opt. Eng.* **2003**, *5221*, 82–91.
- (21) Yonzon, C. R.; Haynes, C. L.; Zhang, X.; Walsh, J. T. J.; Van Duyne, R. P. *Anal. Chem.* **2004**, *76*, 78–85.
- (22) McFarland, A. D. Ph.D. Thesis, Northwestern University, 2004.
- (23) Farquharson, S.; Gift, A. D.; Maksymuk, P.; Inscore, F. E. *Appl. Spectrosc.* **2004**, *58*, 351–354.

SERS Measurement of Glucose and Lactate - MR Glucksberg, PI

used to clean the substrate, and (2) base treatment, 5:1:1 H₂O/NH₄OH/30% H₂O₂ with sonication for 1 h was used to render the surface hydrophilic. Approximately 2 μ L of the nanosphere suspension (4% solids) was drop coated onto each substrate and allowed to dry in ambient conditions. The metal films were deposited in a modified Consolidated Vacuum Corporation vapor deposition system with a base pressure of 10^{-6} Torr.²⁴ The deposition rates for each film (10 Å/s) were measured using a Leybold Inficon XTM/2 quartz crystal microbalance (QCM) (East Syracuse, NY). AgFON substrates were stored in the dark at room temperature prior to use.

UV-Vis Diffuse Reflectance Spectroscopy. Measurements were carried out using an Ocean Optics (Dunedin, FL) SD2000 spectrometer coupled to a reflection probe (Ocean Optics) and a halogen lamp (Model F-O-Lite H, World Precision Instruments, Sarasota, FL). The reflection probe consists of a tight bundle of 13 optical fibers (12 illumination fibers around a collection fiber) with a usable wavelength range of 400–900 nm. All reflectance spectra were collected against a mirrorlike Ag film over glass substrate as a reference.

SERS Apparatus. A battery-powered Raman spectrometer (model Inspector Raman, diode laser excitation wavelength $\lambda_{\text{ex}} = 785$ nm) was purchased from DeltaNu (Laramie, WY),²⁵ which was used to demonstrate the feasibility of a field-portable device for spore detection. The remaining data were acquired using a macro-Raman system. This system consists of an interference filter (Coherent, Santa Clara, CA), a 1 in. holographic edge filter (Physical Optics Corporation, Torrance, CA), a single-grating monochromator with the entrance slit set at 100 μ m (model VM-505, Acton Research Corporation, Acton, MA), a liquid-N₂-cooled CCD detector (Model Spec-10:400B, Roper Scientific, Trenton, NJ), and a data acquisition system (Photometrics, Tucson, AZ). A titanium-sapphire laser (CW Ti:Sa, Model 3900, Spectra Physics, Mountain View, CA) pumped by a solid-state diode laser (Model Millennia Vs, Spectra Physics) was used to generate λ_{ex} of 750 nm. All of the measurements were performed in ambient conditions.

Results and Discussion

Optimization of SERS Substrates for Near-Infrared (NIR)

Laser Excitation. One goal of this work is to demonstrate the feasibility of using SERS for rapid detection of the anthrax biomarker, CaDPA, using a low-cost, battery-powered, and portable Raman spectrometer. Typically, such spectrometers use an NIR diode laser as the excitation source. One popular diode laser excitation wavelength is 785 nm. To mimic a 785 nm diode laser, we have used a CW Ti:Sa laser tuned to 750 nm as the laser excitation source. It should also be noted that NIR excitation reduces the native fluorescence background from microorganisms.

Previously, an important correlation between nanoparticle structure, as reported by the spectral position of the LSPR relative to the laser excitation wavelength, and the SERS intensity was demonstrated.^{18,22} The maximum SERS intensity is obtained from a AgFON surface when the laser excitation wavelength coincides with the LSPR maximum. Since AgFONs are not optically transparent, the reflectivity minimum was used to locate the LSPR maximum.

AgFON substrates for SERS measurements using 750 nm laser excitation were optimized by first measuring the dependence of the LSPR spectral position on nanosphere diameter. Figure 1 shows the UV-vis diffuse reflectance spectra of AgFON substrates with nanospheres having diameters of 390, 510, and 600 nm. A AgFON sample was also fabricated using

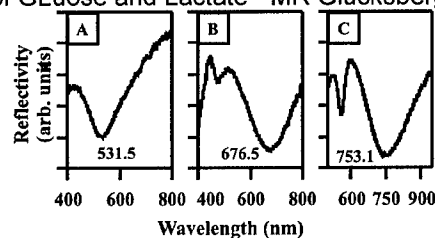


Figure 1. UV-vis diffuse reflectance spectra of different AgFON substrates in air. (A) $D = 390$ nm, $d_m = 200$ nm; (B) $D = 510$ nm, $d_m = 200$ nm; and (C) $D = 600$ nm, $d_m = 200$ nm.

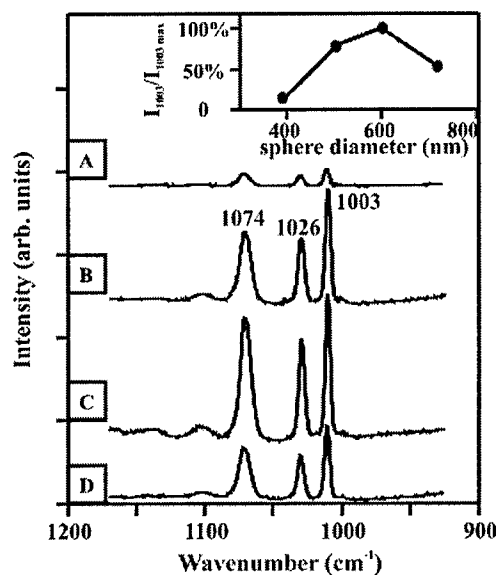


Figure 2. SERS spectra of 20 μ L, 1 mM benzenethiol in ethanol on different AgFON substrates. (A) $D = 390$ nm, $d_m = 200$ nm; (B) $D = 510$ nm, $d_m = 200$ nm; (C) $D = 600$ nm, $d_m = 200$ nm; and (D) $D = 720$ nm, $d_m = 200$ nm. The inset shows the variation of the benzenethiol SERS intensity ratio ($I_{1003}/I_{1003,\text{max}}$) with sphere sizes. $I_{1003,\text{max}}$ is taken from spectrum 2C. For all spectra, $\lambda_{\text{ex}} = 750$ nm, $P_{\text{ex}} = 3$ mW, acquisition time = 1 min.

720 nm diameter spheres; however, the spectrum is not shown because the reflectance minimum is shifted beyond the red limit (~ 900 nm) of the CCD detector. In Figure 1, the reflectance spectrum of AgFON substrate C (nanosphere diameter, $D = 600$ nm, and mass thickness of Ag film, $d_m = 200$ nm) shows a reflectivity minimum near 753 nm, attributable to the excitation of the LSPR of the silver film. This substrate is expected to show the largest intensity for 750 nm laser excitation. To further confirm this expectation, SERS spectra of 1 mM benzenethiol in 20 μ L of ethanol on the AgFON substrates with $D = 390, 510, 600$, and 720 nm (Figure 2) were measured. The largest SERS enhancement of benzenethiol was, in fact, observed from the AgFON with $D = 600$ nm and $d_m = 200$ nm (Figure 2C). Therefore, this AgFON substrate was chosen as optimal for the bacillus spore detection experiments which follow.

Extraction of CaDPA from Spores. CaDPA was extracted from spores by sonicating in 0.02 M HNO₃ solution for 10 min. This concentration of the HNO₃ solution was selected because of its capability of extraction and its benign effect on the AgFON SERS activity. The sonication procedure was performed because no SERS signal of CaDPA was observed from the spore solution prior to sonication (data not shown). To test the efficiency of

(24) Hulteen, J. C.; Van Duyne, R. P. *J. Vac. Sci. Technol. A* **1995**, *13*, 1553–1558.

(25) DeltaNu Company Home Page; <http://www.deltanu.com> (accessed July, 2004).

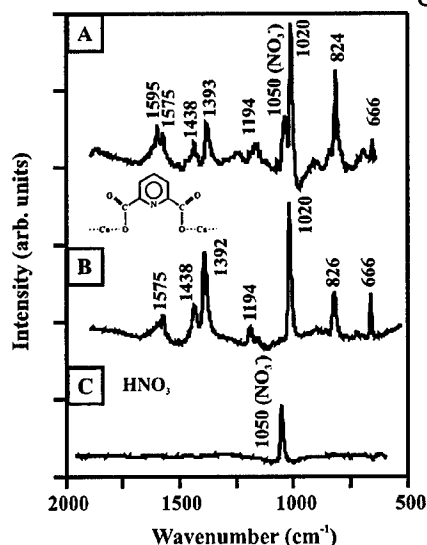


Figure 3. (A) SERS spectrum of 3.1×10^{-13} M spore suspension (3.7×10^4 spores in $0.2 \mu\text{L}$, 0.02 M HNO_3) on a AgFON substrate. (B) SERS spectrum of 5.0×10^{-4} M CaDPA. (C) SERS spectrum of $0.2 \mu\text{L}$ of 0.02 M HNO_3 ; $\lambda_{\text{ex}} = 750 \text{ nm}$, $P_{\text{ex}} = 50 \text{ mW}$, acquisition time = 1 min, $D = 600 \text{ nm}$, $d_{\text{m}} = 200 \text{ nm}$.

this extraction method, a 3.1×10^{-13} M spore suspension (3.7×10^4 spores in $0.2 \mu\text{L}$, 0.02 M HNO_3) was deposited onto a AgFON substrate ($D = 600 \text{ nm}$, $d_{\text{m}} = 200 \text{ nm}$). The sample was allowed to evaporate for less than 1 min. A high signal-to-noise ratio (S/N) SERS spectrum was obtained in 1 min (Figure 3A). For comparison, a parallel SERS experiment was conducted using 5.0×10^{-4} M CaDPA (Figure 3B). The SERS spectrum of *B. subtilis* spores is dominated by bands associated with CaDPA, in agreement with the previous Raman studies on bacillus spores.^{16,23} The SERS spectra in Figure 3, however, display noticeable differences at 1595 cm^{-1} , which are from the acid form of dipicolinate.²⁶ The peak at 1050 cm^{-1} in Figure 3A is from the symmetrical stretching vibration of NO_3^- .²⁷ Because of its prominence, this peak is used as an internal standard to reduce the sample-to-sample deviations.

Temporal Stability of AgFON Substrates. An ideal detection system should run unattended for long periods of time, require infrequent maintenance, and operate at low cost. Previous work has demonstrated that bare AgFON surfaces display extremely stable SERS activity when challenged by negative potentials in electrochemical experiments²⁰ and high temperatures in ultrahigh vacuum experiments.²⁸ In this work, the temporal stability of AgFON substrates was studied over a period of 40 days. SERS spectra of 4.7×10^{-14} M spores (5.6×10^3 spores in $0.2 \mu\text{L}$, 0.02 M HNO_3), well below the anthrax infectious dose of 10^4 spores, were captured on AgFON substrates of different ages (Figure 4). The intensity ratios between the strongest CaDPA peak at 1020 cm^{-1} and the NO_3^- peak at 1050 cm^{-1} (I_{1020}/I_{1050}) were measured to quantitatively compare the AgFON substrates of different ages (shown in Figure 4 inset). Both the CaDPA spectral band positions and intensity patterns remained constant over the course of 40 days,

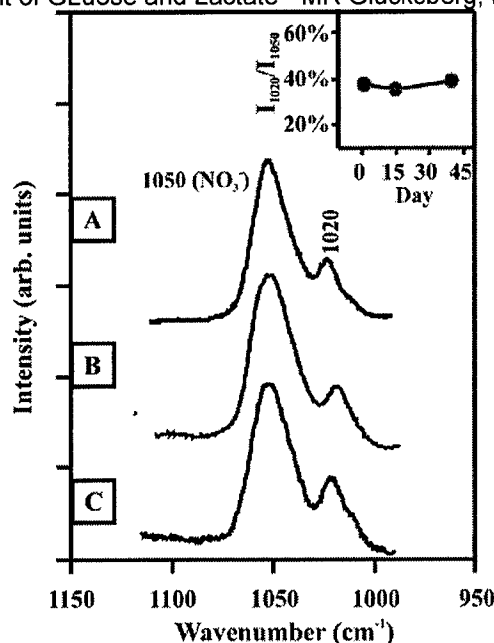


Figure 4. SERS spectra demonstrate the long-term stability of AgFON substrates, monitored for 1–40 days. SERS spectra of 4.7×10^{-14} M spore suspension (5.6×10^3 spores in $0.2 \mu\text{L}$, 0.02 M HNO_3) on AgFON substrates. (A) A 1 day old AgFON, (B) a 15 day old AgFON, and (C) a 40 day old AgFON. The inset shows the intensity ratio (I_{1020}/I_{1050}) variation with time: $\lambda_{\text{ex}} = 750 \text{ nm}$, $P_{\text{ex}} = 50 \text{ mW}$, acquisition time = 1 min, $D = 510 \text{ nm}$, and $d_{\text{m}} = 200 \text{ nm}$.

indicating the long-term stability of the AgFON as SERS substrates for potential field-sensing applications.

Adsorption Isotherm and LOD for Bacillus Spores on AgFON Substrates. The quantitative relationship between SERS signal intensity and spore concentration is demonstrated in Figure 5A. Each data point represents the average intensity at 1020 cm^{-1} from three samples, with the standard deviation shown by the error bars. At low spore concentrations, the peak intensity increases linearly with concentration (Figure 5A inset). At higher spore concentrations, the response saturates as the adsorption sites on the AgFON substrate become fully occupied. Saturation occurs when the spore concentrations exceed $\sim 2.0 \times 10^{-13} \text{ M}$ (2.4×10^4 spores in $0.2 \mu\text{L}$, 0.02 M HNO_3).

To be practical for long-term health and safety monitoring, a SERS-based detection system has to be capable of detecting less than the life-threatening dose of a pathogen in real or near-real time. In this study, the LOD is defined as the concentration of spores for which the strongest SERS signal of CaDPA at 1020 cm^{-1} is equal to 3 times the background SERS signal within a 1 min acquisition period. The background signal refers to the SERS intensity from a sample with a spore concentration equal to 0, which is calculated to be the intercept of the low concentration end of the spore adsorption isotherm (Figure 5A). Although lower detection limits can be achieved using longer acquisition times, these parameters are reasonable for high throughput, real-time, and on-site analysis of potentially harmful species. The LOD for *B. subtilis* spores, evaluated by extrapolation of the linear concentration range of the adsorption isotherms (Figure 5A inset), is found to be $2.1 \times 10^{-14} \text{ M}$ (2.6×10^3 spores in $0.2 \mu\text{L}$, 0.02 M HNO_3). Furthermore, when a similar spore concentration ($2.1 \times 10^{-14} \text{ M}$, 2.6×10^3 spores in $0.2 \mu\text{L}$, 0.02 M HNO_3) is deposited onto a AgFON surface, a

(26) Carmona, P. *Spectrochim. Acta, Part A* **1980**, *36A*, 705–712.

(27) Mosier-Boss, P. A.; Lieberman, S. H. *Appl. Spectrosc.* **2000**, *54*, 1126–1135.

(28) Litorja, M.; Haynes, C. L.; Haas, A. J.; Jensen, T. R.; Van Duyne, R. P. *J. Phys. Chem. B* **2001**, *105*, 6907–6915.

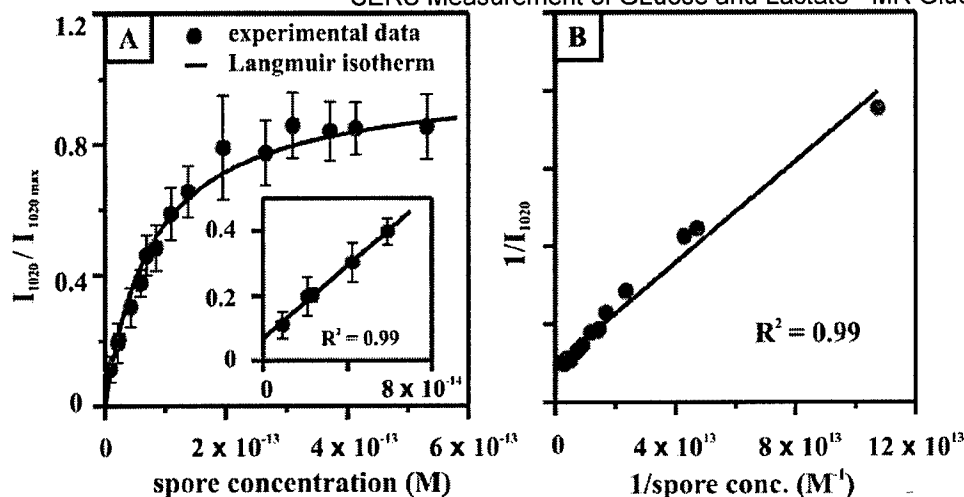


Figure 5. (A) Adsorption isotherm for *B. subtilis* spore suspension onto a AgFON substrate. I_{1020} was taken from SERS spectra that correspond to varying spore concentrations in 0.2 μL of 0.02 M HNO_3 on AgFON substrates; $\lambda_{\text{ex}} = 750$ nm, $P_{\text{ex}} = 50$ mW, acquisition time = 1 min, $D = 600$ nm, and $d_m = 200$ nm. A Langmuir curve was generated using eq 1 with $K_{\text{spore}} = 1.3 \times 10^{13} \text{ M}^{-1}$. The inset shows the linear range that is used to determine the LOD. Each data point represents the average value from three SERS spectra. Error bars show the standard deviations. (B) Adsorption data fit with the linear form of the Langmuir model (eq 2). The slope and intercept values are used to calculate the adsorption constant.

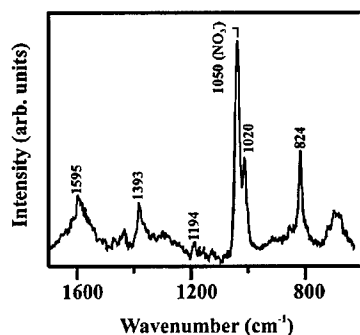


Figure 6. SERS spectrum of $2.1 \times 10^{-14} \text{ M}$ spore suspension (2.6×10^3 spores in 0.2 μL , 0.02 M HNO_3) on AgFON; $\lambda_{\text{ex}} = 750$ nm, $P_{\text{ex}} = 50$ mW, acquisition time = 1 min, $D = 600$ nm, and $d_m = 200$ nm.

1 min acquisition yields a SERS spectrum that clearly displays the spore Raman features at 1595, 1393, 1020, and 824 cm^{-1} (Figure 6). These data clearly demonstrate that the SERS LOD is below the anthrax infectious dose of 10^4 spores.

To determine the adsorption capacity of extracted CaDPA on a AgFON, the Langmuir adsorption isotherm was used to fit the data:^{29,30}

$$\theta = \frac{I_{1020}}{I_{1020, \text{max}}} = \frac{K_{\text{spore}} \times [\text{spore}]}{1 + K_{\text{spore}} \times [\text{spore}]} \quad (1)$$

$$\frac{1}{I_{1020}} = \frac{1}{K_{\text{spore}} \times I_{1020, \text{max}}} \times \frac{1}{[\text{spore}]} + \frac{1}{I_{1020, \text{max}}} \quad (2)$$

where θ is the coverage of CaDPA on the AgFON; $I_{1020, \text{max}}$ is the maximum SERS signal intensity at 1020 cm^{-1} when all the SERS active sites on AgFON are occupied by CaDPA; $[\text{spore}]$ is the concentration of spores (M), and K_{spore} is the adsorption constant of CaDPA extracted from spores on AgFON (M^{-1}). From eq 2, K_{spore} is calculated from the ratio between the intercept and the slope. Slope and intercept analyses of the linear

fit (Figure 5B) lead to the value of the adsorption constant, $K_{\text{spore}} = 1.7 \times 10^{13} \text{ M}^{-1}$.

Adsorption Isotherm and Extraction Efficiency of CaDPA.

Parallel studies of SERS intensities versus CaDPA concentrations indicate that the LOD is $3.1 \times 10^{-6} \text{ M}$ in 0.2 μL , 0.02 M HNO_3 (Figure 7A inset), and the adsorption constant for CaDPA, K_{CaDPA} , is $9.0 \times 10^3 \text{ M}^{-1}$. Under the assumption that there is no influence from the other constituents of spores on the adsorption of CaDPA from spore suspensions, the ratio between K_{spore} and K_{CaDPA} represents the extracted amount of CaDPA. Accordingly, it can be estimated that approximately 1.9×10^9 mol DPA is extracted from 1 mol spores, which corresponds to 3.0% of spore weight. Previous research found that *B. subtilis* spores contain approximately 8.9% DPA by weight.¹ Therefore, the DPA extraction efficiency of 10 min sonication in 0.02 M HNO_3 is $\sim 34\%$.

Use of Field-Portable Raman Spectrometer for Anthrax Detection. The final goal of this project was to demonstrate the use of SERS as a field-portable screening tool by using a compact Raman spectrometer. Many field-sensing applications require the portability and flexibility not available from conventional laboratory scale spectroscopic equipment. As a first step in this direction, the Raman spectrum from 10^4 *B. subtilis* spores dosed onto a 1 month old AgFON substrate was readily acquired using a commercially available portable Raman instrument. A high S/N spectrum was achieved within 5 s (Figure 8A). The SERS peak positions and intensity pattern for the spore sample were similar to those of CaDPA recorded utilizing the same device (Figure 8B). This is the first example of using a compact, portable Raman spectrometer for the detection of bacillus spores. Coupling the portability and ease of use of this type of device with the molecular specificity and spectral sensitivity inherent to SERS, a range of possibilities are now open in the area of detecting bioagents and other chemical threats. In practical field applications of the detection method described, there might be difficulties in collecting *B. anthracis* spores out of the air and dissolving them into a small liquid volume. Most sensor modalities must face this problem.

(29) Jung, L. S.; Campbell, C. T. *J. Phys. Chem. B* **2000**, *104*, 11168–11178.

(30) Jung, L. S.; Campbell, C. T. *Phys. Rev. Lett.* **2000**, *84*, 5164–5167.

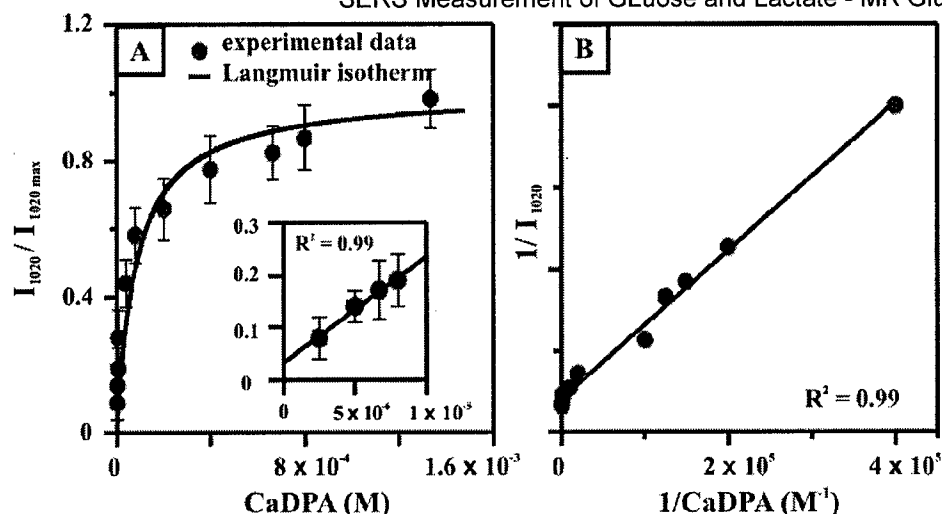


Figure 7. (A) Adsorption isotherm for CaDPA suspension onto a AgFON substrate. I_{1020} was taken from SERS spectra that correspond to varying CaDPA concentrations in 0.2 μL of 0.02 M HNO_3 on AgFON substrates; $\lambda_{\text{ex}} = 750 \text{ nm}$, $P_{\text{ex}} = 50 \text{ mW}$, acquisition time = 1 min, $D = 600 \text{ nm}$, and $d_{\text{m}} = 200 \text{ nm}$. A Langmuir curve was generated using eq 1 with $K_{\text{CaDPA}} = 9.5 \times 10^3 \text{ M}^{-1}$. The inset shows the linear range that is used to determine the LOD. Each data point represents the average value from three SERS spectra. Error bars show the standard deviations. (B) Adsorption data of CaDPA fit with the linear form of the Langmuir model (eq 2). The slope and intercept values are used to calculate the adsorption constant.

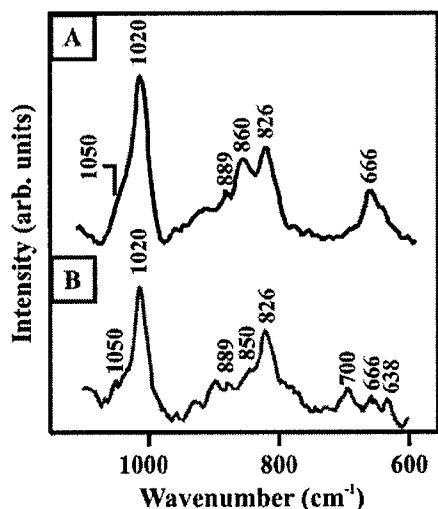


Figure 8. SERS spectra obtained by the portable Raman spectrometer. (A) SERS spectrum of $8.3 \times 10^{-14} \text{ M}$ spore suspension (1.0×10^4 spores in 0.2 μL , 0.02 M HNO_3) on 30 day old AgFON. (B) SERS spectrum of 10^{-4} M CaDPA in 0.2 μL of 0.02 M HNO_3 on 30 day old AgFON substrate; $\lambda_{\text{ex}} = 785 \text{ nm}$, $P_{\text{ex}} = 35 \text{ mW}$, acquisition time = 5 s, resolution = 15 cm^{-1} , $D = 600 \text{ nm}$, and $d_{\text{m}} = 200 \text{ nm}$.

Conclusions

These results represent a significant step toward the real-time detection of anthrax spores using SERS. AgFON surfaces ($D = 600 \text{ nm}$ and $d_{\text{m}} = 200 \text{ nm}$) were determined to be SERS intensity-optimized substrates for 750 nm laser excitation. CaDPA was rapidly extracted from *B. subtilis* spores using a 10 min sonication in 0.02 M HNO_3 , with an extraction efficiency of $\sim 34\%$. The peaks associated with CaDPA dominate the SERS spectrum of spores. The strongest peak of CaDPA at 1020 cm^{-1} was used to measure SERS intensity versus spore concentration profiles that yield an adsorption constant, $K_{\text{spore}} = 1.7 \times 10^{13} \text{ M}^{-1}$. On the basis of the linear portion of the

response curve, the LOD of *B. subtilis* spores was estimated to be $2.1 \times 10^{-14} \text{ M}$ (2.6×10^3 spores in 0.2 μL , 0.02 M HNO_3) for a 1 min data acquisition period. Furthermore, the SERS spectrum of $2.1 \times 10^{-14} \text{ M}$ spore suspension (2.6×10^3 spores in 0.2 μL , 0.02 M HNO_3), well below the anthrax infectious dose of 10^4 spores, was easily measured within this acquisition time. These studies showed a lower LOD of spores and a lower incident laser power (50 mW) than any of the previously reported studies on the detection of bacillus spores based on SERS or NRS. In related experiments,²⁰ we demonstrated that the affinity between silver surfaces and dipicolinate is the key factor to lowering the LOD. Increasing the affinity binding constant by developing an appropriate capture layer on AgFON to preconcentrate CaDPA is an important future goal. The shelf life of AgFON substrates in air at room temperature is shown to exceed 40 days. Finally, preliminary integration of this novel SERS sensor with a field-portable spectrometer shows that it is possible to detect bacillus spores at the desired limit of detection ($\sim 10^4$ spores) within 5 s on a 30 day old AgFON substrate. This experiment demonstrates a necessary but not sufficient result to show the specificity of the *B. anthracis* detection based on SERS. Further confirmation awaits the SERS measurements in the presence of potential interferences.

Acknowledgment. The authors acknowledge Dr. Haitao Ji at Northwestern University for the technical assistance with the *B. subtilis* spore culture. We also are grateful to Dr. Douglas A. Stuart, Dr. Adam D. McFarland, Dr. Amanda J. Haes, and Ms. Chanda R. Yonzon for helpful comments. This research was supported by the National Science Foundation (DMR-0076097), the Air Force Office of Scientific Research MURI program (F49620-02-1-0381), and a Northwestern University MRSEC Fellowship (X.Z.).

JA043623B

Wavelength-Scanned Surface-Enhanced Raman Excitation Spectroscopy

Adam D. McFarland,[†] Matthew A. Young,[†] Jon A. Dieringer, and Richard P. Van Duyne*

Department of Chemistry, Northwestern University, Evanston, Illinois 60208-3113

Received: January 28, 2005; In Final Form: April 8, 2005

A detailed wavelength-scanned surface-enhanced Raman excitation spectroscopy (WS SERES) study of benzenethiol adsorbed on Ag nanoparticle arrays, fabricated by nanosphere lithography (NSL), is presented. These NSL-derived Ag nanoparticle array surfaces are both structurally well-characterized and extremely uniform in size. The WS SERES spectra are correlated, both spatially and spectrally, with the corresponding localized surface plasmon resonance (LSPR) spectra of the nanoparticle arrays. The surface-enhanced Raman scattering (SERS) spectra were measured in two excitation wavelength ranges: (1) 425–505 nm, and (2) 610–800 nm, as well as with the 532-nm line from a solid-state diode-pumped laser. The WS SERES spectra have line shapes similar to those of the LSPR spectra. The maximum SERS enhancement factor is shown to occur for excitation wavelengths that are blue-shifted with respect to the LSPR λ_{max} of adsorbate-covered nanoparticle arrays. Three vibrational modes of benzenethiol (1575, 1081, and 1009 cm^{-1}) are studied simultaneously on one substrate, and it is demonstrated that the smaller Raman shifted peak shows a maximum enhancement closer to the LSPR λ_{max} than that of a larger Raman shifted peak. This is in agreement with the predictions of the electromagnetic (EM) enhancement mechanism of SERS. Enhancement factors of up to $\sim 10^8$ are achieved, which is also in good agreement with our previous SERES studies.

Introduction

Noble metal nanoparticles have gained widespread interest because of their application to chemical and biological sensing,^{1–5} optical device fabrication,^{6–8} and surface-enhanced spectroscopies.^{9–13} The signature optical property of these nanoparticles is the localized surface plasmon resonance (LSPR). The LSPR occurs under conditions where the frequency of photons incident on the nanoparticle is resonant with the collective excitation of its conduction electrons. Excitation of the LSPR is characterized by strong, wavelength-selective extinction¹⁴ and enhanced electromagnetic fields at the nanoparticle surface.¹² It is this field enhancement that is responsible for the observation of all surface-enhanced spectroscopies, and it is the basis for the electromagnetic (EM) enhancement mechanism, which is used to account for the large enhancement in scattering intensity relative to what it would be in the absence of a surface. Surface-enhanced Raman scattering (SERS) is characterized by typical enhancements of 10^6 in the Raman cross section of analytes bound to nanoscale noble metal features, and reports in 1997 of single-molecule detection using SERS have rejuvenated interest in this analytical technique.^{15,16} It is generally accepted that the electromagnetic mechanism of SERS accounts for the majority of the enhancement factors (EF) typically observed; however, a clear understanding of the mechanism responsible for the 10^{14} – 10^{15} enhancement required for the detection of single molecules remains elusive.

Surface-enhanced Raman excitation spectroscopy (SERES) can provide key insights into the mechanism of SERS and could facilitate the understanding of the single-molecule SERS (SM-SERS) phenomenon. Detailed comparison of SERES profiles with the LSPR spectra of SERS substrates could further

substantiate the validity of the EM mechanism and possibly uncover the optical properties of electromagnetic hot spots in nanoparticle aggregates that are hypothesized to be responsible for SMSERS.^{17,18} Even though SERES has the potential to improve the understanding of SERS, less than one percent of SERS literature has focused on this topic. The lack of SERES literature is primarily due to the difficulty of performing a SERES experiment, which generally requires a broadly tunable laser source for excitation and a three-stage spectrometer for efficient rejection of Rayleigh scattered light.

Wavelength-scanned SERES (WS SERES) involves the measurement of SERS enhancement for several laser excitation wavelengths, λ_{ex} . This technique was recognized as a useful tool for probing the EM mechanism immediately following the discovery of SERS. An obvious limitation of this technique is that the number of data points is determined by the tunability of the excitation laser and detection system. These substantial instrumental requirements have led to the majority of SERES publications suffering from low data point density and/or limited spectral coverage.^{19–23} These limitations prevent the establishment of conclusive generalizations from SERES data. Additionally, most SERES experiments have been performed using surface-enhancing substrates with an unknown or poorly characterized distribution of roughness features. In the few cases where the surfaces are carefully characterized, it is shown that there is a wide distribution of roughness feature sizes.^{23,24} Other studies do not include characterization of the LSPR of the substrate,^{19,20} which prevents any direct comparison of the excitation profiles to the spectral location of the LSPR λ_{max} . The most common substrates historically employed in SERES experiments are Ag island films and Ag colloidal solutions. In these cases, the majority of the SERS excitation profiles peak at excitation wavelengths ($\lambda_{\text{ex,max}}$) near 500–600 nm.^{24–28} The peaks of the excitation profiles have been shown to shift to the red with increased aggregation,^{22,24,26,27} which is a qualitative

* To whom correspondence should be addressed. E-mail: vanduyne@chem.northwestern.edu.

[†] These authors contributed equally to this work.

result predicted by the EM mechanism. With these substrates it is difficult to make a direct comparison between the LSPR of the substrate and the SERS excitation profile because the LSPR of the substrate is a superposition of a wide variety of LSPR wavelengths corresponding to the different roughness features.

Two exceptions to the above statements regarding roughness features are the well-known experiments by Liao and co-workers on microlithographically prepared Ag posts²⁹ and recent work by Felidj and co-workers on e-beam lithographically produced arrays of gold elongated nanoparticles.²¹ The former groundbreaking work demonstrated excitation profiles where $\lambda_{\text{ex,max}}$ shifts to the red with increased particle aspect ratio and with increased dielectric constant of the medium surrounding the particles. These results qualitatively agree with the EM mechanism, but the LSPR of these substrates was not measured for a direct comparison. In the latter work, the SERS enhancement was shown to peak at halfway between the excitation wavelength and the wavelength of the Raman scattered photon. This important experiment was the first observation of precisely what is predicted by the EM mechanism. Unfortunately, this result was only obtained on one sample with a profile consisting of only three data points.

The limitation of laser and detection tunability has been circumvented by several researchers using a unique approach that involves investigating substrates with variations in the spectral location of the LSPR λ_{max} .^{30–32} These variations allow investigation of the relationship between the LSPR and SERS enhancement using a single excitation wavelength. Our previous work using plasmon-sampled SERES (PS SERES) on well-defined arrays of nanoparticles was the first systematic study using this technique. The conclusion of that study was that the condition for maximum enhancement occurred when the peak extinction wavelength of the LSPR, λ_{max} , is located between λ_{ex} and the wavelength that is Raman-scattered by the analyte molecules, λ_{vib} . This conclusion supports the EM mechanism, which predicts that maximum SERS intensity is achieved when the LSPR strongly enhances both the incident and scattered photon intensities. However, because of inefficient detection of the Raman scattering, EFs could only be measured down to 1 order of magnitude lower than the peak enhancement. In addition, while this work represented a significant step forward in SERES, the noise levels prevented drawing detailed conclusions from the data.

The work presented herein utilizes a broadly tunable Raman system to measure excitation profiles with the greatest number of data points ever achieved in a WS SERES experiment. A broadly tunable laser system, a versatile detection system, and a well-characterized surface-enhancing substrate are all employed in order to overcome the traditional shortcomings of WS SERES experiments. The use of a CW-modelocked Ti:Sapphire and its harmonics allow for continuous tunability over the spectral ranges 350–500 and 700–1000 nm. The visible region not covered by the Ti:Sapphire system was augmented with the use of a solid-state laser and a tunable dye laser. A triple spectrograph equipped with a CCD camera allows for rapid, multichannel spectral acquisition with efficient rejection of Rayleigh-scattered photons. The SERS substrates used in this work are triangular nanoparticle arrays fabricated by nanosphere lithography (NSL). These substrates have been well characterized by previous work.^{14,33,34} They present a significant advantage over many of the traditional SERS substrates for SERES studies because NSL-fabricated triangular nanoparticles exhibit extremely narrow size distributions, making them an indispen-

SERS Measurement of GLucose and Lactate - MR Glucksberg, PI

sable tool for probing the fundamental characteristics of SERS. Tunability of the LSPR λ_{max} of these nanoparticles throughout the visible and NIR wavelengths can be achieved by systematically varying the dimension of the nanoparticles.¹⁴ Even though the surface coverage of these nanoparticles is $\sim 7\%$, strong SERS intensities are observed from analytes adsorbed to these substrates due to the strong enhancement ($\text{EF} \sim 10^8$, vide infra) NSL-fabricated arrays exhibit.³⁰

The present work demonstrates the most detailed set of WS SERES experiments ever performed on optically and topographically characterized SERS substrates. The relative SERS enhancement of these substrates has been shown to vary by 3 orders of magnitude over the spectral range investigated. It is worth noting that this is not a study on the practical application of SERS for chemical analysis. Factors such as spectrograph throughput, detector efficiency, and the ν^4 scattering dependence of Raman photons play an important role in the practice of Raman spectroscopy. Instead, this study seeks to contribute fundamental insights into the origins of the SERS effect and to test various aspects of the EM mechanism not previously studied. This work demonstrates that for substrates with LSPR λ_{max} values throughout the visible spectrum, the maximum SERS enhancement consistently occurs at excitation wavelengths slightly shorter than the LSPR λ_{max} , such that both the incident photon and the Raman scattered photon are strongly enhanced. The largest EF measured was $\sim 10^8$ for NSL-fabricated nanoparticles, which is consistent with values previously reported using these substrates.

Experimental Methods

Materials. Glass substrates (18-mm diameter, No. 1 coverslips) and cyclohexane were purchased from Fisher Scientific (Hampton, NH). Silicon(111) was purchased from Silicon Quest International (Santa Clara, CA) and cut into $\sim 1.5 \times 1.5$ -cm pieces. Pretreatment of substrates utilized H_2SO_4 , H_2O_2 , and NH_4OH , which were purchased from Fisher Scientific (Pittsburgh, PA). Benzenethiol was purchased from Aldrich (Milwaukee, WI) and used as received. Surfactant-free white carboxyl-substituted polystyrene latex nanospheres were obtained from Interfacial Dynamics (Portland, OR). Ag (99.99%, 0.04-in. diameter) was purchased from D. F. Goldsmith (Evanston, IL), and tungsten vapor deposition boats were purchased from R. D. Mathis (Long Beach, CA). For all steps of substrate preparation, ultrapure water ($18.2 \text{ M}\Omega \text{ cm}^{-1}$) from a Millipore academic system (Marlborough, MA) was used.

Preparation of Nanoparticle Samples. The glass coverslips (for triangular nanoparticle fabrication) used as substrates were pretreated in two steps: (1) piranha etch, 3:1 $\text{H}_2\text{SO}_4/30\% \text{H}_2\text{O}_2$ at 80 °C for 1 h, to clean the substrate, and (2) base treatment, 5:1:1 $\text{H}_2\text{O}/\text{NH}_4\text{OH}/30\% \text{H}_2\text{O}_2$ with sonication for 1 h, to render the surface hydrophilic. After pretreatment of the substrates, 2–3 μL of undiluted nanosphere solution was drop-coated onto the substrates. The substrates were then allowed to dry under ambient conditions, resulting in large areas of close-packed monolayers of nanospheres. Metal films were deposited onto the substrates in a modified Consolidated Vacuum Corporation vapor deposition system with a base pressure of 10^{-7} Torr. Deposition rate and mass thickness were measured using a Leybold Inficon XTM/2 quartz crystal microbalance. The nanospheres were removed from the substrate after the metal deposition by sonicating the samples in ethanol for 5 min. Before the SERS experiments, the samples were incubated in 1 mM benzenethiol in methanol for > 3 h and then rinsed with methanol.

SERES Instrumentation. Figure 1 shows a schematic of the instrumentation used for the SERES experiments. All optical

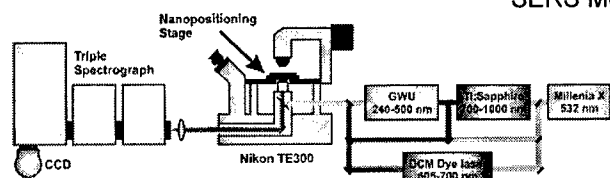


Figure 1. Schematic diagram of the WS SERES apparatus.

measurements were performed using a Nikon Eclipse TE300 inverted microscope (Fryer Co., Huntley, IL) equipped with a 20 \times objective (NA = 0.5). Substrates were mounted on a piezoelectric stage (model P-517.3CD, Polytech PI, Auburn, MA) to allow for sample positioning and raster-scanning during spectral acquisition. The light scattered by the samples was analyzed with a TriplePro three-stage spectrograph equipped with a liquid nitrogen-cooled, deep-depletion Spec-10:400BR CCD detector (Roper Scientific, Trenton, NJ). A color video camera was also attached to the front port of the microscope to facilitate laser alignment and positioning of the samples. Laser excitation was provided by the following systems: (1) a Spectra-Physics (Mountain View, CA) Millennia Xs (λ_{ex} = 532 nm), (2) a Spectra-Physics Tsunami with GWU harmonic generator (λ_{ex} = 350–500, 700–1000 nm), and (3) a Coherent (Santa Clara, CA) model 590 dye laser (λ_{ex} = 610–700 nm). The laser light from the tunable laser systems was filtered using Pellin-Broca prisms or a diffraction grating to ensure monochromatic illumination of the sample. For the NSL-fabricated triangular nanoparticles, in-situ measurement of the LSPR spectrum was achieved by illuminating the sample with the microscope lamp and analyzing the transmitted light with a fiber-optically coupled miniature spectrometer (model SD2000, Ocean Optics, Dunedin, FL). Atomic force micrographs of the SERS substrates were collected in noncontact mode using a Molecular Imaging (Tempe, AZ) PicoPlus microscope.

SERES Methods. During spectral acquisition, the substrates were linearly scanned over a range of 100 μm at a rate of 2 Hz to prevent sample degradation. It is worthwhile to note that all illumination powers reported in this work were the laser powers incident on the microscope beam splitter, not the power incident on the sample. On the basis of experimental measurements, approximately 5–10% of the reported power is incident on the sample; however, because of the intensity standard the absolute power at the sample is not a critical measurement.

To correct for any variation of the SERS intensity not due to the enhancement by the substrate, the 1444 cm^{-1} normal Raman scattering band of neat cyclohexane was used as an intensity standard. This standard was used to correct for the inherent ν^4 behavior of Raman scattering, spectral dependence of the detection system, and differences in the illumination power. This was accomplished by mounting each sample face down as the bottom window of a transparent flow cell. When the flow cell was filled with cyclohexane, the nanoparticle array with an adsorbed benzenethiol monolayer was not in contact with the cyclohexane liquid. In this way, following each SERS acquisition, an intensity standard spectrum of cyclohexane could be taken by translating the inverted microscope objective $\sim 400 \mu\text{m}$ vertically. A schematic depiction of this setup is shown in Figure 2.

Results and Discussion

WS SERES Results. A representative SERS spectrum of benzenethiol on a Ag nanoparticle array is shown in Figure 3. An AFM image of the sample from which this spectrum was taken is shown in the inset. This array was fabricated by

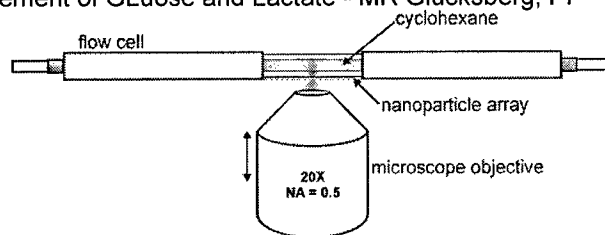


Figure 2. Schematic diagram of flow cell containing cyclohexane for intensity standard measurements.

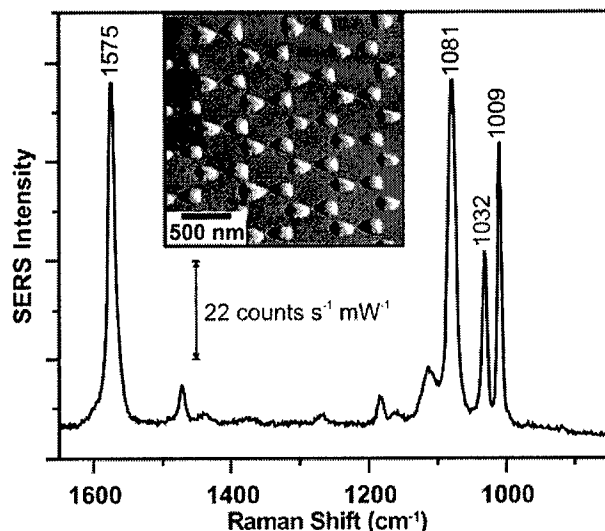


Figure 3. Representative SERS spectrum of benzenethiol-dosed NSL substrate. λ_{ex} = 620 nm, P = 3.0 mW, acquisition time = 150 s. An atomic force micrograph of the sample is shown in the inset.

depositing 55 nm of Ag through a mask formed with 450 nm diameter nanospheres. Figure 4 shows four excitation profiles for the 1575 cm^{-1} peak of benzenethiol, each with an LSPR λ_{max} at a distinctly different location. The SERES profile in Figure 4A consists of 13 data points measured over the spectral range 420–500 nm. Because the formation of a monolayer of benzenethiol on these nanoparticle arrays results in a significant red shift in the position of the LSPR λ_{max} , it was necessary to anneal this sample under vacuum at 300 $^{\circ}\text{C}$ for 1 h prior to benzenethiol addition in order to achieve a final LSPR λ_{max} at a wavelength shorter than 500 nm. It has been previously shown that annealing NSL-derived samples results in a large blue shift of the LSPR due to changing the shape of the nanoparticles.¹⁴ The LSPR λ_{max} of this substrate was measured to be 489 nm (20450 cm^{-1}). The largest SERS enhancement occurs at λ_{ex} = 485 nm. Fitting a Gaussian line shape to the data reveals that the peak of the excitation profile, $\lambda_{\text{ex,max}}$, is 480 nm (20833 cm^{-1}). The peak enhancement factor (EF) value for this sample was calculated to be 5.5×10^5 . This value is low in comparison to the values determined for the other samples because the shape of the nanoparticles is made more ellipsoidal by annealing. In addition to shifting the LSPR λ_{max} to shorter wavelengths, this change decreases the intensity of the electromagnetic fields at the nanoparticle surfaces.

The SERES profile in Figure 4B consists of 14 data points measured over the spectral range 532–690 nm. The LSPR λ_{max} of this substrate was measured to be 663 nm (15083 cm^{-1}). The largest SERS enhancement occurs for λ_{ex} = 625 nm. The maximum of a Gaussian line shape fit to the data is 625 nm (16000 cm^{-1}). The peak EF value for this sample is 1.2×10^7 . The SERES profile in Figure 4C consists of 15 data points measured over the spectral range 532–740 nm. The LSPR λ_{max}

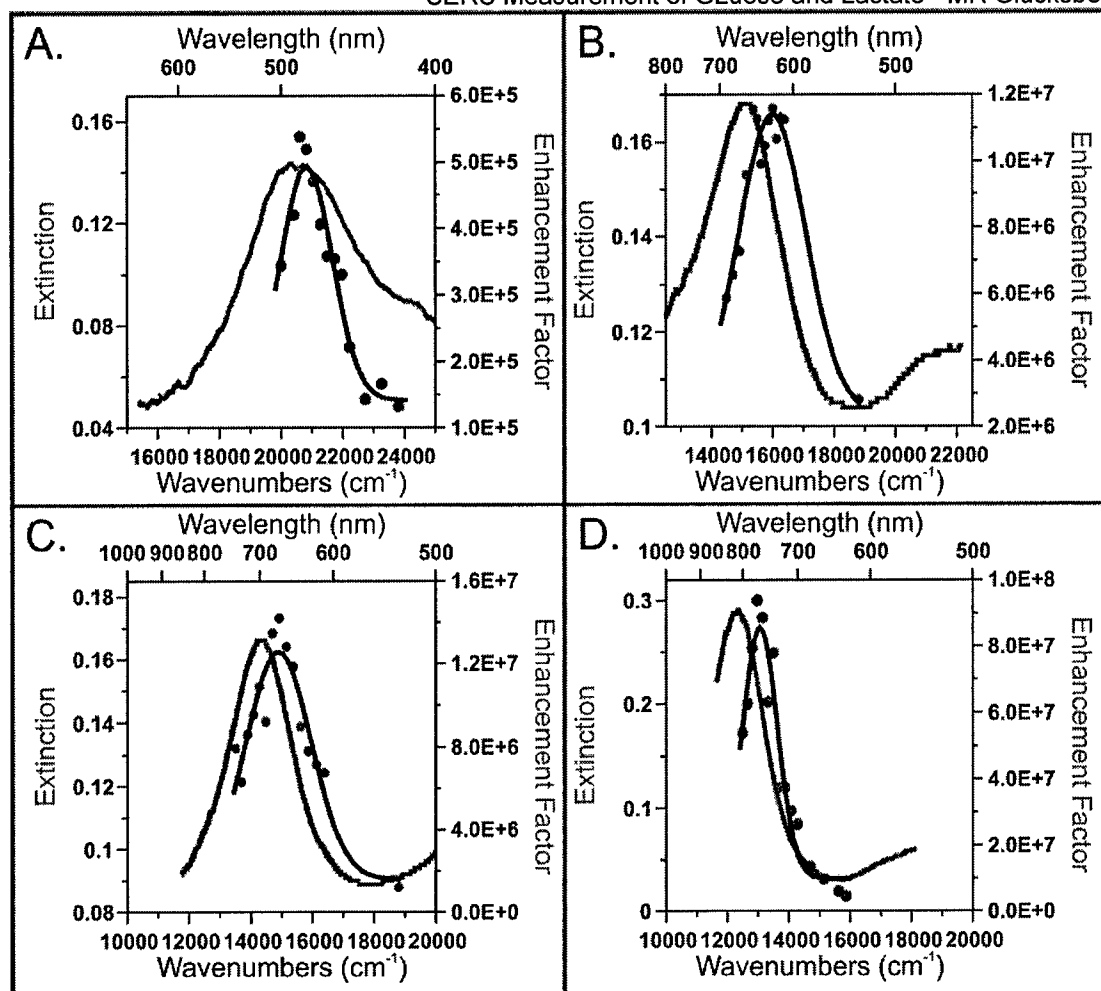


Figure 4. Surface-enhanced Raman excitation spectra of the 1575 cm^{-1} peak of benzenethiol with cyclohexane as intensity standard. (A) Substrate annealed at $300\text{ }^{\circ}\text{C}$ for 1 h. LSPR $\lambda_{\text{max}} = 489\text{ nm}$, profile fit maximum at $\lambda_{\text{ex,max}} = 480\text{ nm}$. (B) LSPR $\lambda_{\text{max}} = 663\text{ nm}$, profile fit maximum at $\lambda_{\text{ex,max}} = 625\text{ nm}$. (C) LSPR $\lambda_{\text{max}} = 699\text{ nm}$, profile fit maximum at $\lambda_{\text{ex,max}} = 671\text{ nm}$. (D) LSPR $\lambda_{\text{max}} = 810\text{ nm}$, profile fit maximum at $\lambda_{\text{ex,max}} = 765\text{ nm}$.

of this substrate was measured to be 699 nm (14306 cm^{-1}). The largest SERS enhancement occurs for $\lambda_{\text{ex}} = 670\text{ nm}$. The maximum of a Gaussian line shape fit to the data is 671 nm (14903 cm^{-1}). The peak EF value for this sample is 1.4×10^7 . The SERES profile in Figure 4D consists of 15 data points measured over the spectral range $630\text{--}800\text{ nm}$. The LSPR λ_{max} of this substrate was measured to be 810 nm (12346 cm^{-1}). The largest SERS enhancement occurs for $\lambda_{\text{ex}} = 770\text{ nm}$. The maximum of a Gaussian line shape fit to the data is 765 nm (13072 cm^{-1}). The peak EF value for this sample is 9.3×10^7 .

To verify that this behavior can be generalized, two SERES experiments were undertaken in which a different benzenethiol band (1081 cm^{-1}) and intensity standard were monitored. In this case, the intensity standard was the 520 cm^{-1} phonon mode of silicon. The wavelength-dependent absorptivity of silicon requires that the measured Raman intensities must be corrected for differences in laser penetration depth. The penetration depth was calculated at all of the excitation wavelengths using the silicon absorptivities measured by Aspnes and Studna.³⁵ The silicon spectra were then normalized so that the intensities were representative of equivalent probe volumes. In addition, a correction was performed to account for the fact that the 520 cm^{-1} band of Si scatters at a significantly different wavelength than the 1081 cm^{-1} band of benzenethiol, particularly at redder excitation wavelengths. No correction was performed to account

for variation in the Raman scattering cross section of silicon because over the range of excitation wavelengths utilized in this work, the differences in the experimentally determined values of the polarizability of silicon are negligible.³⁶ The excitation spectra are shown in Figure 5. The SERES profile in Figure 5A consists of 13 data points measured over the spectral range $475\text{--}700\text{ nm}$. The LSPR λ_{max} of this substrate was measured to be 690 nm (14493 cm^{-1}). The largest SERS enhancement occurs for $\lambda_{\text{ex}} = 660\text{ nm}$. The maximum of a Gaussian line shape fit to the data is 662 nm (15106 cm^{-1}). The peak EF value for this sample is 1.9×10^7 . The SERES profile in Figure 5B consists of 17 data points measured over the spectral range $630\text{--}790\text{ nm}$. The LSPR λ_{max} of this substrate was measured to be 744 nm (13441 cm^{-1}). The largest relative SERS intensity occurs for $\lambda_{\text{ex}} = 700\text{ nm}$. The maximum of a Gaussian line shape fit to the data is 715 nm (13986 cm^{-1}). The peak EF value for this sample is 1.8×10^7 .

Each substrate exhibits a SERES profile that has a similar line shape to the extinction spectrum of the substrate. Also, the $\lambda_{\text{ex,max}}$ for the NSL-fabricated substrates is consistently shorter than the LSPR λ_{max} . In all cases, the maximum SERS enhancement occurs when the substrate LSPR λ_{max} is located between λ_{ex} and λ_{vib} . Under these conditions, both the incident and scattered photons experience enhancement by the LSPR. These

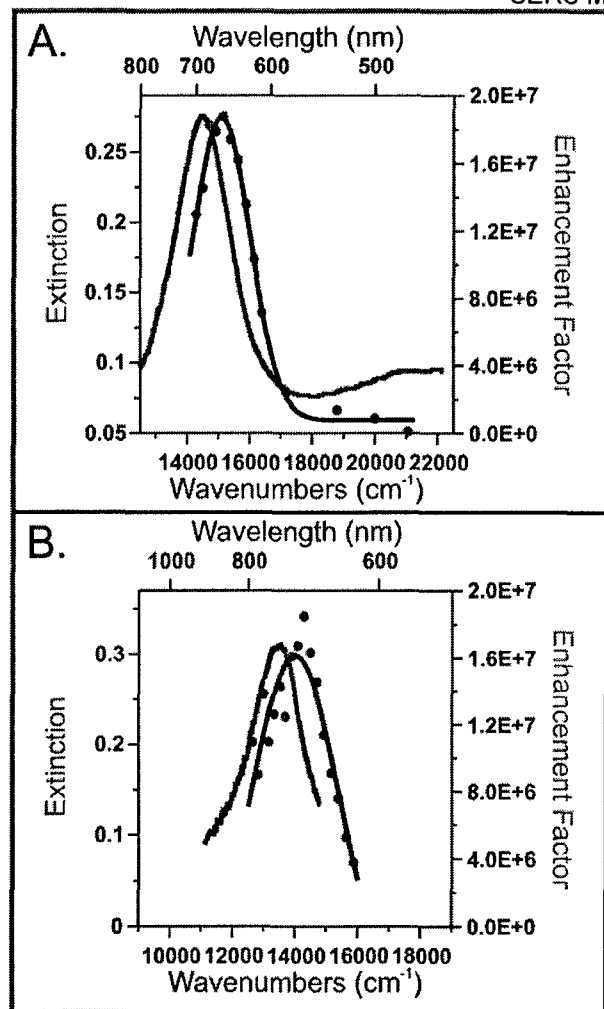


Figure 5. Surface-enhanced Raman excitation spectra of the 1081 cm^{-1} peak of benzenethiol with Si as intensity standard. (A) LSPR $\lambda_{\text{max}} = 690$ nm, profile fit maximum at $\lambda_{\text{ex,max}} = 662$ nm. (B) LSPR $\lambda_{\text{max}} = 744$ nm, profile fit maximum at $\lambda_{\text{ex,max}} = 715$ nm.

data are in accordance with the EM mechanism of SERS and the experimental work performed previously using PS SERES.

If the peak in the SERS enhancement occurs when the LSPR λ_{max} of the sample is equal to $(\lambda_{\text{ex}} + \lambda_{\text{vib}})/2$, then $\lambda_{\text{ex,max}}$ should be different for the various Raman bands of benzenethiol on a single sample. It is expected that $\lambda_{\text{ex,max}}$ will have a larger separation from the LSPR λ_{max} for a large Raman shift than for a small shift. Excitation profiles for three benzenethiol peaks on a single substrate are shown in Figure 6. For this substrate, the LSPR λ_{max} is 729 nm. Figure 6A shows the SERS excitation profile for the 1575 cm^{-1} peak of benzenethiol, normalized to the 1444 cm^{-1} peak of liquid cyclohexane. The separation in wavenumbers between the LSPR λ_{max} and $\lambda_{\text{ex,max}}$ is 734 cm^{-1} . In Figure 6B, the excitation profile for the 1081 cm^{-1} benzenethiol peak (normalized to the 1028 cm^{-1} peak of cyclohexane) is shown. The separation in wavenumbers between the LSPR λ_{max} and $\lambda_{\text{ex,max}}$ is 569 cm^{-1} . Finally, in Figure 6C, the excitation profile for the 1009 cm^{-1} benzenethiol peak (normalized to the 1028 cm^{-1} peak of cyclohexane) is shown, and the separation in wavenumbers between the LSPR λ_{max} and $\lambda_{\text{ex,max}}$ is 488 cm^{-1} . These data demonstrate the qualitative trend whereby the $\lambda_{\text{ex,max}}$ in the excitation spectra of larger Raman shifted bands yield a larger separation from the LSPR λ_{max} than those of smaller Raman shifted bands, and this once again lends support to the EM mechanism.

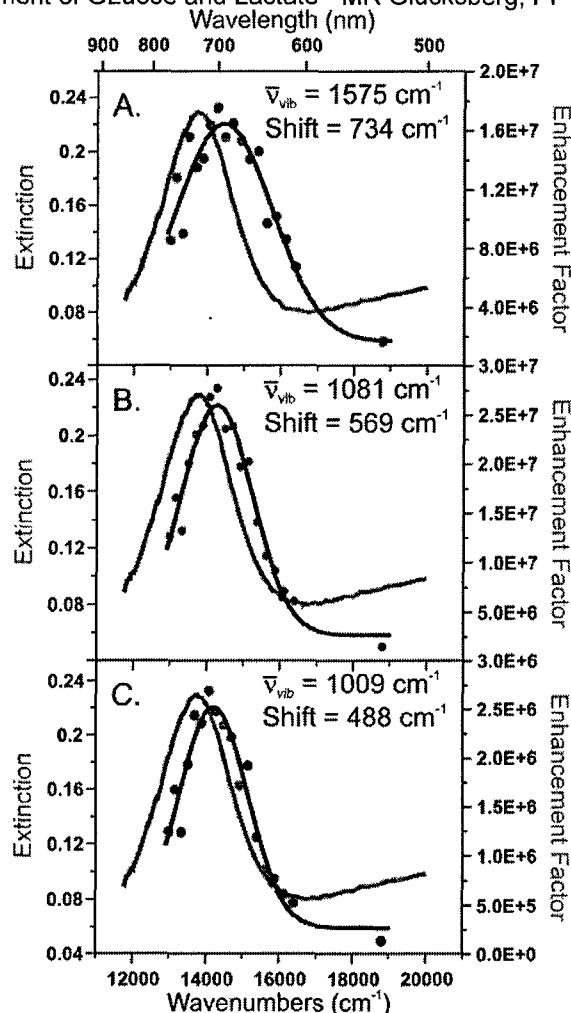


Figure 6. Effect of Stokes Raman shift. (A) Profile of the 1575 cm^{-1} vibrational mode of benzenethiol. Distance between LSPR λ_{max} and excitation profile fit line $\lambda_{\text{ex,max}} = 734$ cm^{-1} . EF = 1.8×10^7 . (B) 1081 cm^{-1} vibrational mode, shift = 569 cm^{-1} , EF = 2.8×10^7 . (C) 1009 cm^{-1} vibrational mode, shift = 488 cm^{-1} , EF = 2.7×10^6 .

Previous work has demonstrated that the spectral location of the LSPR is sensitive to the presence of molecular adsorbates.^{1,4,37} Therefore, it is important to note that the relationship between the LSPR spectra and SERES profiles depicted in Figures 4–6 pertains to LSPR spectra measured after adsorption of the analyte molecule. Figure 7 demonstrates the importance of considering this point. For a bare nanoparticle array, the LSPR λ_{max} was measured to be 672 nm. After incubation in 1 mM benzenethiol for >3 h, thorough rinsing with methanol, and drying, the LSPR λ_{max} was observed to have red-shifted by 57 nm to 729 nm. Measurement of the WS SERES profile yields $\lambda_{\text{ex,max}} = 692$ nm. This is blue-shifted with respect to the LSPR λ_{max} of the adsorbate-covered sample, as observed for the other samples used in this study, but red-shifted with respect to the LSPR λ_{max} of the bare nanoparticle array. This demonstrates that it is critical to characterize the LSPR of a SERS substrate after analyte adsorption in order to choose the appropriate laser excitation wavelength for maximizing EF or to draw any conclusions about the fundamental mechanism of the SERS effect.

SERS Enhancement Factor Calculation. SERS EF values were calculated by comparing the intensity of the appropriate benzenethiol peak (1081 or 1575 cm^{-1}) measured in the SERS experiments to the corresponding peak measured from liquid

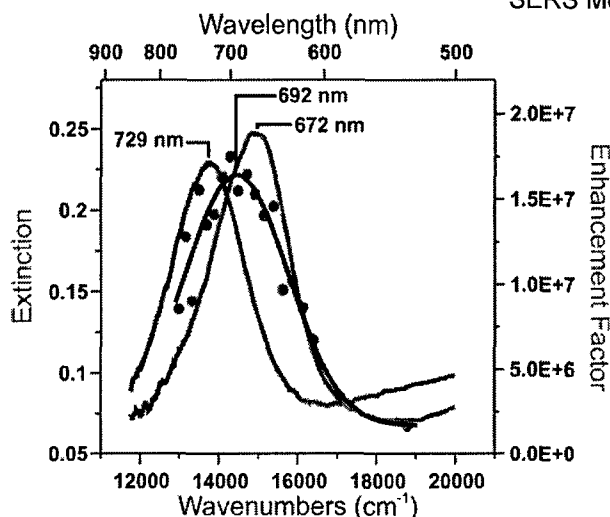


Figure 7. LSPR shift and SERES profile for the 1575 cm⁻¹ peak of benzenethiol. The line with $\lambda_{\text{max}} = 672$ nm is the LSPR extinction of the bare nanoparticle array. The line with $\lambda_{\text{max}} = 729$ nm is the LSPR extinction of the nanoparticle array with an adsorbed monolayer of benzenethiol. The line with $\lambda_{\text{ex,max}} = 692$ nm is the best fit to the SERES data points.

benzenethiol. The normal Raman spectrum was measured at $\lambda_{\text{ex}} = 480, 532$, and 670 nm from a $37 \mu\text{m}$ -thick cell filled with benzenethiol. When the intensities are normalized for laser power and acquisition time, under the same collection conditions, the SERS EF is given by

$$\text{EF} = \frac{N_{\text{vol}} I_{\text{surf}}}{N_{\text{surf}} I_{\text{vol}}}$$

where N_{vol} and N_{surf} are the number of molecules probed in the liquid sample and on the SERS substrates, respectively, and I_{vol} and I_{surf} are the corresponding normal Raman and SERS intensities. On the basis of scanning silicon knife edge measurements, the beam waist of the $20\times$ objective is $4.0 \mu\text{m}$ with $\lambda_{\text{ex}} = 532$ nm. Assuming a benzenethiol packing density of 6.8×10^{14} molecules cm⁻² and the 7.4% surface coverage of nanoparticles, approximately 6.3×10^6 molecules are probed on the triangular nanoparticle array substrates (N_{surf}). For the normal Raman experiment, the probe volume was approximated as a cylinder with a radius of $2.0 \mu\text{m}$ and a height of $37 \mu\text{m}$, resulting in 2.7×10^{12} molecules being probed (N_{vol}). The values for N_{surf} and N_{vol} , along with the SERS intensities for the 1081 and 1575 cm⁻¹ peaks (measured with one of the excitation wavelengths listed above), were substituted into the above equation to calculate the EFs. The peak EF values were calculated by compensating for the differences in the relative SERS intensity measured at $\lambda_{\text{ex,max}}$ versus an excitation wavelength at which a liquid benzenethiol spectrum was measured. Figure 8 shows the spectra necessary for calculating the peak EF for a single SERES profile. This example pertains to the spectrum where $\lambda_{\text{max}} = 810$ nm and $\lambda_{\text{ex,max}} = 765$ nm (Figure 4D). Figure 8A shows the SERS spectrum of benzenethiol on a nanoparticle array taken at $\lambda_{\text{ex}} = 670$ nm. The 1575 cm⁻¹ peak intensity is 22.9 ADU s⁻¹ mW⁻¹ (I_{surf}). Figure 8B shows the normal Raman spectrum of benzenethiol in the $37.0 \mu\text{m}$ -thick cell at $\lambda_{\text{ex}} = 670$ nm. The 1575 cm⁻¹ peak intensity is 0.792 ADU s⁻¹ mW⁻¹ (I_{vol}). When substituted into the EF equation, these values yield an EF of 1.24×10^7 . This EF is for $\lambda_{\text{ex}} = 670$, but because the maximum normalized SERS intensity for this profile was $\lambda_{\text{ex}} = 770$ nm, this value needs to be multiplied by an appropriate

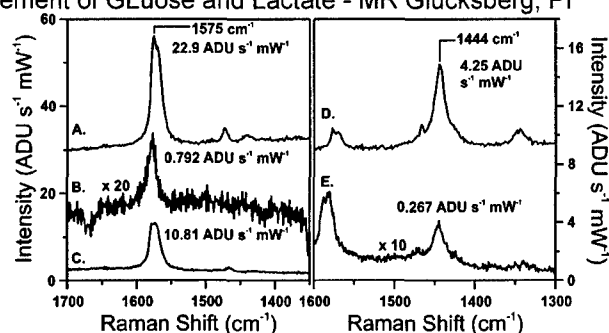


Figure 8. Example of EF calculation. (A) SERS spectrum of benzenethiol on a nanoparticle array at $\lambda_{\text{ex}} = 670$ nm. (B) Raman spectrum of neat benzenethiol at $\lambda_{\text{ex}} = 670$ nm. (C) SERS spectrum of benzenethiol on the same sample as (A) at $\lambda_{\text{ex}} = 770$ nm (the peak of the excitation profile). (D) Raman spectrum of cyclohexane at $\lambda_{\text{ex}} = 670$ nm. (E) Raman spectrum of cyclohexane at $\lambda_{\text{ex}} = 770$ nm.

scale factor to calculate the peak EF. The normalized SERS intensity at $\lambda_{\text{ex}} = 670$ nm is calculated by dividing the SERS intensity of the 1575 cm⁻¹ benzenethiol peak in Figure 8A (22.9 ADU s⁻¹ mW⁻¹) by the normal Raman intensity of the 1444 cm⁻¹ peak of cyclohexane at the same excitation wavelength, Figure 8D (4.25 ADU s⁻¹ mW⁻¹), yielding a relative intensity of 5.39. The normalized SERS intensity at $\lambda_{\text{ex}} = 770$ nm is calculated by dividing the intensity in Figure 8C (10.81 ADU s⁻¹ mW⁻¹) by that in Figure 8E (0.267 ADU s⁻¹ mW⁻¹), which yields a relative intensity of 40.4. Therefore, the normalized SERS intensity at $\lambda_{\text{ex}} = 770$ nm is larger than that at $\lambda_{\text{ex}} = 670$ nm by a factor of $40.4/5.39 = 7.50$. Multiplying the EF value at $\lambda_{\text{ex}} = 670$ nm by this factor yields a peak EF of 9.3×10^7 . This value, the largest peak EF in this study, was measured from the substrate with the longest-wavelength LSPR λ_{max} . The values for EF reported in this paper are conservative estimates because the probe volume assumed for the normal Raman experiment is likely to be an underestimation of the actual value. Also, the calculated number of adsorbate molecules is most likely an overestimation because the calculation assumes perfect array formation. The nanoparticle arrays contain a small number of defects, which can be assumed to contribute little to the observed characteristics of the SERES profiles. If Raman scattering from the defects were contributing significantly, it is unlikely that the systematic trends demonstrated by this work would be observed. Even with consideration of these points, the peak EF calculated for the triangular nanoparticle arrays is consistent with the average values reported in other experimental work using these same substrates³⁰ and theoretical modeling of triangular Ag nanoparticles.³⁸

Conclusions

This work demonstrates the most thorough WS SERES experiments ever performed on optically and topographically characterized SERS substrates. The experimental apparatus utilized has proven effective for the measurement of relative SERS enhancements that vary by 3 orders of magnitude. This work demonstrates that the relationship between the substrate LSPR and the SERES profile for size-homogeneous nanoparticles is consistent throughout the visible range. In all cases, the experimentally observed behavior is consistent with that predicted by the EM mechanism. Specifically, the strongest SERS enhancement occurs under conditions where the incident and Raman scattered photons are both strongly enhanced. The largest EF measured was $\sim 10^8$ for the triangular nanoparticle arrays studied. Ultimately, refinement of the experimental

apparatus and optimization of SERS enhancement will allow SERES to be performed using single nanoparticle substrates. This level provides the best possible case in terms of reducing sample heterogeneity. These experiments are expected to provide key information to validate the EM mechanism of SERS and will present an additional technique that can be used to study the SMSERS effect.

Acknowledgment. The authors gratefully acknowledge support from the Air Force Office of Scientific Research MURI program (Grant F49620-02-1-0381) and the National Science Foundation (EEC-0118025, DMR-0076097, CHE-0414554, DGE-0114429).

References and Notes

- (1) McFarland, A. D.; Van Duyne, R. P. *Nano Lett.* **2003**, *3*, 1057–1062.
- (2) Kim, Y.; Johnson, R. C.; Hupp, J. T. *Nano Lett.* **2001**, *1*, 165–167.
- (3) Haes, A. J.; Stuart, D. A.; Nie, S.; Van Duyne, R. P. *J. Fluoresc.* **2004**, *14*, 355–367.
- (4) Malinsky, M. D.; Kelly, K. L.; Schatz, G. C.; Van Duyne, R. P. *J. Am. Chem. Soc.* **2001**, *123*, 1471–1482.
- (5) Riboh, J. C.; Haes, A. J.; McFarland, A. D.; Yonzon, C. R.; Van Duyne, R. P. *J. Phys. Chem. B* **2003**, *107*, 1772–1780.
- (6) Flaugh, P. L.; O'Donnell, S. E.; Asher, S. A. *Appl. Spectrosc.* **1984**, *38*, 847–850.
- (7) Asher, S. A.; Chang, S.-Y.; Tse, A.; Liu, L.; Pan, G.; Wu, Z.; Li, P. *Mater. Res. Soc. Symp. Proc.* **1995**, *374*, 305–310.
- (8) Lidorikis, E.; Li, Q.; Soukoulis, C. M. *Phys. Rev. E* **1997**, *55*, 3613–3618.
- (9) Zou, S.; Williams, C. T.; Chen, E. K. Y.; Weaver, M. J. *J. Am. Chem. Soc.* **1998**, *120*, 3811–3812.
- (10) Pipino, A. C. R.; Schatz, G. C.; Van Duyne, R. P. *Phys. Rev. B* **1994**, *49*, 8320–8330.
- (11) Yang, W.-H.; Hulteen, J.; Schatz, G. C.; Van Duyne, R. P. *J. Chem. Phys.* **1996**, *104*, 4313–4323.
- (12) Schatz, G. C.; Van Duyne, R. P. Electromagnetic Mechanism of Surface-Enhanced Spectroscopy. In *Handbook of Vibrational Spectroscopy*; Chalmers, J. M., Griffiths, P. R., Eds.; Wiley: New York, 2002; Vol. 1, pp 759–774.
- (13) Schmidt, J. P.; Cross, S. E.; Buratto, S. K. *J. Chem. Phys.* **2004**, *121*, 10657–10659.
- (14) Jensen, T. R.; Malinsky, M. D.; Haynes, C. L.; Van Duyne, R. P. *J. Phys. Chem. B* **2000**, *104*, 10549–10556.
- (15) Nie, S.; Emory, S. R. *Science* **1997**, *275*, 1102–1106.
- (16) Kneipp, K.; Wang, Y.; Kneipp, H.; Perelman, L. T.; Itzkan, I.; Dasari, R. R.; Feld, M. S. *Phys. Rev. Lett.* **1997**, *78*, 1667–1670.
- (17) Michaels, A. M.; Jiang, J.; Brus, L. *J. Phys. Chem. B* **2000**, *104*, 11965–11971.
- (18) Jiang, J.; Bosnick, K.; Maillard, M.; Brus, L. *J. Phys. Chem. B* **2003**, *107*, 9964–9972.
- (19) Vlckova, B.; Gu, X. J.; Moskovits, M. *J. Phys. Chem. B* **1997**, *101*, 1588–1593.
- (20) Gregory, B. W.; Clark, B. K.; Standard, J. M.; Avila, A. J. *Phys. Chem. B* **2001**, *105*, 4684–4689.
- (21) Felidj, N.; Aubard, J.; Levi, G.; Krenn, J. R.; Hohenau, A.; Schider, G.; Leitner, A.; Aussenegg, F. R. *Appl. Phys. Lett.* **2003**, *82*, 3095–3097.
- (22) Blatchford, C. G.; Campbell, J. R.; Creighton, J. A. *Surf. Sci.* **1982**, *120*, 435–455.
- (23) Van Duyne, R. P.; Hulteen, J. C.; Treichel, D. A. *J. Chem. Phys.* **1993**, *99*, 2101–2115.
- (24) Von Raben, K. U.; Chang, R. K.; Laube, B. L.; Barber, P. W. *J. Phys. Chem.* **1984**, *88*, 5290–5296.
- (25) Weitz, D. A.; Garoff, S.; Gramila, T. J. *Opt. Lett.* **1982**, *7*, 168–170.
- (26) Kerker, M.; Siiman, O.; Wang, D. S. *J. Phys. Chem.* **1984**, *88*, 3168–3170.
- (27) Fornasiero, D.; Grieser, F. J. *J. Chem. Phys.* **1987**, *87*, 3213–3217.
- (28) Feilchenfeld, H.; Siiman, O. *J. Phys. Chem.* **1986**, *90*, 2163–2168.
- (29) Liao, P. F.; Bergman, J. G.; Chemla, D. S.; Wokaun, A.; Melngailis, J.; Hawryluk, A. M.; Economou, N. P. *Chem. Phys. Lett.* **1981**, *82*, 355–359.
- (30) Haynes, C. L.; Van Duyne, R. P. *J. Phys. Chem. B* **2003**, *107*, 7426–7433.
- (31) Weimer, W. A.; Dyer, M. J. *Appl. Phys. Lett.* **2001**, *79*, 3164–3166.
- (32) Oldenburg, S. J.; Westcott, S. L.; Averitt, R. D.; Halas, N. J. *J. Chem. Phys.* **1999**, *111*, 4729–4735.
- (33) Hulteen, J. C.; Treichel, D. A.; Smith, M. T.; Duval, M. L.; Jensen, T. R.; Van Duyne, R. P. *J. Phys. Chem. B* **1999**, *103*, 3854–3863.
- (34) Haynes, C. L.; Van Duyne, R. P. *J. Phys. Chem. B* **2001**, *105*, 5599–5611.
- (35) Aspnes, D. E.; Studna, A. A. *Phys. Rev. B* **1983**, *27*, 985–1009.
- (36) Grimsditch, M.; Cardona, M. *Phys. Status Solidi B* **1980**, *102*, 155–161.
- (37) Haes, A. J.; Van Duyne, R. P. *J. Am. Chem. Soc.* **2002**, *124*, 10596–10604.
- (38) Hao, E.; Schatz, G. C. *J. Chem. Phys.* **2004**, *120*, 357–366.

Plasmonic Materials for Surface-Enhanced Sensing and Spectroscopy

Amanda J. Haes, Christy L. Haynes,
Adam D. McFarland, George C. Schatz,
Richard P. Van Duyne, and Shengli Zou

Abstract

Localized surface plasmon resonance (LSPR) excitation in silver and gold nanoparticles produces strong extinction and scattering spectra that in recent years have been used for important sensing and spectroscopy applications. This article describes the fabrication, characterization, and computational electrodynamics of plasmonic materials that take advantage of this concept. Two applications of these plasmonic materials are presented: (1) the development of an ultrasensitive nanoscale optical biosensor based on LSPR wavelength-shift spectroscopy and (2) the use of plasmon-sampled and wavelength-scanned surface-enhanced Raman excitation spectroscopy (SERES) to provide new insight into the electromagnetic-field enhancement mechanism.

Keywords: *localized surface plasmon resonance spectroscopy, nanosensing, plasmonic materials, surface-enhanced Raman spectroscopy.*

Introduction

Plasmonics is an emerging branch of nanophotonics that examines the properties of the collective electronic excitations in noble metal films or nanoparticles known colloquially as surface plasmons. The excitement of plasmonics lies in its potential to achieve highly miniaturized and sensitive photonic devices by controlling, manipulating, and amplifying light on the nanometer length scale.¹⁻³

To date, a variety of passive plasmonic devices have been demonstrated, including filters,¹ waveguides,^{1,3} polarizers,⁴ Bragg reflectors,¹ and nanoscopic light sources.⁵ On the horizon are active plasmonic devices, such as light-output enhancers for organic light-emitting diodes^{6,7} as well as switches and modulators.⁸ Furthermore, our rapidly improving understanding of the interactions between adsorbed molecules and plasmonic nanostructures (i.e., molecular plasmonics)⁹ is having a significant impact on a broad spectrum of other

applications, including nanoscale optical spectroscopy,¹⁰ surface-enhanced Raman spectroscopy,¹¹ surface plasmon resonance sensing,^{12,13} and nanolithography.¹⁴

There are two types of surface plasmon resonance—localized and propagating. This article will mostly be concerned with the former, which we term localized surface plasmon resonance (LSPR). This occurs in silver and gold nanoparticles in the 10–200 nm size range and results in amplification of the electric field E near the particle surfaces such that $|E|^2$ can be 100–10,000 times greater in intensity than the incident field. The field has a spatial range on the order of 10–50 nm and is strongly dependent on nanoparticle size, shape, and local dielectric environment. Propagating plasmons, which are often called surface plasmon polaritons (SPPs), are associated with smooth, thin films of silver and gold with thicknesses in the 10–200 nm range. Propagating plasmons

lead to smaller field enhancements (10–100 times) and a larger spatial range (~1000 nm).

This article will focus on the fabrication and characterization of plasmonic materials that show promise in chemical/biological sensing and surface-enhanced spectroscopy applications. In the first part, the simple, massively parallel method of nanosphere lithography (NSL) and its use in the fabrication of size- and shape-controlled nanostructures is briefly reviewed. Also, the essential physics of LSPR and the theoretical methods used to understand it are described, and key results concerning the short- and long-range distance dependences of the electromagnetic fields surrounding the nanoparticles are summarized. In the second part of this article, we focus on the relationship between LSPR spectroscopy and surface-enhanced Raman spectroscopy (SERS), as revealed by surface-enhanced Raman excitation spectroscopy (SERES). SERES provides a systematic, reproducible way to optimize the signal intensity in SERS experiments.

Nanosphere Lithography

Nanosphere lithography (NSL)¹⁵ is a surprisingly powerful yet simple approach to the fabrication of nanoparticle arrays with precisely controlled shape, size, and interparticle spacing.

Nanosphere lithography (Figure 1) begins with the self-assembly of monodisperse polystyrene or SiO₂ nanospheres of diameter D to form a single- or double-layer colloidal crystal mask for material deposition. A substrate (Figure 1a) is prepared so that the nanospheres can freely move until they reach their lowest energy configuration. This is achieved by chemically modifying the nanosphere surface with a negative charge that is electrostatically repelled by a negatively charged substrate such as mica or chemically treated glass. As the solvent (water) evaporates, capillary forces draw the nanospheres together, and they crystallize into an hcp pattern on the substrate. As in all naturally occurring crystals, nanosphere masks include a variety of defects that arise as a result of nanosphere polydispersity, site randomness, point defects (vacancies), line defects (slip dislocations), and polycrystalline domains. Typical defect-free domain sizes are in the 10–100 μm range. Following self-assembly of the nanosphere mask, a metal or other material is then deposited by physical vapor deposition from a collimated source normal to the substrate through the nanosphere mask to a controlled thickness. The resulting surface is referred to as a metal (e.g., Ag) "film over nanosphere" (FON) surface. Ag FON surfaces are robust plasmonic materials for

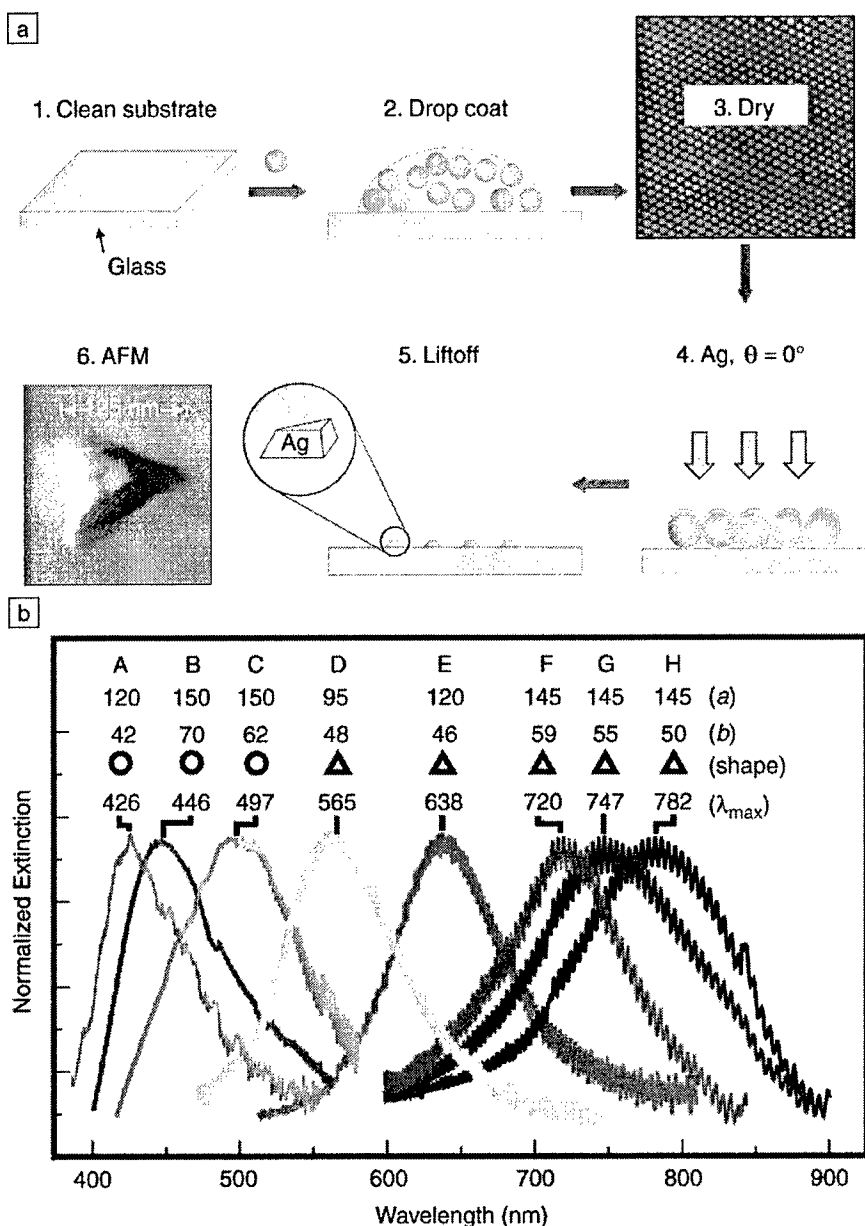


Figure 1. (a) Schematic representation of the nanosphere lithography (NSL) fabrication process. The AFM image in step 3 is 5 $\mu\text{m} \times 5 \mu\text{m}$. (b) Size- and shape-tunable localized surface plasmon resonance spectra of various Ag nanoparticles (labeled A–H) fabricated by NSL. The wavelength of maximum extinction, λ_{max} , is changed by varying the in-plane width a and out-of-plane height b of the nanoparticles.

SERS applications.^{16,17} If the nanosphere mask is removed, typically by sonicating the entire sample in a solvent, surface-confined nanoparticles are left behind that have a triangular footprint. In a typical NSL process, the deposition of 50 nm of Ag over a single-layer mask self-assembled from nanospheres with $D = 400$ nm produces nanotriangles with an in-plane width

$a \approx 100$ nm, height $b \approx 50$ nm, and interparticle separation distance $d_{\text{ip}} \approx 230$ nm.

Size- and Shape-Tunable Localized Surface Plasmon Resonance Spectra

NSL-derived nanoparticles exhibit intense UV–visible extinction (i.e., the sum of absorption and scattering) bands that are

not present in the spectrum of the bulk metal. Figure 1b shows that the LSPR spectra can easily be tuned all the way from the near-UV through the visible spectrum¹⁸ and even into the mid-IR¹⁹ by changing the size or shape (triangle or hemisphere) of the nanoparticles. Note that the LSPR bandwidth does not change significantly as the wavelength at peak maximum, λ_{max} , is tuned. Additionally, several other surprising LSPR optical properties have been discovered for NSL-derived Ag nanoparticles: (1) λ_{max} shifts by 2–6 nm per 1 nm variation in nanoparticle width or height,¹⁸ (2) the molar decadic (tenfold) extinction coefficient is $\epsilon = 3 \times 10^{11} \text{ M}^{-1} \text{ cm}^{-1}$,¹⁸ (3) the LSPR oscillator strength per atom is equivalent to that of atomic silver in gas or liquid phases,¹⁸ (4) resonant Rayleigh scattering^{20,21} occurs with an efficiency equivalent to that of 10^6 fluorophores,²² and (5) local electromagnetic fields are amplified by factors of $|E|^2 \approx 10^4$, leading to intense signals in all surface-enhanced spectroscopies.¹¹

Fundamentals of Localized Surface Plasmon Resonance Spectroscopy

The simplest theoretical approach available for modeling the optical properties of nanoparticles is classical electrodynamics (i.e., solving Maxwell's equations with the metal dielectric constant taken from bulk measurements). For spherical particles, this leads to the following (Mie theory) expression for the extinction coefficient $E(\lambda)$ in the long-wavelength limit:²³

$$E(\lambda) = \frac{24\pi N_A a^3 \epsilon_m^{3/2}}{\lambda \ln(10)} \times \left[\frac{\epsilon_r}{(\epsilon_r + 2\epsilon_m)^2 + \epsilon_i^2} \right] \quad (1)$$

Here, N_A is the areal density of the nanoparticles, a is the radius of the metallic nanosphere, ϵ_m is the dielectric constant of the medium surrounding the nanosphere (assumed to be a positive, real number), λ is the wavelength, and ϵ_r and ϵ_i are the real and imaginary parts of the metal dielectric function. This formula predicts a resonant peak when $\epsilon_r = -2\epsilon_m$, which for silver and gold occurs in the visible portion of the spectrum. In addition, any change in the dielectric constant of the medium (e.g., when molecules adsorb on the particle) leads to a change in the resonance wavelength.

When one considers spheroidally shaped particles, the term $\epsilon_r + 2\epsilon_m$ in the denominator in Equation 1 is replaced by $\epsilon_r + \chi\epsilon_m$, where χ is a parameter that depends on the shape of the spheroid, increasing from 2 for a sphere to 17 for a spheroid with an aspect ratio of 5:1. This leads to strong de-

pendence of λ_{\max} on particle shape, and there is also a strong size dependence that arises from electrodynamic effects that are not contained in Equation 1. In addition, many of the samples considered in this work contain an ensemble of nanoparticles that are supported on a substrate, leading to a dependence on interparticle spacing² and substrate dielectric constant.²⁴

Electrodynamic Calculations

Equation 1 provides useful insight, but it only applies to spherical particles. In order to describe particles like those pictured in Figure 1a, it is necessary to use a numerical method. Several methods have been developed for solving Maxwell's equations using finite-element-based approaches, and one that we have found to be particularly useful is the discrete dipole approximation (DDA).^{25–27} In this method, the particle is subdivided into an array of cubical, polarizable elements. When a plane wave field is applied to the particle, the resulting induced polarizations in the elements are calculated, and from these the extinction and local fields are determined. Figure 2a shows extinction cross sections that have been calculated with this approach for several particle shapes, all for silver particles with the same volume. This shows that a sphere has a plasmon nearer the blue end of the spectrum (Figure 2b), and the particles with points (cubes, prisms, pyramids) are nearer the red end of the spectrum (Figures 2c and 2d).

The electromagnetic (EM) mechanism of SERS¹¹ predicts an enhancement factor proportional to $|E(\omega)|^2 |E(\omega')|^2$, where ω and ω' are the incident and Stokes-shifted frequencies, respectively. To estimate the enhancement factor, in Figures 2b–2d we show contours of $|E|^2$ around three of the particles for wavelengths corresponding to λ_{\max} and for polarizations that lead to the largest $|E|^2$. These figures show that the peak field for a sphere is on the order of 10^2 , while that for the tetrahedron is 10^4 . If we approximate the enhancement factor as $|E(\omega)|^4$, we see that the highest enhancements are on the order of 10^8 , which, as noted later, is about what is found for NSL-derived particles.

Distance Dependence of the Localized Surface Plasmon Resonance

The electrodynamic results in Figure 2 show that the electromagnetic fields surrounding Ag nanoparticles excited at λ_{\max} drop off quickly as one moves a few nanometers away from the particle surface. How can the range of these fields be measured experimentally? Scanning near-field optical microscopy is certainly a pos-

sibility; however, the resolution currently obtainable (~ 10 nm) would only provide a rough picture.

We have pursued an alternative strategy to experimentally measure the range of the electromagnetic fields. It is apparent from Equation 1 that λ_{\max} of noble metal nanoparticles is highly dependent on the dielectric properties of the surrounding environment. For NSL-derived Ag nanoparticles, it has been demonstrated experimentally that λ_{\max} is a linear function of the solvent refractive index, n_m (where the external dielectric constant, ϵ_m , is equal to n_m^2) with a slope of approximately 200 nm per refractive index unit (RIU, defined as a change of 1 in the refractive index).²⁸ In addition, λ_{\max} is responsive to molecule-induced changes in the local dielectric environment. For example, the chemisorption of one monolayer of hexadecanethiol causes λ_{\max} of a NSL-derived Ag nanotriangle (in-

plane width $a = 100$ nm, out-of-plane height $b = 50$ nm) to shift by $\Delta\lambda_{\max} = 40$ nm (Figure 3a).^{29,30}

The chemisorption-induced LSPR shift experiment provides a method for probing the short-range (~ 0.5 – 3.5 nm) distance dependence of the electromagnetic fields surrounding NSL-derived nanoparticles. Figure 3c demonstrates that the dependence of $\Delta\lambda_{\max}$ on the chain length of an alkanethiol monolayer is linear with a remarkably large slope of 3.1 nm per CH_2 unit.^{29,30} These results can be interpreted using a model of the refractive-index response of propagating SPPs on a planar noble metal surface:³¹

$$\Delta\lambda_{\max} = m\Delta n[1 - \exp(-2d/l_d)], \quad (2)$$

where $\Delta\lambda_{\max}$ is the wavelength shift, m is the refractive-index sensitivity, Δn is the change in refractive index induced by

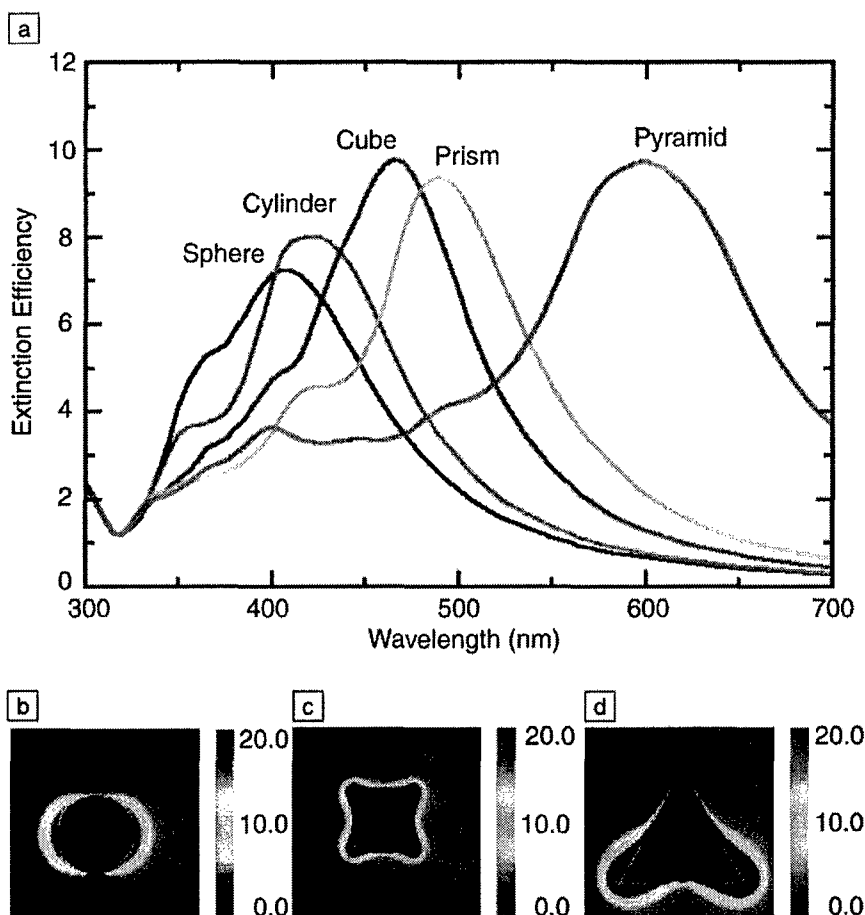


Figure 2. (a) Extinction efficiency (ratio of cross section to effective area) of silver nanoparticles in vacuum having the shapes indicated. Each particle has the same volume, taken to be that of a sphere with a radius of 50 nm. $|E|^2$ contours (E is electric field) for a (b) sphere, (c) cube, and (d) pyramid, plotted for wavelengths corresponding to the plasmon peak in (a), with peak $|E|^2$ values of 54, 745, and 9770, respectively.

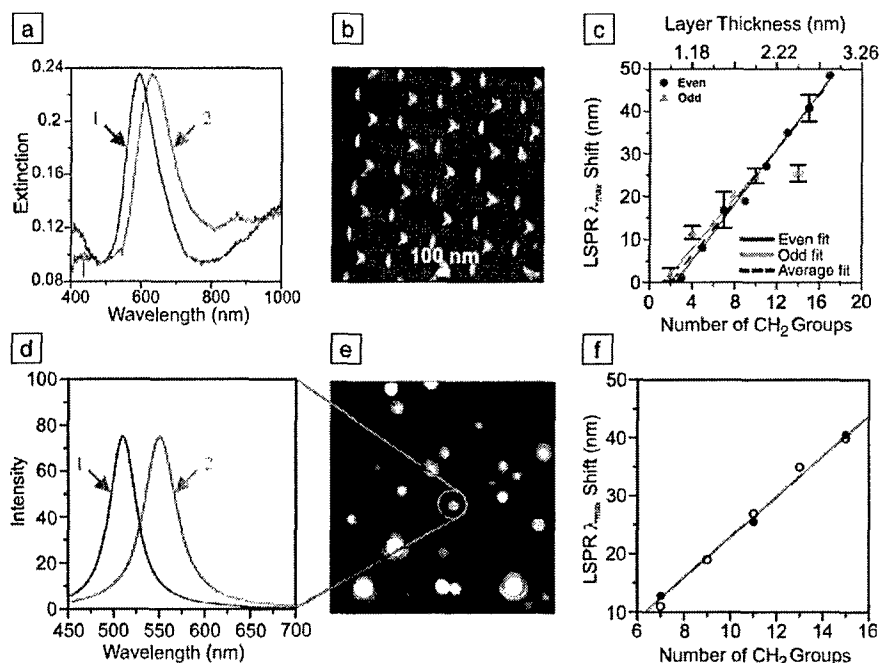


Figure 3. (top row) Localized surface plasmon resonance (LSPR) spectroscopy of a Ag nanoparticle array fabricated by nanosphere lithography in a N₂ environment: (a) Extinction spectrum of the array (curve 1) before chemical modification, wavelength of extinction maximum $\lambda_{max} = 594.8$ nm, and (curve 2) after modification with 1 mM hexadecanethiol, $\lambda_{max} = 634.8$ nm. (b) Tapping-mode atomic force microscopy (AFM) image of the array in (a); nanosphere diameter $D = 390$ nm, deposited mass thickness $d_m = 50$ nm; Ag on mica substrate; scan area, $3.0 \mu m^2$. After solvent annealing, nanoparticle in-plane width is 100 nm and out-of-plane height is 51 nm. (c) Alkanethiol chain length dependence on the LSPR spectral peak shifts for the array. Even and odd carbon chain lengths are depicted with different symbols to emphasize the difference in the terminal bond orientation with respect to the substrate, which leads to different observed trends for the two cases. (bottom row) LSPR spectroscopy of single Ag nanoparticles produced by chemical synthesis: (d) scattering spectrum of a single Ag nanoparticle (curve 1) before chemical modification, $\lambda_{max} = 510.2$ nm, and (curve 2) after modification with 1 mM hexadecanethiol, $\lambda_{max} = 550.9$ nm. The circled nanoparticle in (e) produced the signal for these curves. (e) Dark-field resonant Rayleigh scattering image of a random array of chemically synthesized Ag nanoparticles (image dimensions, $130 \mu m \times 130 \mu m$). (f) Alkanethiol chain length dependence on the LSPR spectral peak shifts for a single Ag nanoparticle. The open circles represent an overlay of the array data from (c). The solid circles are single nanoparticle measurements.

an adsorbate, d is the effective adsorbate layer thickness, and l_d is the characteristic electromagnetic-field decay length. This model assumes exponential decay of the electromagnetic field normal to the planar surface, which is accurate for a SPP, but is undoubtedly an oversimplification for the electromagnetic fields associated with noble metal nanoparticles. Nevertheless, Equation 2 does a remarkably good job of accounting for the data in Figure 3c if one assumes a value $l_d = 5-6$ nm. We will return to a justification of this value in a moment.

Recently, it has become possible to use dark-field resonant Rayleigh scattering to perform the $\Delta\lambda_{max}$ measurement for isolated single nanoparticles, and it was found that for chemically synthesized Ag triangular prisms (Figure 3e), $\Delta\lambda_{max}$ is a linear func-

tion of the refractive index of the external medium (Figure 3d) with a slope of ~ 200 nm/RIU.³² In addition, the same LSPR shift of ~ 40 nm as seen for the NSL particle array was observed for a monolayer of hexadecanethiol on a single particle; more important, the dependence of $\Delta\lambda_{max}$ on the chain length of the alkanethiol monolayer (Figure 3f) was found to be linear, with a large slope of 3.5 nm per CH₂ unit.³²

The similarity of the adsorbate-induced LSPR shift behavior for both NSL-derived nanoparticle arrays and single nanoparticles leads to the following important conclusions: (1) the short-range distance dependences for both systems can be described by Equation 2, and (2) interparticle coupling effects are minimal at the d_{ip} values imposed

by the NSL nanofabrication technique. In addition, it should be pointed out that from the viewpoint of chemical sensing, these single-nanoparticle LSPR shift results are truly remarkable. Based on the average surface area of the nanoparticles prepared and the monolayer packing density of molecules on Ag, this saturation response corresponds to the detection of fewer than 60,000 surface-confined molecules of hexadecanethiol. Additional experiments (not described here) demonstrate a limit of detection of ~ 2000 molecules.³² The real-time kinetics of adsorbates binding to single nanoparticles is also accessible from this experiment.³²

LSPR spectroscopy can also be used to probe the long-range (up to 40 nm) distance dependence of the electromagnetic fields surrounding NSL-derived Ag nanoparticles.³³ Figure 4 (see 4a and the solid triangles in 4c) shows that the dependence of $\Delta\lambda_{max}$ on the thickness of multilayer adsorbate shells synthesized through the interaction of $HOOC(CH_2)_{10}SH$ and Cu^{2+} is nonlinear. The multilayer thickness required to saturate the LSPR shift response was found to be dependent on the composition (Ag versus Au), shape (triangle versus hemisphere), in-plane width, and out-of-plane height of the nanoparticles. These results verify that the linear distance dependence found in the case of alkanethiol monolayers was the thin-shell limit of a longer-range, nonlinear dependence. They can be understood on the basis of an exponentially decaying electromagnetic field with l_d in the range of 5–6 nm for Ag nanotriangles ($a \approx 100$ nm, $b \approx 50$ nm). A more accurate simulation of the data has been provided by DDA calculations,³³ and the results are in quantitative agreement with experiment. Comparison of the long-range LSPR spectroscopy results for Ag (Figure 4a and solid circles in 4d) versus Au (Figure 4b and red triangles in 4d) shows that Ag has a longer spatial electromagnetic range and is more sensitive to adsorbates than Au.

Nanoscale Optical Biosensors Based on LSPR Spectroscopy

The LSPR wavelength shift response, $\Delta\lambda_{max}$, has been used to develop a new class of nanoscale optical biosensors.^{34–38} Two model systems, biotin–streptavidin³⁴ and biotin–anti-biotin,³⁵ were studied to illustrate the desirable attributes of LSPR-based nanoscale affinity biosensors. Streptavidin, a tetrameric protein, can bind up to four biotinylated molecules (i.e., antibodies, inhibitors, nucleic acids, etc.) with minimal impact on its biological activity, and therefore it provides a ready pathway for extending the analyte accessibility of the LSPR nanobiosensor. Anti-biotin, an antibody,

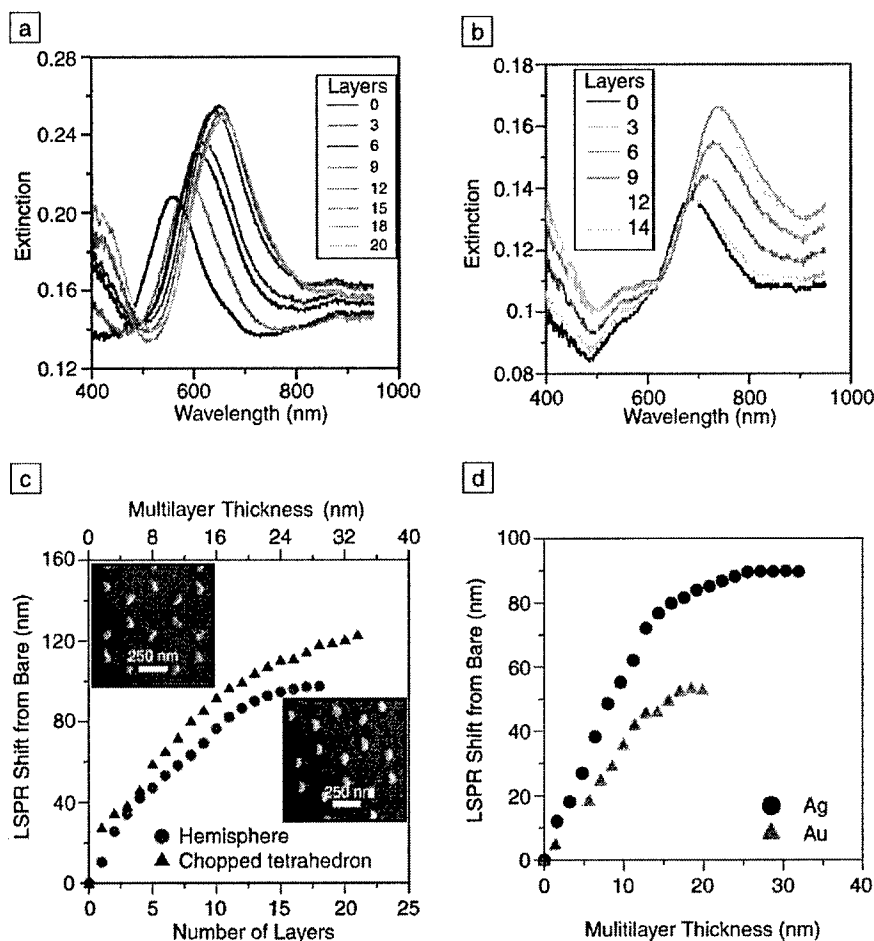


Figure 4. Localized surface plasmon resonance (LSPR) spectra for Ag and Au nanoparticles fabricated by nanosphere lithography. Long-range distance dependence: (a) Ag nanoparticles (in-plane width $a = 100$ nm, out-of-plane height $b = 50.0$ nm) for 0–20 layers of $\text{Cu}^{2+}/\text{HS}-(\text{CH}_2)_{10}\text{COOH}$; (b) Au nanoparticles ($a = 70$ nm, $b = 50.0$ nm) for 0–14 layers of $\text{Cu}^{2+}/\text{HS}-(\text{CH}_2)_{10}\text{COOH}$. (c) Shape dependence for Ag nanoparticles: (solid triangles) LSPR shift versus number of layers in the self-assembled monolayer (SAM) thickness for solvent-annealed Ag nanoparticles; (blue circles) LSPR shift versus number of layers in the SAM thickness for thermally annealed (600°C for 1 h) Ag nanoparticles. (inset, upper left) Atomic force microscopy (AFM) image of solvent-annealed nanoparticles ($a = 114$ nm, $b = 54$ nm). (inset, lower right) AFM image of thermally annealed nanoparticles ($a = 110$ nm, $b = 61$ nm). (d) Composition dependence: (solid circles) LSPR shift versus layer thickness for Ag nanoparticles ($a = 70$ nm, $b = 50.0$ nm); (red triangles) LSPR shift versus layer thickness for Au nanoparticles ($a = 70$ nm, $b = 50.0$ nm).

provides a straightforward platform to extend the LSPR nanosensor technology to immunoassay technology. The $\Delta\lambda_{\text{max}}$ for biotin-functionalized Ag NSL nanoparticle arrays was measured as a function of the concentration of streptavidin (SA) over the concentration range 10^{-15} M $< [\text{SA}] < 10^{-6}$ M. Fitting the data to the theoretical normalized response expected for 1:1 binding of a ligand to a multivalent receptor with different sites but invariant affinities yielded the following values: saturation response $R_{\text{max}} = 26.5$ nm, surface-confined thermodynamic binding

constant $K_{\text{a,surf}} = 10^{11}$ M $^{-1}$, and limit of detection $\text{LOD} < 1$ pM SA.³⁴ Similarly, the LSPR response curve for the binding of anti-biotin (AB) to biotin-functionalized Ag NSL nanoparticles was measured, and the data analysis yielded $R_{\text{max}} = 38.0$ nm, $K_{\text{a,surf}} = 4.5 \times 10^7$ M $^{-1}$, and $\text{LOD} < 7 \times 10^{-10}$ M AB.³⁵ As predicted, the LOD of the nanobiosensor studied is lower for systems with higher binding affinities, such as for the well-studied biotin–streptavidin couple, and higher for systems with lower binding affinities, as seen in the anti-biotin system.

A comparative analysis of real-time responses of a commercial propagating SPR sensor (planar thin film of gold) and the LSPR sensor (Ag NSL nanoparticle array) was carried out using the binding of Concanavalin A (ConA), a mannose-specific plant lectin, to mannose-functionalized self-assembled monolayers (SAMs).³⁶ During the association phase in the real-time binding studies, both sensors exhibited qualitatively similar signal-versus-time curves. However, in the dissociation phase, the SPR sensor showed an approximately five times greater loss of signal than the LSPR sensor. A comprehensive set of nonspecific binding studies demonstrated that this signal difference was not the consequence of greater nonspecific binding to the LSPR sensor, but rather a systematic function of nanoparticle structure. Ag nanoparticles with larger aspect ratios showed larger dissociation phase responses than those with smaller aspect ratios. DDA calculations demonstrated that this response is a consequence of the similarity in length scale between the electromagnetic-field decay length and the physical size of ConA.³⁶

Recently, the LSPR sensor has been successfully used for the detection of an Alzheimer's disease biomarker from both synthetic^{37,38} and human patient³⁹ samples (see also the article by Thaxton et al. in this issue). In this work, the interactions between the biomarker (antigen), amyloid- β derived diffusible ligands (ADDLs), and specific anti-ADDL antibodies were studied. Using the sandwich assay format, the LSPR sensor provided quantitative binding information for both antigen and second antibody detection that permits the determination of ADDL concentration. This unique capability offers the possibility of analyzing the aggregation mechanisms of this putative Alzheimer's disease pathogen at physiologically relevant monomer concentrations. Monitoring the LSPR-induced shifts from both ADDLs and a second polyclonal anti-ADDL antibody as a function of ADDL concentration reveals two ADDL epitopes (the exact binding site on an antigen that binds to an antibody) that have binding constants to the specific anti-ADDL antibodies of 7.3×10^{12} M $^{-1}$ and 9.5×10^8 M $^{-1}$. Furthermore, this study demonstrated for the first time that the LSPR nanosensor was successful at analyzing human brain extract and cerebrospinal fluid (CSF) samples. Examination of these results from both Alzheimer's disease and control patients reveals that the LSPR nanosensor provides new information relevant to the understanding and possible diagnosis of Alzheimer's disease. This exciting advance is one of the first examples in which nanotechnology has been applied to clinical materials for biomolecular diagnostics.³⁸

It is important to note that this technology is in its infancy. There are at least two main research objectives that must be met before it becomes available. First, the sensor must undergo rigorous testing using CSF samples from many more patients. In order for this objective to be met, we must integrate this technology with a redesigned chip. Currently, approximately 250 μ l of CSF is required for each assay. Because spinal taps are painful, it is ideal to minimize the amount of sample needed. By incorporating microfluidics and miniaturizing the sample cell, this objective will be met.

The examples just given all involved NSL-derivatized Ag nanoparticle arrays as the sensor platform. It has now been demonstrated that all of the outstanding attributes of the propagating SPR sensor, the "gold standard" in optical biosensing, are retained or exceeded in a single-nanoparticle sensor.^{32,39} Dark-field LSPR scattering spectroscopy and microscopy were used to demonstrate zeptomole (10^{-21}) sensitivity coupled with real-time kinetic analysis.³² Streptavidin biosensing has also been demonstrated on single Ag nanoparticles. A 12.7 nm redshift in the LSPR λ_{max} arises from the detection of <700 streptavidin molecules.⁴⁰

Surface-Enhanced Raman Spectroscopy

The local electromagnetic fields that accompany photon excitation of the LSPR are a key factor leading to the intense signals observed in all surface-enhanced spectro-

scopies.¹¹ Surface-enhanced Raman spectroscopy (SERS) is characterized by an ensemble-averaged intensity enhancement factor, EF, of $\sim 10^6$, for analytes bound to noble metal surfaces that possess random roughness,⁴¹ or EF $\approx 10^7$ – 10^8 , for surfaces with intentionally nanofabricated feature sizes in the ~ 100 nm range.⁴² Recent reports of single-molecule detection^{43,44} using SERS on Ag nanoparticle clusters have rejuvenated interest in this widely used analytical technique. A clear understanding of the mechanism responsible for the enormous enhancement factors ($\sim 10^{14}$ – 10^{15}) observed in single-molecule SERS remains elusive.

The electromagnetic (EM) mechanism of SERS mentioned earlier predicts that there is a well-defined relationship between the LSPR spectrum and the SERS spectrum of a SERS-active surface. In particular, very specific quantitative predictions for the magnitude of the enhancement factor on nanoparticle size, shape, and local dielectric environment are made. Wavelength-scanned SERES experiments on microfabricated surfaces were carried out in the early 1980s at Bell Laboratories,^{45,46} with a view toward verifying these predictions of the EM mechanism. Both as a consequence of experimental difficulty and the dissolution of the Bell group, many EM predictions remain purely in the domain of theory. The plasmonic materials that are now readily available from NSL and electron-beam lithography (EBL) provide a new platform for the detailed study of the electromagnetic-field enhancement mechanism associated

with SERS. Consequently, there is renewed experimental effort in SERES seeking to verify various aspects of the EM theory.

We will now discuss some recent results from our laboratory obtained using two approaches—plasmon-sampled (PS)⁴² and wavelength-scanned (WS) SERES. WS-SERES requires both a broadly tunable laser and detection system. This is not commonly available; however, with the size- and shape-tunable LSPR spectra obtainable with NSL- or EBL-derived plasmonic materials, this problem can be circumvented. NSL and EBL are used to prepare many samples with different LSPR λ_{max} values. Each sample is thoroughly characterized structurally by atomic force microscopy or scanning electron microscopy. Correlated, spatially resolved LSPR and SERS spectra are measured with a single excitation wavelength at multiple locations on each sample using a Raman microscope. Figure 5 shows representative LSPR spectra (Figures 5a–5c) and SERS spectra (Figures 5d–5f) for benzenethiol adsorbed on NSL-fabricated Ag nanoparticles excited at three common, fixed, excitation wavelengths. The SERS enhancement factors for Figures 5d–5f are 7.6×10^7 , 6.3×10^7 , and 9.0×10^7 , respectively,⁴² which are results that roughly agree with theoretical estimates (the electrodynamic calculations described earlier). PS-SERES plots (enhancement factor versus LSPR λ_{max}) for the 1575 cm^{-1} band of benzenethiol excited at three different laser wavelengths each showed a well-defined maximum

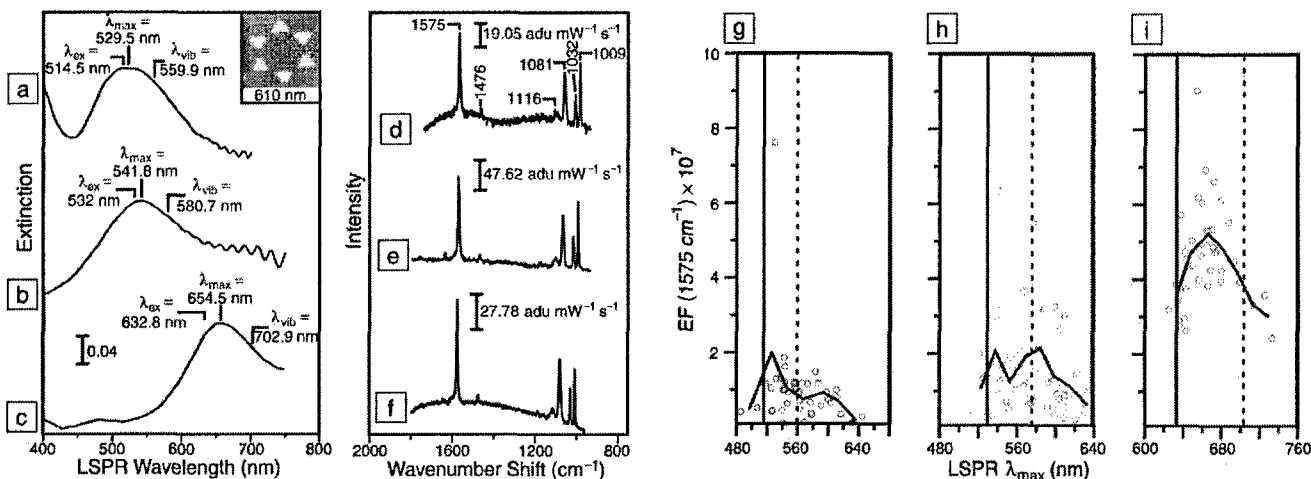


Figure 5. (a)–(f) Correlated, spatially resolved, localized surface plasmon resonance (LSPR) and surface-enhanced Raman spectroscopy (SERS) results for benzenethiol adsorbed on Ag nanoparticle arrays fabricated by nanosphere lithography. (a), (d) Ag nanoparticles fabricated with nanosphere diameter $D = 280$ nm and deposited mass thickness $d_m = 36$ nm, probed with an excitation wavelength $\lambda_{\text{ex}} = 514.5$ nm, power = 0.7 mW. A representative atomic force micrograph of the substrate is shown in the inset. (b), (e) Ag nanoparticles fabricated with $D = 280$ nm, $d_m = 36$ nm, probed with $\lambda_{\text{ex}} = 532.0$ nm, power = 0.7 mW. (c), (f) Ag nanoparticles fabricated with $D = 400$ nm, $d_m = 56$ nm, probed with $\lambda_{\text{ex}} = 632.8$ nm, power = 1.2 mW. (g)–(i) Plasmon-sampled surface-enhanced Raman excitation spectroscopy (PS-SERES) results for the 1575 cm^{-1} band of benzenethiol with three different excitation wavelengths: (g) $\lambda_{\text{ex}} = 514.5$ nm, (h) $\lambda_{\text{ex}} = 532.0$ nm, and (i) $\lambda_{\text{ex}} = 632.8$ nm. For each λ_{ex} , both the wavelength location of the excitation (solid line) and the scattering (dashed line) are marked. The overlaid curves represent the bin-averaged values of the LSPR λ_{max} and the enhancement factor. Bin widths are (g) 24 nm, (h) 16 nm, and (i) 16 nm.

representing the highest intensity SERS signal (Figures 5g–5i).⁴² In each case, these PS-SERES spectra follow the behavior predicted by the EM theory, that is, the largest enhancement factor occurs when the energy corresponding to the LSPR maximum is located near the midpoint between the energy of laser excitation and the energy of the Raman photons. These results unambiguously demonstrate (1) a systematic approach to the optimization of SERS spectra on nanoparticle substrates and (2) that large, ensemble-averaged, SERS enhancement factors ($\sim 1 \times 10^6$) are readily obtainable from Ag NSL-derived nanoparticle array surfaces. Recently, these results have been corroborated using Au nanoparticle array surfaces fabricated by EBL.⁴⁷

Figure 6a shows the SERS spectrum of benzenethiol adsorbed on a Ag FON surface. The nanostructure of Ag FON surfaces can be quantitatively characterized by atomic force microscopy (Figures 6b and 6c). Ag FON surfaces have a nanostructure size distribution that is less broad than that of a randomly roughened surface but not as narrow as a NSL-derived surface. Consequently, Ag FON surfaces have well-defined LSPR spectra (Figures 6d and 6e, solid curves), albeit broader than the LSPR spectra for Ag NSL-derived nanoparticle arrays. WS-SERES spectra for the 1081 cm^{-1} band of benzenethiol are shown in Figures 6d and 6e (data points). Using neat liquid benzenethiol as the normal Raman standard, the peak enhancement factor values were calculated to be 2.7×10^6 and 1.9×10^6 for Figure 6d and 6e, respectively. Two different behaviors are observed in the WS-SERES spectra for these surfaces. In one case, the WS-SERES spectrum peaks to the red of the LSPR spectrum (Figure 6d, data points) and in the other, it tracks the LSPR spectrum (Figure 6e, data points). This outcome is attributed to the different nanostructure size distributions for each surface. From a practical perspective, we point out that it is not yet possible to determine the optimum laser excitation wavelength for an Ag FON without doing SERES.

Figure 6f shows the SERS spectrum of benzenethiol adsorbed on a Ag NSL-derived nanoparticle array surface. A typical atomic force micrograph of a Ag NSL surface is shown in the inset in Figure 6g. The LSPR spectrum of a Ag NSL array is shown in Figure 6g (solid red line), along with the corresponding WS-SERES spectrum for the 1081 cm^{-1} band of benzenethiol adsorbed on the same Ag NSL array (data points). The peak enhancement factor for the 1081 cm^{-1} band of benzenethiol adsorbed on this surface is 1.9×10^7 , again using neat liquid benzenethiol as the normal Raman standard. Note that the peak

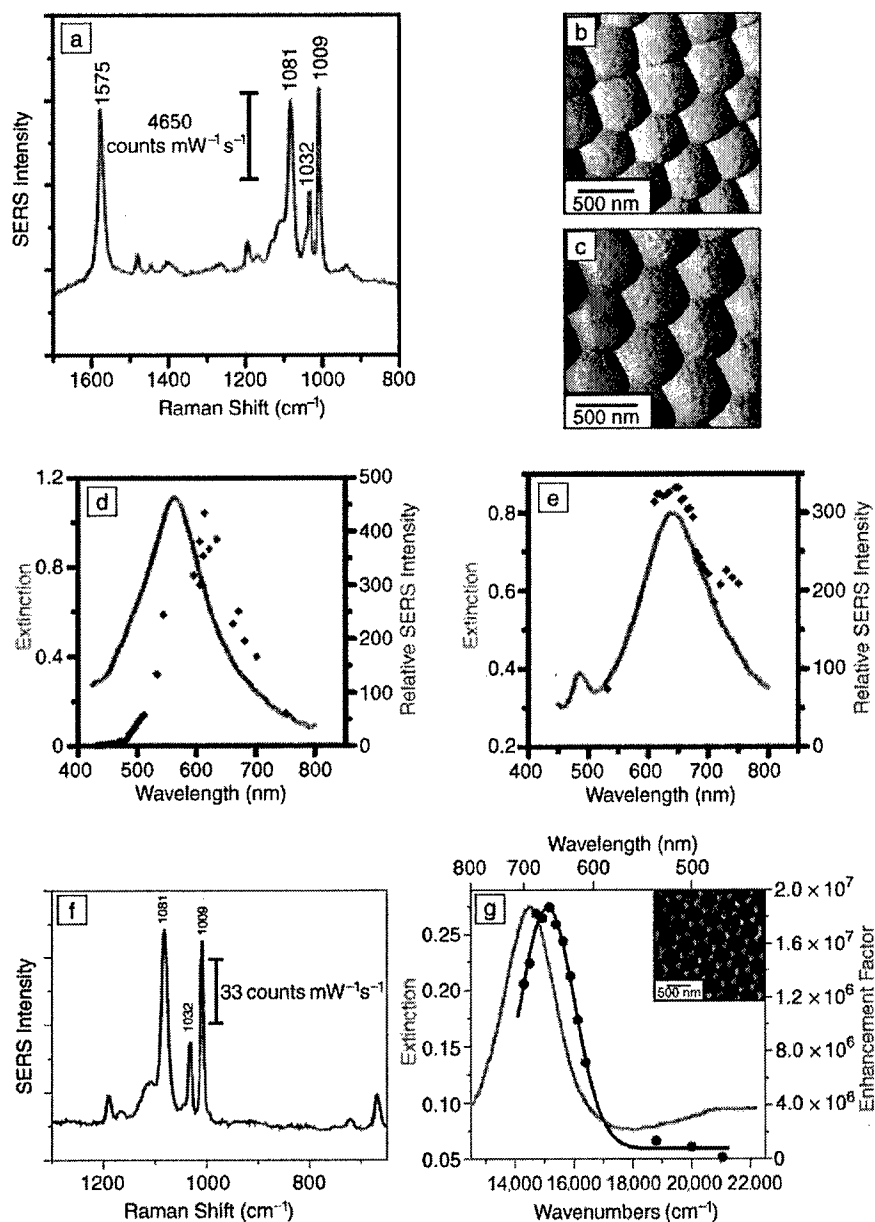


Figure 6. Localized surface plasmon resonance (LSPR), surface-enhanced Raman spectroscopy (SERS), and wavelength-scanned surface-enhanced Raman excitation spectroscopy (WS-SERES) results for benzenethiol adsorbed on Ag film-over-nanosphere (Ag FON) surfaces and nanoparticle arrays fabricated by nanosphere lithography (NSL). (a) SERS spectrum measured from Ag FON surface with excitation wavelength $\lambda_{\text{ex}} = 532 \text{ nm}$, power = 3.0 mW, and 100 s data acquisition time. (b) Contact-mode atomic force microscopy (AFM) image of Ag FON surface (nanosphere diameter $D = 410 \text{ nm}$, deposited mass thickness $d_m = 200 \text{ nm}$) used for SERS in (a). (c) Contact-mode AFM image of Ag FON surface ($D = 500 \text{ nm}$, $d_m = 250 \text{ nm}$) used for WS-SERES in (e). (d) LSPR spectrum (solid line, $\lambda_{\text{max}} = 562 \text{ nm}$, FWHM = 144 nm) and WS-SERES spectra (data points) for the 1081 cm^{-1} band of benzenethiol measured from the Ag FON surface in (b). (e) LSPR spectrum (solid line, $\lambda_{\text{max}} = 638 \text{ nm}$, FWHM = 131 nm) and WS-SERES spectra (data points) for the 1081 cm^{-1} band of benzenethiol measured from Ag FON surface in (c). (f) SERS spectrum measured from Ag nanoparticle array surface ($\lambda_{\text{ex}} = 532 \text{ nm}$, power = 3.0 mW, 100 s data acquisition time). (g) LSPR spectrum (solid line, $\lambda_{\text{max}} = 688 \text{ nm}$, FWHM = 95 nm) and WS-SERES spectra (data points) for the 1081 cm^{-1} band of benzenethiol measured from a Ag nanoparticle array surface. (inset) Tapping-mode AFM image of a representative array surface.

of the WS-SERES spectrum is blueshifted by 613 cm^{-1} (76 meV) with respect to the LSPR λ_{max} . The blueshift is an important prediction of EM theory that has not been previously observed. The results in Figures 5 and 6 are, to the best of our knowledge, the first correlated LSPR and SERES measurements for a nanofabricated surface.^{48,49}

Conclusions

The results presented here demonstrate the strength and versatility of silver and gold nanoparticles for biosensing based on extinction and surface-enhanced Raman spectroscopy and on single-particle Rayleigh scattering. These capabilities are based on the unique optical properties of localized surface plasmon resonances, including their sensitivity to particle shape and size, and to local changes in the surrounding refractive index due to molecular adsorption. In addition, plasmon excitation leads to strong local field enhancements that yield 10^8 enhancements in SERS. For all of these properties, theory can be used to provide important guidance to the design of these experiments. Recent theoretical work has suggested that new directions for nanoparticle-based sensing may be developed for interacting nanoparticle structures, including nanoparticle dimers⁵⁰ and large-scale arrays.⁵¹ Thus, there is much yet to do in this field.

Acknowledgments

The authors gratefully acknowledge support from the Air Force Office of Scientific Research MURI program (grant F49620-02-1-0381), the National Science Foundation (EEC-0118025, DMR-0076097, CHE-0414554), the Institute for Bioengineering and Nanoscience in Advanced Medicine at Northwestern University, and the National Institutes of Health (1 R21 DK066990-01A1).

References

- W.L. Barnes, A. Dereux, and T.W. Ebbesen, *Nature* **424** (2003) p. 824.
- C.L. Haynes, A.D. McFarland, L. Zhao, R.P. Van Duyne, G.C. Schatz, L. Gunnarsson, J. Prikkulis, B. Kasemo, and M. Käll, *J. Phys. Chem. B* **107** (2003) p. 7337.
- S.A. Maier, P.G. Kik, H.A. Atwater, S. Meltzer, E. Harel, B.E. Koel, and A.A.G. Requicha, *Nature Mater.* **2** (2003) p. 229.
- C.L. Haynes and R.P. Van Duyne, *Nano Lett.* **3** (2003) p. 939.
- H.J. Lezec, A. Degiron, E. Devaux, R.A. Linke, L. Martin-Moreno, F.J. Garcia-Vidal, T.W. Ebbesen, *Science* **297** (2002) p. 820.
- L.H. Smith, J.A.E. Wasey, and W.L. Barnes, *Appl. Phys. Lett.* **84** (2004) p. 2986.
- S. Wedge, J.A.E. Wasey, W.L. Barnes, and I. Sage, *Appl. Phys. Lett.* **85** (2004) p. 182.
- P. Andrew and W.L. Barnes, *Science* **306** (2004) p. 1002.
- R.P. Van Duyne, *Science* **306** (2004) p. 985.
- B. Pettinger, B. Ren, G. Picardi, R. Schuster, and G. Ertl, *Phys. Rev. Lett.* **92** 096101 (2004).
- G.C. Schatz and R.P. Van Duyne, in *Handbook of Vibrational Spectroscopy*, Vol. 1 (Wiley, New York, 2002) p. 759.
- A.J. Haes and R.P. Van Duyne, *Anal. Bioanal. Chem.* **379** (2004) p. 920.
- J.M. Brockman, B.P. Nelson, and R.M. Corn, *Ann. Rev. Phys. Chem.* **51** (2000) p. 41.
- W. Srituravanich, N. Fang, C. Sun, Q. Luo, and X. Zhang, *Nano Lett.* **4** (2004) p. 1085.
- J.C. Hulthen and R.P. Van Duyne, *J. Vac. Sci. Technol., A* **13** (1995) p. 1553.
- L.A. Dick, A.D. McFarland, C.L. Haynes, and R.P. Van Duyne, *J. Phys. Chem. B* **106** (2002) p. 853.
- M. Litorja, C.L. Haynes, A.J. Haes, T.R. Jensen, and R.P. Van Duyne, *J. Phys. Chem. B* **105** (2001) p. 6907.
- T.R. Jensen, M. Duval Malinsky, C.L. Haynes, and R.P. Van Duyne, *J. Phys. Chem. B* **104** (2000) p. 10549.
- T.R. Jensen, R.P. Van Duyne, S.A. Johnson, and V.A. Maroni, *Appl. Spectrosc.* **54** (2000) p. 371.
- A.M. Michaels, M. Nirmal, and L.E. Brus, *J. Am. Chem. Soc.* **121** (1999) p. 9932.
- S. Schultz, D.R. Smith, J.J. Mock, and D.A. Schultz, *Proc. Natl. Acad. Sci. U.S.A.* **97** (2000) p. 996.
- J. Yguerabide and E.E. Yguerabide, *Anal. Biochem.* **262** (1998) p. 157.
- U. Kreibitz and M. Vollmer, *Optical Properties of Metal Clusters*, Vol. 25 (Springer-Verlag, Heidelberg, Germany, 1995).
- C.L. Haynes and R.P. Van Duyne, *J. Phys. Chem. B* **105** (2001) p. 5599.
- B.T. Draine and J.J. Goodman, *Astrophys. J.* **405** (1993) p. 685.
- B.T. Draine and P.J. Flatau, *J. Opt. Soc. Am. A* **11** (1994) p. 1491.
- W.-H. Yang, G.C. Schatz, and R.P. Van Duyne, *J. Chem. Phys.* **103** (1995) p. 869.
- T.R. Jensen, M.L. Duval, L. Kelly, A. Lazarides, G.C. Schatz, and R.P. Van Duyne, *J. Phys. Chem. B* **103** (1999) p. 9846.
- M. Duval Malinsky, L. Kelly, G.C. Schatz, and R.P. Van Duyne, *J. Am. Chem. Soc.* **123** (2001) p. 1471.
- A.J. Haes, S. Zou, G.C. Schatz, and R.P. Van Duyne, *J. Phys. Chem. B* **108** (2004) p. 6961.
- L.S. Jung, C.T. Campbell, T.M. Chinowsky, M.N. Mar, and S.S. Yee, *Langmuir* **14** (1998) p. 5636.
- A.D. McFarland and R.P. Van Duyne, *Nano Lett.* **3** (2003) p. 1057.
- A.J. Haes, S. Zou, G.C. Schatz, and R.P. Van Duyne, *J. Phys. Chem. B* **108** (2004) p. 109.
- A.J. Haes and R.P. Van Duyne, *J. Am. Chem. Soc.* **124** (2002) p. 10596.
- J.C. Riboh, A.J. Haes, A.D. McFarland, C.R. Yonzon, and R.P. Van Duyne, *J. Phys. Chem. B* **107** (2003) p. 1772.
- C.R. Yonzon, E. Jeoung, S. Zou, G.C. Schatz, M. Mrksich, and R.P. Van Duyne, *J. Am. Chem. Soc.* **126** (2004) p. 12669.
- A.J. Haes, W.P. Hall, L. Chang, W.L. Klein, and R.P. Van Duyne, *Nano Lett.* **4** (2004) p. 1029.
- A.J. Haes, L. Chang, W.L. Klein, and R.P. Van Duyne, *J. Am. Chem. Soc.* **127** (2005) p. 2264.
- G. Raschke, S. Kowarik, T. Franzl, C. Soennichsen, T.A. Klar, J. Feldmann, A. Nichtl, and K. Kuerzinger, *Nano Lett.* **3** (2003) p. 935.
- R.P. Van Duyne, A.J. Haes, and A.D. McFarland, *Proc. SPIE—The International Society for Optical Engineering* **5223** (2003) p. 197.
- D.L. Jeanmaire and R.P. Van Duyne, *J. Electroanal. Chem.* **84** (1977) p. 1.
- C.L. Haynes and R.P. Van Duyne, *J. Phys. Chem. B* **107** (2003) p. 7426.
- S. Nie and S.R. Emory, *Science* **275** (1997) p. 1102.
- K. Kneipp, Y. Wang, H. Kneipp, L.T. Perelman, I. Itzkan, R.R. Dasari, and M.S. Feld, *Phys. Rev. Lett.* **78** (1997) p. 1667.
- P.F. Liao, J.G. Bergman, D.S. Chemla, A. Wokaun, J. Melngailis, A.M. Hawryluk, and N.P. Economou, *Chem. Phys. Lett.* **81** (1981) p. 355.
- R.E. Howard, P.F. Liao, W.J. Skocpol, L.D. Jackel, and H.G. Craighead, *Science* **221** (1983) p. 117.
- N. Felidi, S.L. Truong, J. Aubard, G. Levi, J.R. Krenn, A. Hohenau, A. Leitner, and F.R. Aussenegg, *J. Chem. Phys.* **120** (2004) p. 7141.
- A.D. McFarland, "Using Nanoparticle Optics for Ultrasensitive Chemical Detection and Surface-Enhanced Spectroscopy," PhD thesis, Northwestern University, 2004.
- A.D. McFarland, M.A. Young, J.A. Dieringer, and R.P. Van Duyne, *J. Phys. Chem. B* **109** (2005) accepted.
- E. Hao and G.C. Schatz, *J. Chem. Phys.* **120** (2004) p. 357.
- S. Zou, N. Janel, and G.C. Schatz, *J. Chem. Phys.* **120** (2004) p. 10871. □

MRS Materials Connections

www.mrs.org/connections/

Your source for Materials Research-Related Information!

Research news, materials data sources,
materials Web site database,
meetings calendar, and more.

Check it out today!

Advertisers in This Issue

	Page No.
Carl Zeiss MicroImaging, Inc.	361
Chemat Technology, Inc.	348
Cougar Labs, Inc.	Inside back cover
High Voltage Engineering	Inside front cover
Huntington Mechanical Labs, Inc.	Outside back cover
Janis Research Company, Inc.	355
Shiva Technologies, Inc.	395

For free information about the products and services offered in this issue, check <http://advertisers.mrs.org>

A Mixed Decanethiol/Mercaptohexanol Partition Layer Enables Real-Time Glucose Sensing by Surface- Enhanced Raman Spectroscopy in Bovine Plasma

*Olga Lyandres,^{‡§} Nilam C. Shah,^{†§} Chanda Ranjit Yonzon,^{†§} Joseph T. Walsh Jr.,[‡] Matthew R.
Glucksberg,[‡] and Richard P. Van Duyne^{†*}*

[†]Chemistry Department, [‡]Department of Biomedical Engineering, Northwestern University, Evanston,
Illinois 60208.

* To whom correspondence should be addressed: vanduyne@chem.northwestern.edu

§ These authors contributed equally to this work

Abstract: A new mixed decanethiol (DT) partition layer with dramatically improved properties has been developed for glucose sensing by surface-enhanced Raman spectroscopy (SERS). This work represents significant progress towards our long term goal of a minimally invasive, continuous, reusable glucose sensor. The DT/MH-functionalized surface has greater temporal stability, demonstrates rapid, reversible partitioning and departitioning, and is simpler to control compared to the tri(ethylene glycol) monolayer used previously. The data herein show that this DT/MH-functionalized surface is stable for at least 10 days in bovine plasma. Reversibility is demonstrated by exposing the sensor alternately to 0 and 100 mM aqueous glucose solutions (pH ~ 7). The difference spectra show that complete partitioning and departitioning occur. Furthermore, physiological levels of glucose in two complex media were quantified using multivariate analysis. In the first system the sensor is exposed to a solution

consisting of water with 1 mM lactate and 5 mM urea. The root mean squared error of prediction (RMSEP) is 92.17 mg/dL (5.12 mM) with 87% of the validation points falling within the A and B range of the Clarke error grid. In the second, more complex system, glucose is measured in the presence of bovine plasma. The root mean squared error of prediction (RMSEP) is 83.16 mg/dL (4.62 mM) with 85% of the validation points falling within the A and B range of the Clarke error grid. Finally, in order to evaluate the real-time response of the sensor, the 1/e time constant for glucose partitioning and departitioning in the bovine plasma environment was calculated. The time constant is 28 s for partitioning and 25 s for departitioning, indicating the rapid interaction between the SAM and glucose that is essential for continuous sensing.

INTRODUCTION

Diabetes mellitus is a chronic disorder that requires careful regulation of glucose levels in order to maintain the health of diabetic patients. Failure to regulate these levels within tight limits leads to severe secondary health complications to the diabetic patient's retina, kidneys, nerves, and circulatory system.^{1,2} Most commonly, diabetics measure glucose levels 4-6 times per day with the electrochemically based finger-stick method. The finger-stick method is not capable of continuous monitoring and suffers from low patient compliance due to the pain and discomfort associated with blood sampling from the capillaries. Such intermittent testing can fail to detect significant fluctuations in blood glucose levels and place the patient in dangerously hypo- or hyperglycemic conditions. The development of a continuous monitoring device for glucose with as low a degree of invasiveness as possible will clearly have an enormous impact on long-term human health.

In recent years, the development of continuous, implantable glucose sensors has been the focus of various research groups. The most advanced glucose sensors measure glucose indirectly by electrochemical detection methods. Glucose is enzymatically reduced by glucose oxidase in the presence of oxygen resulting in production of hydrogen peroxide.^{3,4} While hydrogen peroxide is

detected, other interfering analytes such as SERS Measurement of Glucose and Lactate in pH-Buffered False positive signals.⁵ Clearly, specificity is very important in the development of glucose sensors.

Infrared (IR) and Raman spectroscopies have recently been explored as useful techniques for glucose detection. The unique vibrational signatures of each molecule allow direct and selective identification of glucose. Arnold and coworkers have demonstrated the detection of glucose both in aqueous solution⁶ and in whole blood in the near-IR region.⁷ However, due to low spectral resolution and overlap with second overtone peaks of water, glucose detection using near-IR spectroscopy is difficult. On the other hand, Raman spectroscopy has higher spectral resolution and significantly reduced interference from water. Moreover, Raman spectroscopy has been able to detect glucose in the physiological range *in vitro* and in aqueous humor.⁸ Due to the inherently weak Raman signals of glucose, however, high power and long acquisition times are required for quantitative detection.⁹ This problem can be overcome by utilizing surface-enhanced Raman spectroscopy (SERS).¹⁰⁻¹² Enhancement is observed when molecules are brought into proximity to nanoscale roughened metal surfaces.¹³ The intensified local electromagnetic field generated by the nanoscale structures is able to enhance the observed Raman scattering by 10^6 to 10^8 ,^{14,15} and in exceptional cases as much as 10^{14} times.^{16,17}

In our previous work, development of a sensing platform for glucose detection using SERS was demonstrated.¹⁰⁻¹² The metal film over nanospheres (MFON) SERS-active surface was functionalized with alkanethiol or an alkanethiol derivative self-assembled monolayer (SAM) to partition and departition glucose closer to the surface. Quantitative measurements were performed using the SAM-functionalized SERS surface in phosphate buffered saline (pH = 7.4) and in presence of bovine serum albumin.¹¹ In addition, SAM stability on the AgFON and AuFON was demonstrated for three and ten days, respectively.¹² Reversibility of glucose partitioning was also demonstrated on these sensors.

Quantitative detection of glucose was demonstrated using tri (ethylene glycol) terminated alkanethiol (EG3) and decanethiol (DT) SAMs on the SERS-active surface. Although EG3 SAM is

known to be biocompatible,¹⁸⁻²⁰ its SERS measurement of glucose and lactate - MR Glucksberg, PI

challenging and, therefore its availability is limited.

DT, on the other hand, is hydrophobic and not

compatible with an aqueous environment. In this

work, a new mixed SAM, based on two

commercially available components, decanethiol

(DT) and mercaptohexanol (MH), was explored to

attain a real-time, quantitative glucose monitoring

device. Combining the longer DT component with

the shorter MH component creates a pocket for

improved glucose partitioning, bringing glucose

even closer to the SERS-active surface than was possible with EG3. In addition, the DT/MH SAM has

dual hydrophobic/hydrophilic functionality analogous to EG3. Based on the stability and reversibility

parameters, we have experimentally confirmed that the DT/MH mixed SAM has better performance as a

partitioning layer than the DT and EG3 SAMs used previously.

Herein, we demonstrate (1) the stability of the DT/MH partition layer on an AgFON surface, (2) partitioning and departitioning of glucose on a DT/MH-functionalized AgFON surface, (3) quantitative detection of glucose in aqueous solution with interfering analytes and in bovine plasma, and (4) real-time kinetics of glucose partitioning and departitioning.

EXPERIMENTAL SECTION

Materials. All the chemicals were reagent grade or better, and used as purchased. Silver pellets (99.99%) were purchased from Kurt J. Lesker Company (Clairton, PA). Oxygen free high conductivity copper was obtained from McMaster-Carr (Chicago, IL) and cut into 18 mm diameter disks. To clean substrates, NH_4OH , H_2O_2 , and $\text{CH}_3\text{CH}_2\text{OH}$ were used from Fisher Scientific (Fairlawn, VA).

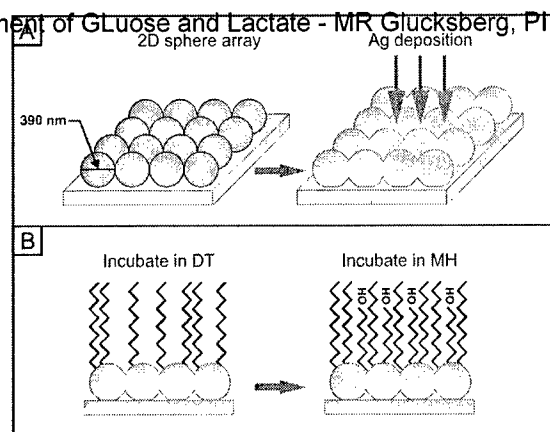


Figure 1. Schematic for fabricating DT/MH-functionalized AgFON. A) Nanospheres (diameter = 390 nm) were self-assembled to form a hexagonal close packed 2D crystal. Metal (Ag) was then deposited via electron beam deposition. B) The FON surface was then incubated in a solution of 1 mM DT in ethanol for 45 minutes and then transferred to 1 mM MH in ethanol for at least 12 hours. This DT/MH SAM creates a pocket for glucose to fit into, bringing glucose closer to the SERS-active surface.

Surfactant-free, white carboxyl-substituted polystyrene nanospheres (diameter, 4% solid) were purchased from Duke Scientific Corporation (Palo Alto, CA). Ultrapure water ($18.2 \text{ M}\Omega \text{ cm}^{-1}$) from a Millipore system (Marlborough, MA) was used for substrate and solution preparation. Bovine plasma was obtained from Hemostat Laboratories (Dixon, CA). Glucose, lactate, and urea were purchased from Sigma (St. Louis, MO). Decanethiol ($\text{CH}_3(\text{CH}_2)_9\text{SH}$), and 6-mercapto-1-hexanol ($\text{HS}(\text{CH}_2)_6\text{OH}$) were purchased from Aldrich (Milwaukee, WI). Disposable filters, pore size $0.45 \text{ }\mu\text{m}$, were acquired from Gelman Sciences (Ann Arbor, MI).

AgFON Fabrication and Incubation Procedure. The copper substrates were cleaned by sonicating in 5:1:1 $\text{H}_2\text{O}/30\% \text{ H}_2\text{O}_2/\text{NH}_4\text{OH}$. Approximately $10 \text{ }\mu\text{l}$ of nanosphere solution was drop-coated onto a clean copper substrate and allowed to dry at room temperature. Then, 200 nm thick Ag films were deposited onto and through the nanosphere mask using the Kurt J. Lesker electron beam deposition system (Clairton, PA) to form AgFON substrates. The mass thickness and deposition rate ($2 \text{ }\text{\AA}/\text{s}$) of the Ag metal were measured by 6 MHz gold plated quartz-crystal microbalance purchased from Sigma Instruments (Fort Collins, CO). AgFON substrates were first incubated in 1 mM DT in ethanol for 45 minutes and then transferred to 1 mM MH in ethanol for at least 12 hours (Figure 1). Then the SAM-functionalized surfaces were mounted into a small volume flow cell for SER spectra collection.

Surface-enhanced Raman Spectroscopy. A Spectra-Physics model Millennia Vs laser ($\lambda_{\text{ex}} = 532 \text{ nm}$) was used to excite a Spectra-Physics model 3900 Ti-sapphire laser to produce the 785 nm excitation wavelength (λ_{ex}); the laser spot size on the sample was less than 0.5 mm in diameter. This excitation wavelength was chosen to minimize autofluorescence of proteins.^{21,22} The SERS measurement system includes an interference filter, an edge filter (Semrock, Rochester, NY), a model VM-505 single-grating monochromator with the entrance slit set at $100 \text{ }\mu\text{m}$ (Acton Research Corp., Acton, MA), and a LN_2 -cooled CCD detector (Roper Scientific, Trenton, NJ). A collection lens with magnification 5 was used to collect the scattered light. The small volume flow cell was used to control the external environment of the AgFON surfaces throughout the SERS experiments.

Quantitative Multivariate Analysis. SERS measurement of glucose and lactate was performed using MATLAB (MathWorks, INC., Natick, MA) and PLS_Toolbox (Eigenvector Research, Inc., Manson, WA). Prior to analysis, the spectra were smoothed using the Savitsky-Golay method with a second order polynomial and window size of 9. Cosmic rays were removed from the spectra using a derivative filter. The slowly varying background, commonly seen in SERS experiments was removed by subtracting a fourth-order polynomial fit. This method greatly reduced varying background levels with minimum effect on the SERS peaks. The chemometric analysis was performed using the partial least-squares (PLS) method and leave-one-out (LOO) cross validation algorithm.

Time Constant Analysis. The data was processed using PeakFit 4.12 software (Systat Software Inc, Richmond, CA). To remove the varying background in SER spectra, a fourth order polynomial was subtracted from the baseline using MATLAB software. The spectra were further preprocessed in PeakFit with linear best fit baseline correction and Savitsky-Golay smoothing. The amplitude of the Raman bands was obtained by fitting the data to the superposition of the Lorentzian amplitude lineshapes.

RESULTS AND DISCUSSION

The results presented below show significant advancement towards an implantable, real-time continuous SERS based glucose sensor. Our previous work demonstrated the ability to detect glucose with SERS using decanethiol as the partition layer.¹⁰ Subsequently, EG3 was used as the partition layer because it is biocompatible and has the ability to resist nonspecific binding of proteins due to its hydrophilic properties.¹¹ Moreover, stability, reversibility, and resistance to serum protein interference of the EG3-functionalized glucose sensor were demonstrated. Finally, the SERS based glucose sensor was optimized for NIR laser excitation wavelength with the EG3 partition layer to reduce photodamage of tissue and optimize signal on Au surfaces.¹² This development showed enhanced spectral stability

and gave more accurate measurements. SERS Measurement of Glucose and Uric Acid in Human Blood Plasma is scarce. In the present work, a new mixed SAM layer, consisting of decanethiol (DT) and mercaptohexanol (MH) has been developed. We also demonstrate (1) long term stability of the DT/MH-functionalized AgFON surface (2) reversibility of the sensor (3) quantitative measurement of glucose, and (4) real-time partitioning and departitioning of the glucose sensor.

Temporal Stability of DT/MH-Modified Substrate. An implantable glucose sensor must be stable for at least 3 days.²³ In our previous work, we demonstrated that SAM-functionalized AgFON substrates were stable for at least 3 days in phosphate buffered saline by electrochemical and SERS measurements.¹² Herein, we demonstrate the stability of the DT/MH-functionalized AgFON surface for

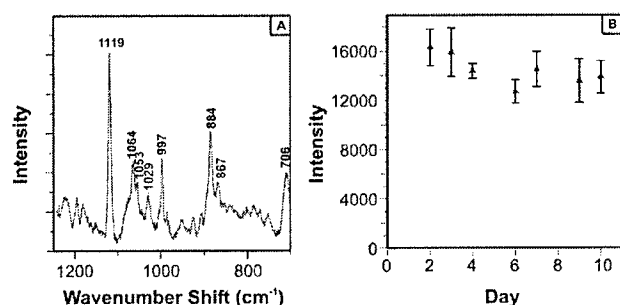


Figure 2. Stability of the DT/MH-functionalized FOM. A) SERS spectrum of DT/MH-functionalized FOM (Day 2) B) Time-course of intensity of 1119 cm⁻¹ peak. Signal intensities stayed stable over a 10 day period with only a 2.08% change in intensity, $\lambda_{\text{ex}} = 785$ nm, $P_{\text{laser}} = 55$ mW, $t = 2$ min.

10 days in bovine plasma (Figure 2). SER spectra were captured every 24 hours from three different samples and three spots on each sample ($\lambda_{\text{ex}} = 785$ nm, $t = 2$ min). Figure 2A represents the DT/MH spectrum acquired on day 2. Figure 2B shows the average intensity of the 1119 cm⁻¹ peak for DT/MH on the AgFON for each day as a function of time. The 1119 cm⁻¹ band corresponds to a

symmetric stretching vibration of a C–C bond.²⁴ The change in intensity of the 1119 cm⁻¹ peak from the first day to the last day is 2.08%, indicating that it did not vary significantly during the ten day period. The 2% change in the intensity can be attributed to the rearrangement of the SAM during the incubation in bovine plasma.²⁵ The temporal stability of the 1119 cm⁻¹ peak intensity indicates that the DT/MH SAM was intact and well ordered, making this SAM-functionalized surface a potential candidate for an implantable sensor.

Reversible Glucose Sensing. An implantable glucose sensor must also be reversible in order to successfully monitor fluctuation in glucose concentration throughout the day. To demonstrate the

reversibility of the sensor, the DT/MH-SERS-Measurement of Glucose and Lactate - MR Glucksberg, P

AgFON sensor was exposed to cycles of 0 and 100 mM aqueous glucose solutions (pH ~ 7) without flushing the sensor in between measurements to simulate real-time sensing (Figure 3 inset). Nitrate was used as an internal standard in all the experiments (1053 cm^{-1} peak) to minimize effective laser power fluctuations. The 1053 cm^{-1} band corresponds to a symmetric stretching vibration of NO_3^- and was used to normalize the spectra.²⁶ SER spectra were collected for each step ($\lambda_{\text{ex}} = 532\text{ nm}$, $P = 10\text{ mW}$,

$t = 20\text{ min}$) (Figure 3A, 3B, 3C, 3D). Figure 3E shows the normal Raman spectrum of a saturated aqueous glucose solution for comparison. In the normal Raman spectrum of a saturated aqueous glucose solution, peaks at 1462 , 1365 , 1268 , 1126 , 915 , and 850 cm^{-1} correspond to crystalline glucose peaks.²⁷ The difference spectra (Figure 3F, 3G) represent partitioning of glucose in DT/MH SAM, which clearly show the glucose features at 1461 , 1371 , 1269 , 1131 , 916 , and 864 cm^{-1} . This corresponds to the peaks in the normal Raman spectrum of glucose in aqueous solution (Figure 3E). Literature has shown that SERS bands can shift up to 25 cm^{-1} when compared to normal Raman bands of the same analyte.²⁸ The sharp peak seen in all of the difference spectra at 1053 cm^{-1} represent imperfect subtraction of the nitrate internal standard. The absence of glucose spectral features in the difference spectra (Figure 3H, 3I) represents complete departitioning of glucose. The DT/MH mixed SAM presents a completely reversible sensing surface for optimal partitioning and departitioning of glucose.

Quantitative Detection of Glucose Using DT/MH Partition Layer. In order for a glucose sensor to be viable, it should be able to detect glucose in the clinically relevant range $10\text{-}450\text{ mg/dL}$ ($0.56\text{-}25$

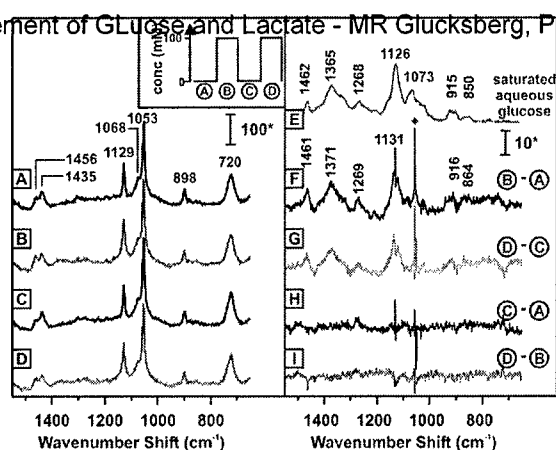


Figure 3. Glucose pulsing sequence on the SAM modified AgFON surface (inset). SER spectra of the sample cycled between 0 and 100 mM aqueous glucose solutions (A, B, C, D), $\lambda_{\text{ex}} = 532\text{ nm}$, $P_{\text{laser}} = 10\text{ mW}$, $t = 20\text{ min}$, $\text{pH} \sim 7$. Normal Raman spectrum of aqueous saturated glucose solution (E). Difference spectra showing partitioning/departitioning of glucose (F, G, H, I). ♦ Imperfect subtraction of the narrow band at 1053 cm^{-1} due to nitrate results in a very sharp peak in the difference spectra. *a.d.u. $\cdot\text{mW}^{-1}\cdot\text{min}^{-1}$.

mM), under physiological pH, and in the presence of glucose and lactate (Figure 4). The data is presented in the Clarke error grid, a standard for evaluating the reliability of glucose sensors in the clinically relevant concentration range (0-450 mg/dL).²⁹ Data points that fall in the A and B range are acceptable values. Values outside the A and B range result in potential failure to detect blood glucose levels outside of the target range and erroneous diagnosis. DT/MH-functionalized AgFON samples were placed in a flow cell containing water (pH ~ 7) with lactate (1 mM) and urea (2.5 mM) in physiological concentrations, which are potential interferents for glucose detection. Glucose solutions ranging from 10 to 450 mg/dL with lactate and urea were then randomly introduced in the cell and incubated for 2 min to ensure complete partitioning. SER spectra were collected using two substrates and multiple spots with a near-infrared laser source ($\lambda_{\text{ex}} = 785 \text{ nm}$, $P = 8.4 \text{ mW}$, $t = 2 \text{ min}$). A calibration model was constructed using partial least squares leave-one-out (PLS-LOO) analysis with 46 randomly chosen independent spectral measurements of known glucose concentrations. The calibration model was based upon 7 latent variables which take into account variation in laser power, the environment in the lab, and SERS enhancement at different locations. The PLS analysis results in a root mean square error of calibration (RMSEC) of 9.89 mg/dL (0.549 mM). This RMSEC value is lower than that reported in our previous work using the EG3-modified AgFON.

In addition to having a low RMSEC, it is important to use an independent validation set to test the calibration model.³⁰ For this model, a set of 23 data points was used to validate the model. The root mean square error of prediction (RMSEP) was calculated to be 92.17 mg/dL (5.12 mM). Figure 4 depicts that 98% of the calibration points and 87% of the validation points

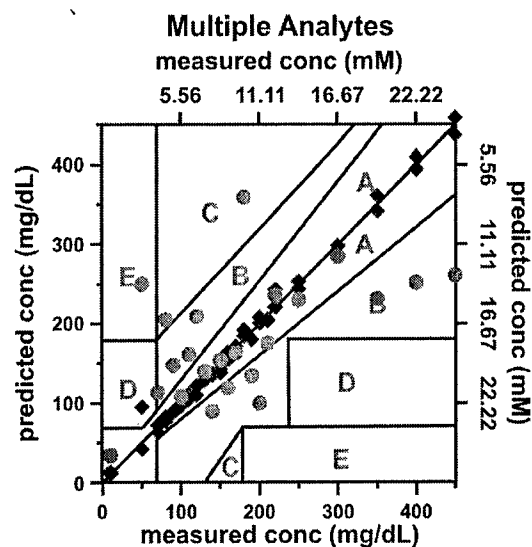


Figure 4. Calibration (♦) and validation (●) plots using two substrates and multiple spots. PLS calibration plot was constructed using 46 data points. The validation plot was constructed using 23 data points taken over a range of glucose concentrations (10 - 450 mg/dL) in 1 mM lactate and 2.5 mM urea at pH~7. RMSEC = 9.89 mg/dL (0.55 mM) and RMSEP = 92.17 mg/dL (5.12 mM). $\lambda_{\text{ex}} = 785\text{nm}$, $P_{\text{laser}} = 8.4\text{mW}$, $t = 2 \text{ min}$.

fall in the A and B range of the Clarke error grid. The RMSEP of the in vivo glucose sensor is 83.16 mg/dL (4.62 mM). The RMSEC of the in vitro glucose sensor is 34.3 mg/dL (1.90 mM). The number of data points in the calibration set.

To transition from the *in vitro* sensor to an *in vivo* sensor, the sensor should also demonstrate quantitative detection in a more complex medium. Bovine plasma was used to simulate the *in vivo* environment of an implantable glucose sensor. Prior to use, bovine plasma was filtered using 0.45 μm diameter pore size. The filtered plasma was then spiked with glucose concentrations ranging from 10-450 mg/dL. DT/MH-functionalized AgFON substrates were placed in the flow cell and exposed to glucose spiked bovine plasma. SER spectra were collected at each concentration using multiple samples and multiple spots in random order to construct a robust calibration model ($\lambda_{\text{ex}} = 785 \text{ nm}$, $P = 10\text{-}30 \text{ mW}$, $t = 2 \text{ min}$). Calibration was constructed using PLS-LOO analysis described above using 7 latent variables and presented in a Clarke error grid (Figure 5). To construct the calibration, 92 randomly chosen data points were used, resulting in an RMSEC of 34.3 mg/dL (1.90 mM). For the validation, 46 data points were used with an RMSEP of 83.16 mg/dL (4.62 mM). In the Clarke error grid, 98% for calibration and 85% for validation fall in the A and B range. The errors in both experiments can be reduced by using more data points for the calibration. In addition, error can also be attributed to variation in SERS enhancement at different spots and different substrates.¹⁴ The results show that the DT/MH-modified AgFON glucose sensor is capable of making accurate glucose measurements in the presence of many interfering analytes.

Real-time Study of Partitioning and Departitioning of Glucose. In addition to reversibility, which is an important characteristic for a viable sensor, the sensor

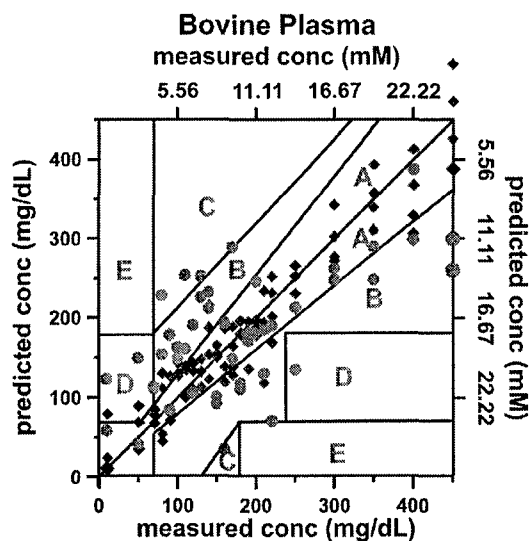


Figure 5. Calibration (\blacklozenge) and validation (\bullet) plots using three substrates and multiple spots acquired in two days. PLS calibration plot was constructed using 92 data points. The validation plot was constructed using 46 data points taken over a range of glucose concentrations (10 - 450 mg/dL) in bovine plasma. RMSEC = 34.3 mg/dL (1.9 mM) and RMSEP = 83.16 mg/dL (4.62 mM). $\lambda_{\text{ex}} = 785 \text{ nm}$, $P_{\text{laser}} = 10\text{-}30 \text{ mW}$, $t = 2 \text{ min}$.

should be able to partition and depart glucose on a reasonable time scale. The real-time response was examined in a system with bovine plasma simulating the *in vivo* environment. In order to evaluate the real-time response of the sensor, the $1/e$ time constant for partitioning and departitioning was calculated.

A DT/MH-functionalized AgFON was placed in bovine plasma for ~5 hours. The AgFON surface was then placed in a flow cell. SER spectra were collected continuously ($\lambda_{\text{ex}} = 785 \text{ nm}$) with a 15 s integration time. To observe partitioning, 50 mM glucose solution in bovine plasma was injected at $t =$

0. At $t = 225 \text{ s}$, 0 mM glucose solution in bovine plasma was injected into the flow cell to evaluate the departitioning of glucose. Excitation wavelength of 785 nm was used to reduce autofluorescence caused by proteins.^{21,22} The amplitude was then plotted versus time as shown in Figure 6C. The $1/e$ time constant was calculated from the exponential curve fitted to the data points.

The spectra shown in Figure 6A and 6B demonstrate real-time amplitude changes in the 1462 cm^{-1} peak as the glucose concentration varies. The amplitude of the 1462 cm^{-1} peak was obtained by fitting the data to the superposition of three Lorentzian lineshapes using PeakFit. The $1/e$ time constant is 28 s for partitioning and 25 s for departitioning, calculated from the exponential fit (Figure 6C). These experiments demonstrate that partitioning and departitioning occur rapidly making the SERS based glucose sensor a potential candidate for implantable, continuous sensing.

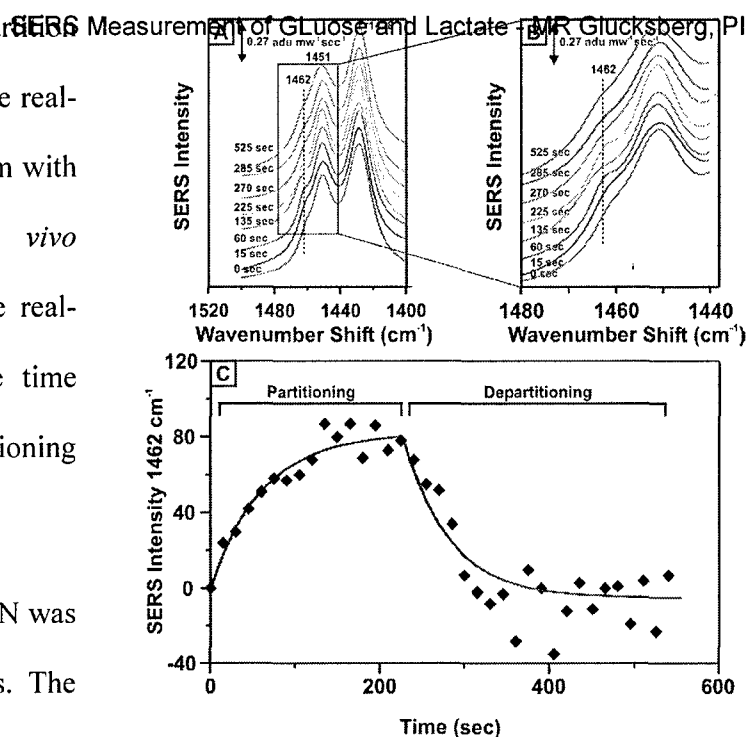


Figure 6. Real-time SERS response to a step change in glucose concentration in bovine plasma. A) SER spectra of the SAM and glucose at various times. Peaks at 1451 cm^{-1} and 1428 cm^{-1} are features of SAM and 1462 cm^{-1} indicates glucose. Glucose was injected at $t = 0 \text{ s}$ and the cell was flushed with bovine plasma at $t = 225 \text{ s}$. B) Expanded scale version of Figure 6A from 1480 to 1440 cm^{-1} . C) Partitioning and departitioning of glucose. $\lambda_{\text{ex}} = 785 \text{ nm}$, $P_{\text{laser}} = 100 \text{ mW}$, $t = 15 \text{ s}$. The $1/e$ time constants were calculated to be 28 s for partitioning and 25 s for departitioning.

CONCLUSIONS

This work demonstrates significant progress towards developing a real-time, continuous, quantitative SERS glucose sensor. A new mixed SAM was explored to partition and departition glucose efficiently. The new SAM consists of decanethiol (DT) and mercaptohexanol (MH) providing the appropriate balance of hydrophobic and hydrophilic groups. The DT/MH-functionalized SERS surface showed temporal stability for at least 10 days in bovine plasma, making it a potential candidate for implantable sensing. Furthermore, quantitative glucose measurements, in the physiological concentration range, in a mixture of interfering analytes and in bovine plasma were also demonstrated. Finally, the DT/MH-functionalized SERS surface also partitioned and departitioned glucose in less than one minute which indicates that the sensor can be used for real-time, continuous sensing.

The temporal stability of the DT/MH-functionalized AgFON surface is evident from the fact that the intensity of a SERS band did not change for a period of 10 days when incubated in bovine plasma. The intensity of the 1119 cm^{-1} SAM peak varied by only 2% during a period of ten days. This fluctuation can be attributed to molecular rearrangement of the SAM.²⁵

Moreover, reversibility of the DT/MH-functionalized glucose sensor was demonstrated by injecting cycles of 0 and 100 mM glucose in water (pH \sim 7). The difference spectra demonstrate complete partitioning and departitioning of glucose. In addition, the time constant for glucose partitioning and departitioning is less than one minute, indicating rapid interaction between the SAM and glucose essential for continuous sensing.

The ability for DT/MH-functionalized AgFON to measure glucose concentrations accurately was evaluated using the Clarke error grid. The sensor was exposed to various concentrations of glucose in an aqueous solution (pH \sim 7), consisting of 1 mM lactate and 2.5 mM urea. The cross-validation error is 92.17 mg/dL and 87% of the validation data fall in the A and B range of the Clarke error grid.

Furthermore, a more complex media, bovine plasma, was used to demonstrate the glucose response of the SERS glucose sensor. In this case, the cross-validation error is 83.16 mg/dL and 85% of the validation data fall in the A and B range of the Clarke error grid.

Significant progress toward developing a continuous, real-time, quantitative glucose sensor is reported. In future work, the SERS glucose sensor will be implanted in an animal to demonstrate *in vivo* glucose sensing, and cross-calibrated with qualified hospital laboratory equipment.

ACKNOWLEDGMENTS

This work was supported by the National Institutes of Health (DK066990-01A1), the U. S. Army Medical Research and Materiel Command (W81XWH-04-1-0630), the National Science Foundation (CHE0414554), and the Air Force Office of Scientific Research MURI program (F49620-02-1-0381).

REFERENCES

- (1) *Diabetes Overview*; National Diabetes Information Clearinghouse (NDIC), <http://diabetes.niddk.nih.gov/dm/pubs/overview/index.htm> (07-26-05).
- (2) Ross, S. A.; Gulve, E. A.; Wang, M. *Chem. Rev.* **2004**, *104*, 1255.
- (3) Heller, A. *Annu. Rev. Biomed. Eng.* **1999**, *1*, 153.
- (4) Wilson, G. S.; Hu, Y. *Chem. Rev.* **2002**, *100*, 2693.
- (5) Park, S. C.; T. C.; Kim, H. C. *Anal. Chem.* **2003**, *75*, 3046.
- (6) Arnold, M. A. *Abstracts of Papers of the American Chemical Society* **2002**, *224*, U114.
- (7) Amerov, A. K.; Chen, J.; Small, G. W.; Arnold, M. A. *Anal. Chem.* **2005**, *77*, Web Release Date: 02.
- (8) Lambert, J.; Storrie-Lombardi, M.; Borchert, M. *IEEE LEOS Newsletter* **1998**, *12*, 19.
- (9) McCreery, R. L. *Raman Spectroscopy for Chemical Analysis*; John Wiley & Sons, Inc.: New York, 2000; Vol. 157.
- (10) Shafer-Peltier, K. E.; Haynes, C. L.; Glucksberg, M. R.; Van Duyne, R. P. *J. Am. Chem. Soc.* **2003**, *125*, 588.
- (11) Yonzon, C. R.; Haynes, C. L.; Zhang, X. Y.; Walsh, J. T.; Van Duyne, R. P. *Anal. Chem.* **2004**, *76*, 78.
- (12) Stuart, D. A.; Yonzon, C. R.; Zhang, X.; Lyandres, O.; Shah, N. C.; Glucksberg, M. R.; Walsh, J. T.; Van Duyne, R. P. *Anal. Chem.* **2005**, *77*, 4013.

- (13) Schatz, G. C.; Van Duyne, R. P. *Measurement of Glucose and Lactate by Surface Plasmon Resonance*; Wiley, New York, 2002; Vol. 1, p 759.
- (14) Haynes, C. L.; Van Duyne, R. P. *J. Phys. Chem. B* **2003**, *107*, 7426.
- (15) McFarland, A. D.; Young, M. A.; Dieringer, J. A.; Van Duyne, R. P. *J. Phys. Chem. B* **2005**, *109*, 11279.
- (16) K. Kneipp, Y. W., H. Kneipp, L.T. Perelman, I. Itzkan, R.R. Dasari, M.S. Feld *Phys. Rev. Lett.* **1997**, *78*, 1667.
- (17) Nie, S.; Emory, S. R. *Science* **1997**, *275*, 1102.
- (18) Mauzac, M. A., N.; Jozefonvicz, J. *Biomaterials* **1982**, *3*, 221.
- (19) Lee, J. H.; Kopecek, J.; Andrade, J. D. *Journal of Biomedical Materials Research* **1989**, *23*, 351.
- (20) Cohn, D. Y., H. *Journal of Biomedical Materials Research* **1988**, *22*, 993.
- (21) Anderson, R. R.; Parrish, J. A. In *The Science of Photomedicine*; Plenum Press: New York, 1982, p 147.
- (22) Weissleder, R. *Nat. Biotechnol.* **2001**, *19*, 316.
- (23) Kaufman, F. R.; Gibson, L. C.; Halvorson, M.; Carpenter, S.; Fisher, L. K.; Pitukcheewanont, P. *Diabetes Care* **2001**, *24*, 2030.
- (24) Bryant, M. A.; Pemberton, J. E. *J. Am. Chem. Soc.* **1991**, *113*, 8284.
- (25) Biebuyck, H. A.; Bain, C. D.; Whitesides, G. M. *Langmuir* **1994**, *10*, 1825.
- (26) Mosier-Boss, P. A.; Lieberman, S. H. *Appl. Spectrosc.* **2000**, *54*, 1126.
- (27) Soderholm, S.; Roos, Y. H.; Meinander, N.; Hotokka, M. *J. Raman Spectrosc.* **1999**, *30*, 1009.
- (28) Stacy, A. M.; Van Duyne, R. P. *Chem. Phys. Lett.* **1983**, *102*, 365.
- (29) Clarke, W. L.; Cox, D.; Gonder-Frederick, L. A.; Carter, W.; Pohl, S. L. *Diabetes Care* **1987**, *10*, 622.
- (30) Beebe, K. R.; Pell, R. J.; Seasholtz, M. B. *Chemometrics: A Practical Guide*; Wiley Interscience: New York, 1998.